

THERMAL DECOMPOSITION OF ENERGETIC MATERIALS: TNCHP, TNAZ,
24DNI, ANTA, DNBT AND HMX

FINAL REPORT

RICHARD BEHRENS.

MARCH 31, 1998

U. S. ARMY RESEARCH OFFICE

GRANT NO. 33655-CH

SANDIA NATIONAL LABORATORIES
COMBUSTION RESEARCH FACILITY
LIVERMORE, CALIFORNIA 94551

APPROVED FOR PUBLIC RELEASE;

DISTRIBUTION UNLIMITED.

19990621 034

THE VIEWS, OPINIONS, AND/OR FINDINGS CONTAINED IN THIS REPORT ARE
THOSE OF THE AUTHOR AND SHOULD NOT BE CONSTRUED AS AN OFFICIAL
DEPARTMENT OF ARMY POSITION, POLICY, OR DECISION, UNLESS SO
DESIGNATED BY OTHER DOCUMENTATION

Foreword

The objective of our research has been to develop a better understanding of the thermal decomposition mechanisms of energetic materials. Over the years, our understanding of the mechanisms has evolved from a relatively simple chemical framework, in which individual bond-breaking processes in a molecule were thought to control the rate of decomposition, to an appreciation of the complex sets of processes that typically control the decomposition of these materials. For example, in our earlier work we observed the mononitroso intermediate of the parent cyclic nitramine. We came to realize that this intermediate provides a means to branch to a different set of decomposition products. Thus, allowing for two different chemical reaction pathways. In another example from our earlier work we also realized that HMX undergoes extensive decomposition within individual particles. We found evidence of bubbles formed within the solid particles.

Since our initial work we have expanded significantly on our understanding of these materials. We have analyzed different classes of energetic compounds in an attempt to understand how molecular and crystal structures, as well as other physical parameters, affect the decomposition process. We have examined different cyclic nitramines, nitrate esters, C-nitro compounds, and several different types of azoles. This current project focuses on HMX and several different types of azoles.

We have found that all of these compounds exhibit a complex thermal decomposition behavior that involves both chemical and physical processes, which are coupled. As the reader will see, from the results presented in this report, our methods of measurement allow us to identify the nature of the underlying decomposition processes. This enables us to formulate mathematical models of the underlying processes, and determine the necessary parameters required to make predictive models. This is done for the first time in the current project for 24DNI. Our success with 24DNI has encouraged us to proceed with formulating models for other materials, such as HMX and TNAZ.

Throughout the years, it has been our pleasure to collaborate with Dr. Surya Bulusu from the U.S. Army, ARDEC. Our collaborations have been stimulating, cordial and highly productive. To our great dismay, Dr. Bulusu passed away last year. He was a dear friend who will be greatly missed.

REPORT DOCUMENTATION PAGE			Form Approved OMB NO. 0704-0188	
Public reporting burden for this collection of information is estimated to average 1 hour per response, including the time for reviewing instructions, searching existing data sources, gathering and maintaining the data needed, and completing and reviewing the collection of information. Send comment regarding this burden estimate or any other aspect of this collection of information, including suggestions for reducing this burden, to Washington Headquarters Services, Directorate for Information Operations and Reports, 1215 Jefferson Davis Highway, Suite 1204, Arlington, VA 22202-4302, and to the Office of Management and Budget, Paperwork Reduction Project (0704-0188), Washington, DC 20503.				
1. AGENCY USE ONLY (Leave blank)		2. REPORT DATE 3/31/98		3. REPORT TYPE AND DATES COVERED FINAL 7/95 TO 12/97
4. TITLE AND SUBTITLE THERMAL DECOMPOSITION OF ENERGETIC MATERIALS: TNCHP, TNAZ, 24DNI, ANTA, DNBT and HMX			5. FUNDING NUMBERS AROMIPR 148-95	
6. AUTHOR(S) Richard Behrens				
7. PERFORMING ORGANIZATION NAME(S) AND ADDRESS(ES) Sandia National Laboratories Combustion Research Facility P.O. Box 969, MS 9052 Livermore, CA 94551-0969			8. PERFORMING ORGANIZATION REPORT NUMBER	
9. SPONSORING / MONITORING AGENCY NAME(S) AND ADDRESS(ES) U.S. Army Research Office P.O. Box 12211 Research Triangle Park, NC 27709-2211			10. SPONSORING / MONITORING AGENCY REPORT NUMBER ARO 33655.2-CH	
11. SUPPLEMENTARY NOTES The views, opinions and/or findings contained in this report are those of the author(s) and should not be construed as an official Department of the Army position, policy or decision, unless so designated by other documentation.				
12a. DISTRIBUTION / AVAILABILITY STATEMENT Approved for public release; distribution unlimited.			12 b. DISTRIBUTION CODE	
13. ABSTRACT (Maximum 200 words) The physical and chemical processes that control the thermal decomposition of several different types of energetic materials have been determined from measurements with a simultaneous thermogravimetric modulated beam mass spectrometer (STMBMS). The compounds studied include HMX, hexahydro-1-nitroso-3,5-dinitro-s-triazine (ONDNTA), 2,4-dinitroimidazole (24DNI), TNAZ, 1-nitroso-3,3-dinitroazetidine (NDNAZ), 3-amino-5-nitro-1,2,4-triazole (ANTA), 5,5'-dinitro-3,3'-bi-1,2,4-triazole (DNBT), and a complex of DNBT•2ANTA. The results on HMX provide new insights on the solid-phase decomposition processes that take place within individual particles. The results on ONDNTA provide new insight to the reaction mechanisms that control the decomposition of this important cyclic nitramine reaction intermediate. The results on 24DNI, TNAZ, and NDNAZ provide sufficient data to construct a model of the underlying chemical and physical processes. A model has been formulated to represent the decomposition of 24DNI and the parameters for the model have been determined from the STMBMS results. The model consists of seven different physical processes, which include the nucleation and growth of a polymeric residue that acts as an "autocatalyst". Global chemical reactions are used in each step. A qualitative model of the thermal decomposition of TNAZ and NDNAZ is presented. Sufficient data has been collected to formulate mathematical models of their decomposition.				
14. SUBJECT TERMS HMX, TNAZ, NDNAZ, 24DNI, ONDNTA, thermal decomposition, kinetics, reaction mechanisms, explosives, propellants			15. NUMBER IF PAGES 93	
			16. PRICE CODE	
17. SECURITY CLASSIFICATION OR REPORT UNCLASSIFIED	18. SECURITY CLASSIFICATION OF THIS PAGE UNCLASSIFIED	19. SECURITY CLASSIFICATION OF ABSTRACT UNCLASSIFIED	20. LIMITATION OF ABSTRACT UL	

Table of Contents

<i>Foreword</i>	2
<i>Table of Contents</i>	3
<i>List of Figures</i>	4
<i>Statement of the Problem</i>	5
<i>Summary of Most Important Results</i>	6
Decomposition of HMX and RDX	7
Decomposition of TNAZ, NDN AZ, 24DNI, ANTA and DNBT	13
Decomposition of 24DNI	15
Decomposition of TNAZ and NDN AZ	16
Decomposition of ANTA, DNBT and the DNBT•2ANTA complex	17
<i>Publications and Technical Reports</i>	21
<i>Scientific Personnel</i>	22
<i>Inventions: none</i>	22
<i>Bibliography</i>	22
<i>Appendix</i>	24

List of Figures

FIGURE 1. GAS FORMATION RATES OF PRODUCTS FORMED FROM THE THERMAL DECOMPOSITION OF HMX AT 235°C FROM THREE DIFFERENT EXPERIMENTS. BY USING DIFFERENT DIAMETER ORIFICES IN EACH EXPERIMENT THE MAXIMUM PRESSURE OF THE GASEOUS DECOMPOSITION PRODUCTS CONTAINED IN THE REACTION CELL WAS CHANGED. THE RESULTS SHOW THAT AS THE PRESSURE OF THE DECOMPOSITION PRODUCTS IN THE REACTION CELL INCREASE THE RATES OF DECOMPOSITION DURING THE LATER STAGES OF THE REACTION CHANGE FROM DECREASING RATES TO INCREASING RATES.....	9
FIGURE 2. SEM OF THE RESIDUE THAT REMAINS AFTER THE DECOMPOSITION OF HMX IN THE SOLID PHASE UNDER LOW GAS PRESSURE CONDITIONS. THE RESIDUE WAS FORMED FROM THE DECOMPOSITION OF ONE HMX PARTICLE. THE REMAINING RESIDUE WAS CUT IN HALF TO EXPOSE THE INSIDE OF THE PARTICLE SHOWN IN THE SEM.	10
FIGURE 3. SEMS OF RESIDUE FROM THE DECOMPOSITION OF ONE HMX PARTICLE THAT WAS DECOMPOSED UNDER LOW CONFINEMENT CONDITIONS. NOTE FLAKE-LIKE APPEARANCE AND SUBMICRON SIZE SHELLS.....	11
FIGURE 4. SEMS OF RESIDUE FROM THE DECOMPOSITION OF ONE HMX PARTICLE THAT WAS DECOMPOSED UNDER <u>HIGH</u> CONFINEMENT CONDITIONS. NOTE ROD-LIKE APPEARANCE AND APPEARANCE OF LAYERS (LIKE LAYERS OF SWISS CHEESE).	12
FIGURE 5. SCHEMATIC REPRESENTATION OF 2,4-DNI DECOMPOSITION PROCESSES IN THE SOLID PHASE.....	16
FIGURE 6. (A) HEATING ANTA WITH A 500 μm ORIFICE RESULTS IN COMPLETE EVAPORATION. (B) HEATING ANTA AT 220°C WITH A 25 μm ORIFICE RESULTS IN SUBSTANTIAL DECOMPOSITION AND LEAVES ~45 % OF THE INITIAL WEIGHT AS NONVOLATILE RESIDUE. NOTE THE INITIAL RISE IN THE WATER SIGNAL AND THE CORRESPONDING DROP IN WEIGHT; THIS LIKELY REPRESENTS LOSS OF ADSORBED WATER. (THE WEIGHT LOSS CURVE IS NORMALIZED SO THE Y-SCALE IS 100 % OF THE INITIAL WEIGHT. THE EVAPORATION AND DECOMPOSITION SIGNALS ARE ON THE SAME SCALE IN ARBITRARY UNITS).	18
FIGURE 7. (TOP) HEATING DNBt WITH A ~500 μm ORIFICE RESULTS IN RAPID WEIGHT LOSS DUE TO EVAPORATION OF DNBt AND DECOMPOSITION, REPRESENTED BY M/Z 30 (MOSTLY NO). ABOUT 34% OF INITIAL WEIGHT IS LEFT AS NONVOLATILE RESIDUE. (BOTTOM) HEATING DNBt AT 240°C WITH A 25 μm ORIFICE RESULTS IN GRADUAL DECOMPOSITION AND LEAVES ~66 % OF THE INITIAL WEIGHT AS NONVOLATILE RESIDUE. (THE WEIGHT LOSS CURVE IS NORMALIZED SO THE Y-SCALE IS 100 % OF THE INITIAL WEIGHT. THE EVAPORATION AND DECOMPOSITION SIGNALS ARE ON THE SAME SCALE IN ARBITRARY UNITS).	19
FIGURE 8A. HEATING DNBt•2ANTA WITH A ~500 μm ORIFICE RESULTS IN RAPID WEIGHT LOSS DUE TO EVAPORATION AND DECOMPOSITION OF BOTH COMPONENTS. ABOUT 28% OF INITIAL WEIGHT IS LEFT AS NONVOLATILE RESIDUE. (THE WEIGHT LOSS CURVE IS NORMALIZED SO THE Y-SCALE IS 100 % OF THE INITIAL WEIGHT. THE EVAPORATION AND DECOMPOSITION SIGNALS ARE ON THE SAME SCALE IN ARBITRARY UNITS).	20
FIGURE 8B. HEATING DNBt•2ANTA AT 190°C WITH A 25 μm ORIFICE RESULTS IN RAPID DECOMPOSITION BUT VERY LITTLE EVAPORATION (NO DNBt IS OBSERVED) AND LEAVES ~54 % OF THE INITIAL WEIGHT AS NONVOLATILE RESIDUE. (THE WEIGHT LOSS CURVE IS NORMALIZED SO THE Y-SCALE IS 100 % OF THE INITIAL WEIGHT. THE EVAPORATION AND DECOMPOSITION SIGNALS ARE ON THE SAME SCALE IN ARBITRARY UNITS).	21

Statement of the Problem

The purpose of this project has been to further our understanding of the chemical reaction mechanisms and physical processes that control the thermal decomposition of energetic materials with two goals in mind. The first goal focuses on applying this knowledge to predict the response of energetic materials, currently used in weapon stockpiles, to heat, impact or shock. The second goal is to develop a new understanding of how to develop new energetic materials for insensitive ordnance. To achieve this goal requires understanding how the processes that control the thermal, impact and shock sensitivity of energetic materials are related to the physical and chemical properties of the compounds. Since the thermal, impact and shock sensitivities are related to the chemical reactions transforming these compounds to their final products, understanding the details of how the thermal decomposition processes are related to the physical and chemical properties of the energetic materials will provide a basis for developing new, less sensitive, energetic materials.

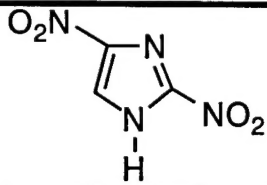
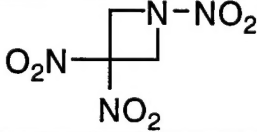
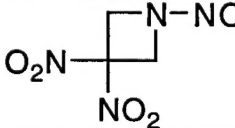
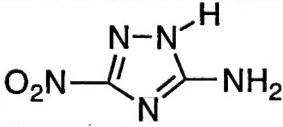
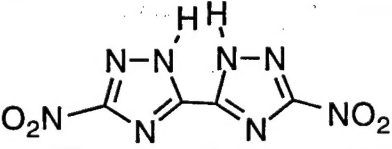
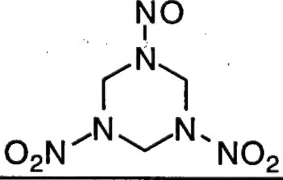
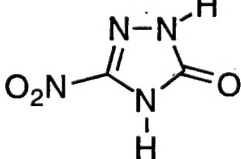
The processes that control the thermal decomposition of energetic materials are complex physicochemical processes. These processes involve multiple chemical reaction pathways coupled with different types of physical processes that are dependent on whether the reaction occurs in the solid, liquid or gaseous state. To accurately characterize the rates of thermal decomposition of energetic materials requires understanding the chemical reaction mechanisms, the physical processes, and how they are coupled to each other. To achieve our first goal requires understanding the processes in compounds such as RDX and HMX. Furthermore, it requires developing mathematical models of the underlying processes and obtaining the quantitative data required to parameterize the physicochemical processes used in the mathematical models. These models will allow the thermal decomposition results to be used in models of ordnance behavior. To achieve the second goal requires understanding how these physicochemical processes are dependent on the physical and chemical properties of different types of energetic materials. This requires obtaining a detailed understanding of the physicochemical processes that control the decomposition of a range of different energetic materials.

To obtain this type of information on the thermal decomposition processes of energetic materials requires the ability to identify the products of the thermal decomposition reactions, to obtain their rates of formation as a function of time, and to correlate the results with morphological changes that occur in condensed-phase reactions or the formation of secondary products that may act as autocatalysts. This is a difficult task. We utilize simultaneous thermogravimetric modulated beam mass spectrometry (STMBMS) to identify the products and measure their rates of formation. We utilize scanning electron microscopy (SEM) to characterize the morphology of condensed-phase processes.

Summary of Most Important Results

Our work on the thermal decomposition of energetic materials has two principal goals: (1) to develop a sufficient understanding of the physical and chemical processes controlling the decomposition of energetic materials to enable development of models for prediction of the response to hazards, such as fire or impact; (2) to gain a better understanding of how functionality, physical properties and molecular structure of energetic materials relate to their behaviors in both normal and abnormal environments and to their long-term aging behavior. We have concentrated our efforts in two areas. First, we have worked to obtain an in-depth understanding of the decomposition of two important cyclic nitramines, RDX and HMX. This work has been supported over several years by both a Memorandum of Understanding between the U.S. Army and DOE and a previous research grant from ARO. Under this grant we have continued our efforts in this area by studying the thermal decomposition of hexahydro-1-nitroso-3,5-dinitro-s-triazine (ONDNTA), the mononitroso analogue of RDX, because our previous studies discovered that the mononitroso analogues of RDX and HMX are important intermediates in their decomposition. We have also initiated new studies on HMX to obtain a better understanding of the solid-phase processes that control its decomposition. Second, we have obtained extensive temperature-dependent data on the decomposition of 1,3,3-trinitroazetidine (TNAZ), 1-nitroso-3,3-dinitroazetidine (NDNAZ) and 2,4-dinitro-1,3-imidazole (24DNI), and have initiated studies on the decomposition of 3-amino-5-nitro-1,2,4-triazole (ANTA), 5,5'-dinitro-3,3'-bi-1,2,4-triazole (DNBT), and a complex of DNBT•2ANTA. This work will examine the effect of changes in functionality and differing molecular environments on the decomposition process. (Molecular structures of the compounds used in this study are listed in Table 1.) Third, we have developed new methods to create mathematical models of the thermal

Table 1. Structures of compounds discussed in report.

Compound	Structure
24DNI	
TNAZ	
NDNAZ	
ANTA	
DNBT	
ONDNTA	
NTO	

decomposition processes of energetic materials, and have obtained parameters for these models from the thermal decomposition data collected with the STMBMS instrument. We have focused our initial efforts on the development of a mathematical model to characterize the thermal decomposition of 24DNI. The details of the work may be found in the copies of the publications of our work included in Appendix A. A summary of the most significant findings from our work on HMX and RDX is presented first, followed by the most significant finding from our work on TNAZ, NDNABZ, 24DNI, ANTA and ANTA•DNBT.

Decomposition of HMX and RDX

The work on the cyclic nitramines, HMX and RDX, has focused on three different studies. First the low temperature decomposition of HMX was examined to extend the data range of our previous work on HMX^{1,2} down to 175°C. Next, the decomposition of the mononitroso analogue of RDX, hexahydro-1-nitroso-3,5-dinitro-s-triazine (ONDNTA), was studied further because it is an important intermediate in the decomposition of RDX. Finally, new studies of the decomposition of HMX were undertaken to obtain a better understanding of the physical processes that occur within the solid phase and how these affect the rates of decomposition.

Low temperature decomposition of HMX. The thermal decomposition of HMX between 175°C and 200°C has been studied using the simultaneous thermogravimetric modulated beam mass spectrometer (STMBMS) apparatus with a focus on the initial stages of the decomposition.³ The identity of thermal decomposition products is the same as that measured in previous higher temperature experiments. The initial stages of the decomposition are characterized by an induction period followed by two acceleratory periods. The Arrhenius parameters for the induction and two acceleratory periods are ($\text{Log}(A) = 18.2 \pm 0.8$, $E_a = 48.2 \pm 1.8$ kcal/mole), ($\text{Log}(A) = 17.15 \pm 1.5$ and $E_a = 48.9 \pm 3.2$ kcal/mole), ($\text{Log}(A) = 19.1 \pm 3.0$ and $E_a = 52.1 \pm 6.3$ kcal/mole), respectively. The data can be used to calculate the time and temperature required to decompose a desired fraction of a test sample that is being prepared to test the effect of thermal degradation on its sensitivity or burn rates. It can also be used to estimate the extent of decomposition that may be expected under normal storage conditions for munitions containing HMX. The data, along with previous mechanistic studies conducted at higher temperatures, suggest that the process that controls the early stages of decomposition of HMX in the solid phase is scission of the N-NO₂ bond, reaction of the NO₂ within a "lattice cage" to form the mononitroso analogue of HMX and decomposition of the mononitroso HMX within the HMX lattice to form gaseous products that are retained in bubbles or diffuse into the surrounding lattice.

The decomposition of ONDNTA. Previous work on the decomposition of hexahydro-1,3,5-trinitro-s-triazine (RDX)^{4,5} and octahydro-1,3,5,7-tetranitro-1,3,5,7-tetrazocine (HMX)^{2,6} has shown that the mononitroso analogues of these compounds play an important role in their decomposition, in both the solid and liquid phases. The mononitroso analogue of RDX, hexahydro-1-nitroso-3,5-dinitro-s-triazine (ONDNTA) was independently synthesized and its decomposition had been studied previously.⁷ Our current thermal decomposition studies of ONDNTA have uncovered a relatively complex decomposition behavior.⁸

We have found that ONDNTA decomposes in two different temperature ranges in an unusual way. As the temperature of the sample is increased, one temperature range ("low") of decomposition is evident between 95°C and 145°C and, after a cessation of the decomposition, the sample resumes decomposition again between 155°C and 210°C. The relative amounts that decompose in the two channels appear to be dependent on the degree of containment of the products in the reaction cell. The amount of containment can be varied by changing the diameter of the reaction cell's orifice through which products exit to the mass spectrometer. Isothermal experiments in the low temperature channel show that the fraction of the sample that decomposes in this channel is fixed and depends on the degree of containment.

The main decomposition products formed in the lower temperature range are either CO or N₂, and CH₂O, NO, N₂O and NO₂. For low degrees of containment, in which approximately 2% to 10% of the sample decomposes in the low temperature channel, small amounts of formamide (NH₂CHO), N-methylformamide (CH₃NHCHO), N,N-dimethylformamide ((CH₃)₂NCHO) and the species, CH₂NO₃ are also observed. For the highest degree of containment, in which all of the ONDNTA decomposes in the low temperature channel, large amounts of water and dimethylnitrosamine, (CH₃)₂NNO, are also formed. The main gaseous products formed in the higher temperature range are the same as those in the low temperature range. In addition, a product of molecular formula C₂H₅N (which may be aziridine) is formed in amounts comparable to CH₂O and N₂O.

Extensive data has been collected on the thermal decomposition of ONDNTA that will allow detailed mathematical models of its decomposition to be created. To date only a qualitative summary of the decomposition processes have been published.⁸ The long illness and subsequent death of one of the authors (Dr. S. Bulusu) has limited the final analysis and publication of the work on ONDNTA. Future efforts will revisit this work and strive to incorporate the results into the overall model for the decomposition of HMX and RDX.

HMX decomposition in the solid phase. In the last six months of this project, it became apparent that significant improvements to the STMBMS instrument would enable us to conduct new experiments on the thermal decomposition of HMX that would advance our understanding beyond our previous work. The ability to confine the gaseous products better in the reaction cell reduces the rate of reactant evaporation, allowing experiments to be conducted on single HMX particles. It also allows the interactions between the gaseous decomposition products and the remaining HMX to be studied in more detail.

Recent results on the thermal decomposition of HMX and 2,4-dinitroimidazole (24DNI) has shown that there is a close coupling between the reaction mechanisms, rates of decomposition and the morphology of the decomposing particles when the decomposition takes place in the solid phase. Increasing the pressure of the confined decomposition products in the reaction cell changes the decomposition process as shown in Figure 1.

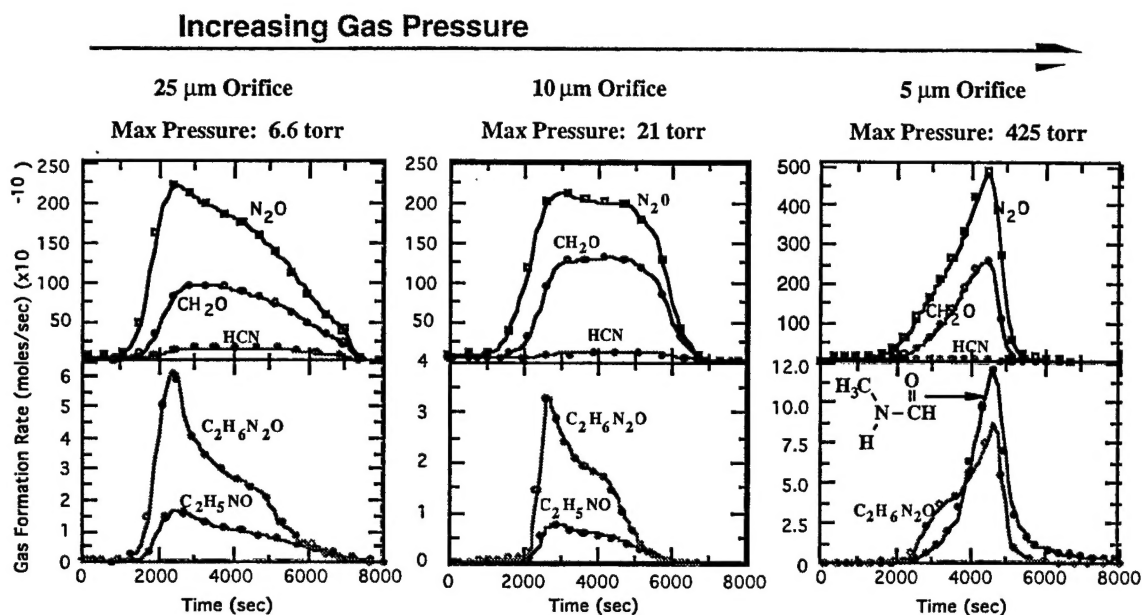


Figure 1. Gas formation rates of products formed from the thermal decomposition of HMX at 235°C from three different experiments. By using different diameter orifices in each experiment the maximum pressure of the gaseous decomposition products contained in the reaction cell was changed. The results show that as the pressure of the decomposition products in the reaction cell increase the rates of decomposition during the later stages of the reaction change from decreasing rates to increasing rates.

As the pressure of the contained decomposition products increases the rate of reaction during the later stages of the decomposition increases. For the low confinement case (25 μm orifice) the rates of decomposition decrease after the acceleratory region (1000 to 2000 seconds). In the high confinement case (5 μm orifice) the rates increase after the acceleratory period (~3500 sec).

A series of experiments using a single HMX particle in each experiment were conducted. Photomicrographs of each particle were taken before and after each decomposition experiment and scanning electron micrographs (SEM) were taken of the particle at the end of each experiment. There is a strong correlation between the morphology of the particle after the experiment and the temporal behaviors of the gas formation rates of the decomposition products.

The SEMs of the non-volatile residue remaining from a particle decomposed under lower confinement conditions are shown in Figures 2 and 3. Note the homogeneous appearance of the residue on the scale of the whole particle. The magnified SEM shows that the residue has a flake-like appearance and evidence of submicron size shells.

The SEMs of the non-volatile residue remaining from a particle decomposed under higher confinement conditions are shown in Figure 4. Note the significantly different appearance of the residue. The residue appears to be formed from layers of material that have holes within each layer.

In all of our experiments in which we observe an increase in the rate of decomposition in the final stages (5 μm behavior in Figure 1) we see a residue that looks like that shown in Figure 4. On the other hand in all of our experiments in which we observe a decreasing

rate of gas formation in the later stages (25 μ m data in Fig. 1), we see a residue that looks like that shown in Figs. 2 and 3.

These results on the thermal decomposition of HMX in the solid phase provide new information on the decomposition processes that occur within the HMX particles. The morphology of the non-volatile residue remaining at the end of the decomposition process provides insight into the reactive processes that occur within the HMX particles. Extension of this work will continue with future funding from ARO.

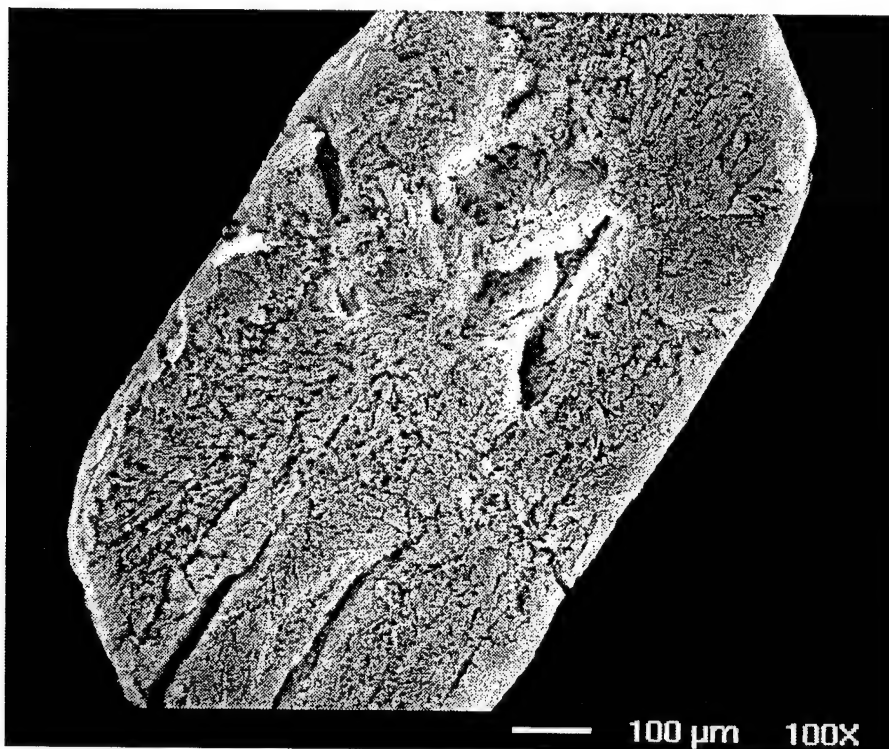


Figure 2. SEM of the residue that remains after the decomposition of HMX in the solid phase under low gas pressure conditions. The residue was formed from the decomposition of one HMX particle. The remaining residue was cut in half to expose the inside of the particle shown in the SEM.

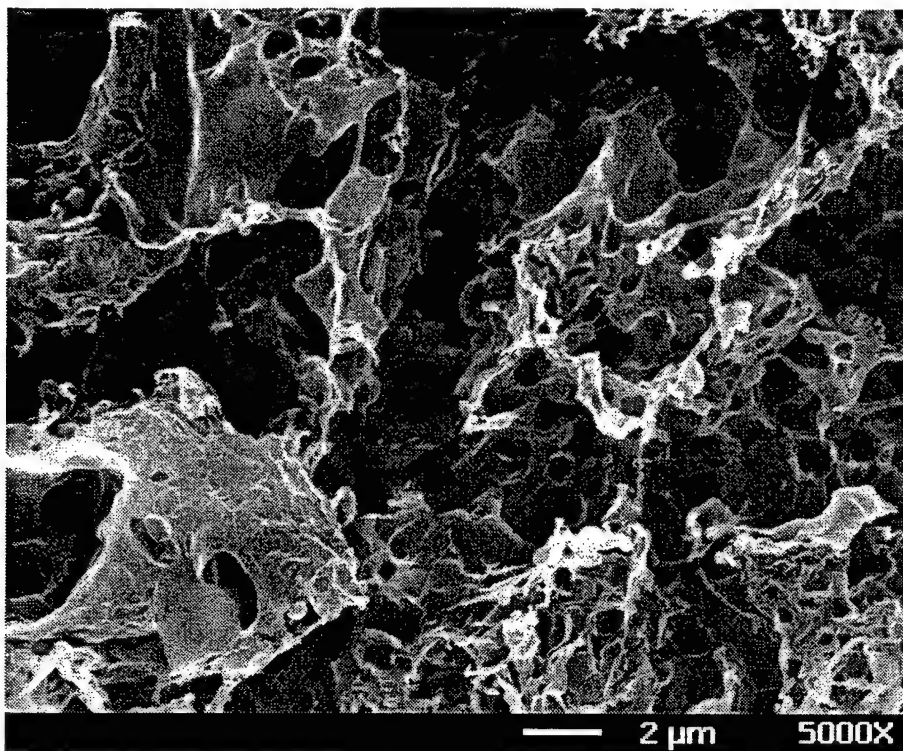


Figure 3. SEMs of residue from the decomposition of one HMX particle that was decomposed under low confinement conditions. Note flake-like appearance and submicron size shells.

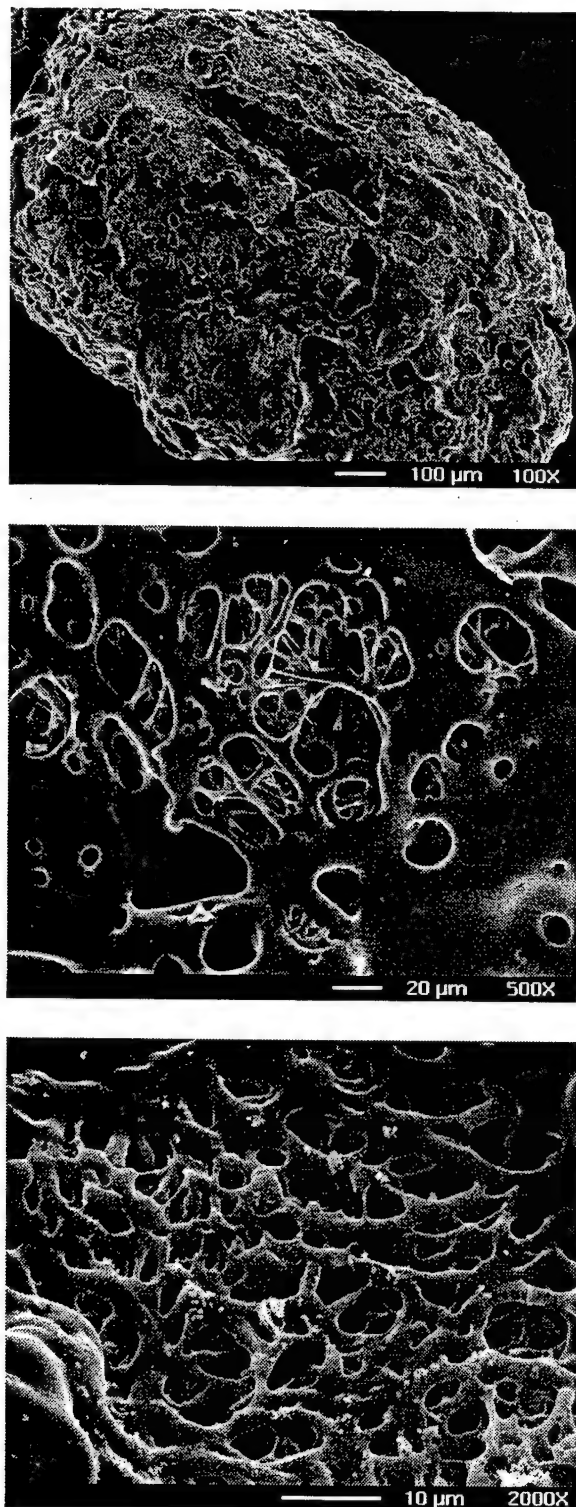


Figure 4. SEMs of residue from the decomposition of one HMX particle that was decomposed under high confinement conditions. Note rod-like appearance and appearance of layers (like layers of Swiss cheese).

Decomposition of TNAZ, NDAZ, 24DNI, ANTA and DNBT

The results of our simultaneous thermogravimetric modulated beam mass spectrometric (STMBMS) studies on TNAZ, NDAZ, 24DNI, ANTA and DNBT have provided several significant insights into the reaction mechanisms that control the decomposition of these compounds, and the role these mechanisms may play in both their combustion and their thermal and impact sensitivities. Our findings may be summarized as follows:

1. **Decomposition of nitro-substituted azoles produce a large fraction of polymeric product.** The decomposition of azoles, 24DNI, ANTA, DNBT and NTO (2,4-dihydro-5-nitro-3H-1,2,4-triazole-3-one, funded by a different source) is characterized by formation of a large fraction of solid polymeric residue and formation of a smaller fraction of gaseous products when compared to other energetic materials such as HMX, RDX or PETN. The fraction of solid residue, formed from the azoles, ranges between 20% and 66%, depending on the compound and reaction conditions.
2. **Nitro-substituted azoles absorb water.** Several of the azoles, 24DNI and NTO, have been observed to absorb water, forming a layer beneath the surface of the particle. During our thermal decomposition experiments, the reaction rates of 24DNI and NTO are increased when they evolve from this water-enriched layer. This suggests that humidity may increase decomposition rates in these materials, potentially limiting their useful life. Experiments on ANTA and DNBT have not addressed the issue of absorption of water in the particles.
3. **Polymeric residue catalyzes decomposition of 24DNI.** The rate of reaction of 24DNI is greatly affected by the presence of the polymeric residue formed during its decomposition. The physical processes controlling this autocatalytic reaction are vaporization of 24DNI, transport and deposition of 24DNI on the residue surface, and reaction of 24DNI with the residue. Reaction between 24DNI and the residue releases gaseous products and incorporates new molecular segments into the polymeric residue. The details of the chemical reaction between 24DNI and the residue is not currently understood. The decomposition behaviors of the other azoles suggest they also undergo autocatalytic reactions.
4. **Formation of isocyanate intermediate may influence sensitivity.** The molecular structure of the nitrated azoles studied in this project, along with the observed gaseous thermal decomposition products, suggest a primary mechanism leading to formation of the polymeric residue. A nitro-nitrite rearrangement, followed by loss of NO and ring scission, forms a reactive isocyanate group (-NCO). The isocyanate group may either react with water to form CO₂ or undergo polymerization reactions.
5. **Correlation of thermal decomposition mechanisms and sensitivity.** Based on our extensive thermal decomposition studies and the known impact sensitivities of the materials studied, we observe two general features of the reaction mechanism that correlate to the impact sensitivities. Insensitivity is related to the complexity of the decomposition pathways and to the fraction of nonvolatile residue versus gaseous products formed. A comparison of PETN, HMX, RDX, and the nitrated azoles (listed in order of decreasing impact sensitivity) illustrates these two principles. The complexity of the thermal decomposition process increases from PETN to the nitrated azoles. Once a PETN molecule starts to decompose, it rapidly forms mostly final gaseous

products, shows no tendency to branch to form a different set of decomposition products, and accumulates only small amounts of solid intermediate products which are volatile and decompose readily to gaseous products. On the other hand, RDX and HMX decompose along several coupled decomposition pathways, producing mainly gaseous products and a small amount of nonvolatile polymeric residue (5%). The nitrated azoles also decompose along several coupled decomposition pathways, but produce significantly less gaseous products than PETN, RDX or HMX, and produce significant amounts of nonvolatile polymeric residue. This correlation makes sense because if the reaction pathways are more complex, the rate of generation of heat and pressure within the sample will be slower. Likewise, if the heat released and the pressure of the gas generated can be reduced by forming a polymeric residue and limiting the extent of reaction, the amount of energy required to generate a runaway reaction will be greater.

6. **Mathematical model of the 24DNI decomposition process.** A complex physicochemical process controls the decomposition of 24DNI. The process is clearly dependent on features of the particle morphology and the formation of a non-volatile product that acts as an "autocatalyst". A mathematical model of the physical and chemical processes that control the thermal decomposition of 24DNI has been developed. The parameters for the model have been determined by optimizing the model to fit the data from a series of STMBMS experiments. This is the first time that such a mathematical model has been used to characterize the various physical and chemical processes that underlie the thermal decomposition of an energetic material in the solid phase.
- 7 **TNAZ decomposition mechanism and kinetics model.** TNAZ decomposes to low molecular weight decomposition products both directly and through the mononitroso analogue of TNAZ, 1-nitroso-,3,3-dinitroazetidine (NDNAZ). The reaction of TNAZ with NO to form NDNAZ is analogous to reactions observed in both RDX and HMX. Recent results from extensive sets of experiments characterizing the decomposition of TNAZ and NDNAZ have shown that TNAZ decomposes extensively between 160 °C and 230 °C, whereas, NDNAZ decomposes extensively between 110°C and 170°C. The NDNAZ is significantly less stable than TNAZ, suggesting that it may play a significant role in the TNAZ decomposition process. We are currently analyzing the results of isothermal decomposition experiments on both of these materials and are developing a model for the decomposition, which will be used to characterize the decomposition behaviors of TNAZ and NDNAZ.
8. **ANTA, DNBT and DNBT•2ANTA decomposition studies.** The unique DNBT•2ANTA complex offers an opportunity to investigate the effects of changing functionality and differing molecular environments on thermal decomposition and sensitivity of high explosives. Work at LLNL has shown that inclusion of DNBT (which is sensitive relative to ANTA), into a hydrogen-bonded complex with ANTA results in a material nearly as insensitive as ANTA itself. In our experiments, the thermal decomposition behaviors of ANTA, DNBT, and the DNBT•2ANTA complex vary significantly. Upon heating at a constant rate with no confinement of evolved gases, ANTA evaporates completely, while DNBT evaporates and decomposes rapidly near 250°C, followed by gradual decomposition and ending with a significant amount of nonvolatile residue. The DNBT•2ANTA complex, by contrast, experiences evaporation and rapid decomposition of *both* compounds near 195°C (a substantially lower temperature than either compound), followed by gradual decomposition and ending with a substantial amount of nonvolatile residue.

With moderate confinement of evolved gases, ANTA experiences evaporation and rapid decomposition near 230°C, leaving a significant amount of nonvolatile residue. An isothermal experiment at 220°C showed a similar rapid decomposition after a short induction period, again leaving significant residue. With moderate confinement at 240°C, DNBT exhibits only gradual decomposition ending with a significant amount of nonvolatile residue. The behavior of the DNBT•2ANTA complex under moderate confinement is similar to its unconfined state, except that less evaporation and more decomposition are observed. Further research will elucidate the decomposition pathways of ANTA, DNBT, and the complex, which we hope will lead to further understanding of the relationships between sensitivity, decomposition pathway complexity, gaseous versus nonvolatile products, and the different molecular environments of the pure compounds versus the complex.

A brief summary of our work in each of these areas, highlighting interesting results, is outlined in the following paragraphs. Copies of papers describing the details of the work in these areas are included in the Appendix.

Decomposition of 24DNI

Our study of the solid-phase thermal decomposition behavior of 2,4-DNI has shown that the decomposition behavior is complex, and not defined by a single dominant process that can be accurately represented with a simple analysis of the quantified results.⁹ The decomposition products consist of several different gases and a polymeric residue that accounts for ~40% of the total decomposition product weight. A first-generation model has been developed to describe the solid-phase pyrolysis of 2,4-DNI, that is based on the temporal behaviors of the gas-evolution rates of the gaseous products of decomposing 2,4-DNI under various conditions. The results of the model show that the decomposition of 2,4-DNI and evolution of gaseous products is controlled by at least six basic processes as illustrated in Figure 5. These processes include: 1) sublimation and decomposition in the gas phase (small contribution), 2) decomposition in a reactive shell on the surface of the particles, 3) enhancement of the reaction rates and reduction of the 2,4-DNI sticking coefficient due to absorbed exogenous water and impurities in the 2,4-DNI sample, 4) the growth of polymeric reactive nuclei in the reactive shell, 5) adsorption of 2,4-DNI on the surface of the reactive nuclei, followed by reaction of the 2,4-DNI on the surface to release gaseous products and add to the polymer, and 6) transformation of the polymer formed by the initial reaction with 2,4-DNI to a more thermally stable polymer, releasing gas in the process. The combination of processes four through six characterizes the autocatalytic nature of the 2,4-DNI decomposition. Global reaction chemistry has been used to characterize each of the basic decomposition processes in the first generation of the model. At the model's present state of development, global chemistry is used to represent the various chemical reactions that occur during each of the processes just described. Differences between the rates of gas formation predicted by the model and the measured data will be used to generate a second-generation model of the 2,4-DNI decomposition processes that include more details on the individual chemical reactions involved in each process.

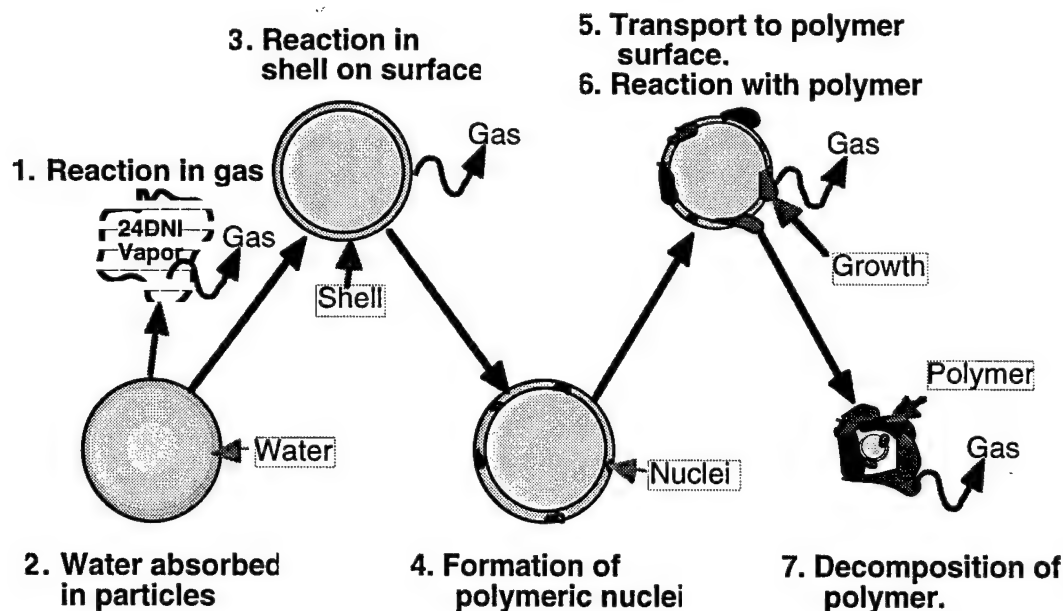


Figure 5. Schematic representation of 2,4-DNI decomposition processes in the solid phase.

Decomposition of TNAZ and NDNaz

The decomposition of TNAZ and NDNaz has been extensively studied.^{10,11} A paper summarizing the most recent results is included in the Appendix.¹² The major products formed in the decomposition of TNAZ are NO_2 and NO , with lesser amounts of H_2O , HCN , CO/N_2 , $\text{CO}_2/\text{N}_2\text{O}$, NDNaz, and a small amount of polymeric residue. The results indicate four likely steps for the first step in the TNAZ decomposition. Three of these generate NO_2 , either by unimolecular cleavage of a nitramine or nitroalkane, or by displacement of the nitramine NO_2 by NO , while the fourth involves a nitro-nitrite rearrangement of the gem-dinitro group (elimination of HNO_2 occurs, but is relatively small). The unimolecular fragmentation pathways are supported because NO_2 generation is initially first order in TNAZ concentration in both liquid and gas phases (additional sources of NO_2 must exist because its signal does not decrease as TNAZ nears depletion). Experiments using $1\text{-}^{15}\text{NO}_2\text{-TNAZ}$ show NO_2 evolution from both sites in the molecule, though occurring first at the weaker nitramine bond; and also indicate, by lack of isotopic shifts, that signals at m/z 28 and 44 are mostly CO and CO_2 rather than N_2 and N_2O . The observation that the rates of formation of NO_2 , NO , and NDNaz increase sequentially indicates NDNaz is formed by direct replacement of the nitramine NO_2 in TNAZ by NO . This and the nitro-nitrite pathway are also suggested because CO_2 , NO , CO/N_2 , HCN , CH_3CN , and NDNaz do not correlate with the first-order NO_2 cleavage. Evolution of $\text{CO}_2/\text{N}_2\text{O}$, NO , HCN , and CO/N_2 after TNAZ depletion indicates they are thermal decomposition products of NDNaz.

The decomposition of independently synthesized NDNaz provides further clues to the overall decomposition process. The major product in the decomposition of NDNaz is NO , followed by lesser amounts of H_2O , HCN , CO/N_2 , $\text{CO}_2/\text{N}_2\text{O}$, and a significant amount of polymeric residue, which actually catalyzes NDNaz decomposition. While

these products are similar to those formed in the TNAZ decomposition, their ratios differ significantly. There are two likely first steps for the decomposition of NDN AZ, either cleavage of the N-nitroso group to form NO and 3,3-dinitroaziridiny l radical, or nitro-nitrite rearrangement of the gem-dinitro group. Because more than one equivalent of NO is evolved, a nitro-nitrite rearrangement as in the second path almost certainly occurs.

The results of our experiments confirm loss of NO₂ as one of the first steps in TNAZ decomposition, as discovered in RSFTIR and IRMPD experiments by other groups, and furthermore, show that the NO₂ arises from both possible sites. Contrary to the RSFTIR experiments, however, HNO₂ elimination is relatively unimportant. We find once again that a mononitroso analog (NDNAZ) is an important intermediate in nitramine decomposition, as we have shown previously for RDX, TNCHP, and HMX.

Several significant improvements have been made to our experimental protocol, allowing the effective use and characterization of 2.5 μ m diameter orifices, despite their inherent difficulties. With these improvements, quantification of our data is more reliable. Coupled with kinetic, mechanistic, and physical information on these decompositions, this will provide the foundation to develop a detailed mathematical model of the decomposition processes of TNAZ and NDN AZ.

Decomposition of ANTA, DNBT and the DNBT•2ANTA complex

We have completed preliminary experiments on ANTA, DNBT, and the DNBT•2ANTA complex at two levels of containment and various temperatures to examine their decomposition behavior. This preview reveals the chemistry of this novel system to be complex and intriguing.

Heating ANTA alone with a large (~500 μ m) orifice resulted in evaporation, with virtually no evidence of decomposition and no solid residue (Figure 6A). Heating ANTA with a small (~25 μ m) orifice at 2°C/min revealed a rapid decomposition event at about 230°C, which resulted in the loss of ~43% of the sample weight, followed by a more gradual period where ~20% of the sample weight was lost, leaving about 37% of the sample weight as nonvolatile residue. Heating ANTA with a small orifice at an isotherm of 220°C resulted in rapid weight loss (44% of initial weight) after short induction period, followed by a more gradual weight loss (11% of initial weight), leaving a significant amount of nonvolatile residue (45% of initial weight, Figure 6B). With the 25 μ m orifice, decomposition was dominant; probably less than 10% of the sample escaped as ANTA. The dominant product m/z values in the rapid decomposition period, their probable identities, and approximate order of importance are: 18 (H₂O), 44 (N₂O, CO₂), 28 (N₂, CO), 27 (HCN), 43, 30 (NO, CH₂O), 45, and 17 (NH₃). Approximately 75% of the signal at m/z 30 is due to NO, with the rest due to CH₂O.

The behavior of DNBT is significantly different. Heating DNBT alone with a large (~500 μ m) orifice at 1°C/min revealed a rapid weight loss at about 250°C which corresponded to ~50% of the original sample weight (Figure 7A). Comparison of the ion signals in this period to the parent mass at m/z 226 indicates that this weight loss is mostly evaporation up until the maximum rate of weight loss, where signals due to decomposition become significant. This period is followed by a gradual weight loss (16% of initial weight), leaving a significant amount of nonvolatile residue (34% of initial weight). The dominant product m/z values in the rapid decomposition period, their probable identities, and approximate order of importance are: 30 (NO, CH₂O), 44 (N₂O, CO₂), 28 (N₂, CO), 18 (H₂O), 43, 27 (HCN), 68, 46 (NO₂), 29 (CHO), 42, and 45. The proportion of NO to CH₂O for m/z 30 in this period has not been determined. The dominant product m/z values

in the gradual decomposition period, their probable identities, and approximate order of importance are: 30 (NO, CH₂O), 18 (H₂O), 46 (NO₂), 44 (N₂O, CO₂), 28 (N₂, CO), 29 (CHO), 42, 27 (HCN), 43, 68, and 45. Approximately 75% of the signal at m/z 30 in this phase is due to NO, with the rest due to CH₂O. Since this decomposition occurs while using a large orifice, the evolving gases are not contained for a significant period of time and therefore the decomposition must occur in the condensed phases. Heating DNBT with a small (25 μ m) orifice at 240°C (Figure 7B) resulted in a gradual weight loss due to decomposition (34% of initial weight), leaving a significant amount of nonvolatile residue (66% of initial weight). The dominant product m/z values in this gradual decomposition period, their probable identities, and approximate order of importance are: 30 (NO, CH₂O), 18 (H₂O), 44 (N₂O, CO₂), 46 (NO₂), 28 (N₂, CO), 43, 111, 29 (CHO), and 45. At least 85% of the signal at m/z 30 is due to NO.

The behavior of the DNBT•2ANTA complex is significantly different from either compound alone. Heating DNBT•2ANTA using a large (~500 μ m) orifice at 1°C/min (Fig. 8A) revealed a rapid weight loss at about 195°C which corresponded to ~44% of the original sample weight, followed by a gradual weight loss (26% of initial weight), leaving a significant amount of nonvolatile residue (28% of initial weight). Comparison of the ion signals in the rapid weight loss period to parent masses 129 (ANTA) and 226 (DNBT) indicates that this weight loss is due to evaporation of both ANTA and DNBT and decomposition of one or both. Considering that this initial weight loss corresponds to only 44% of the initial sample weight, that significant evaporation occurs for both compounds in

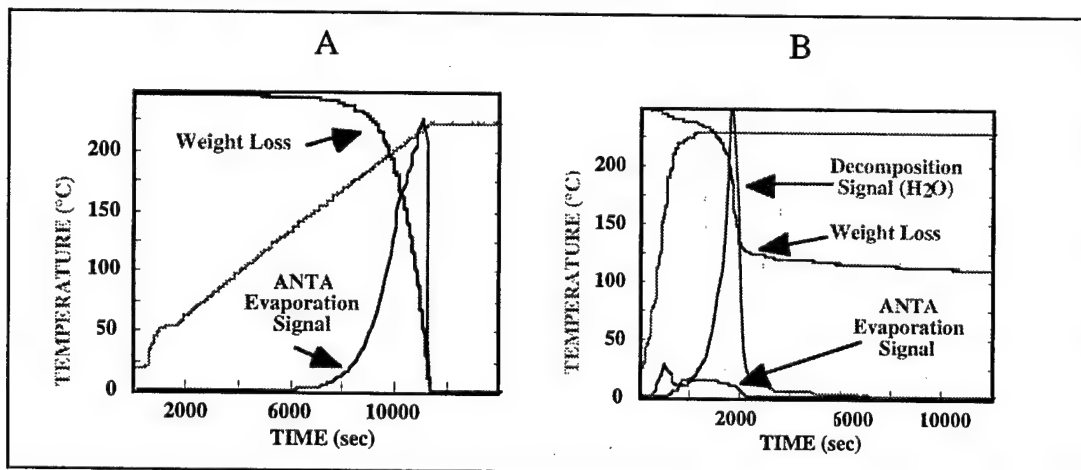


Figure 6. (A) Heating ANTA with a 500 μ m orifice results in complete evaporation. (B) Heating ANTA at 220°C with a 25 μ m orifice results in substantial decomposition and leaves ~45 % of the initial weight as nonvolatile residue. Note the initial rise in the water signal and the corresponding drop in weight; this likely represents loss of adsorbed water. (The weight loss curve is normalized so the Y-scale is 100 % of the initial weight. The evaporation and decomposition signals are on the same scale in arbitrary units).

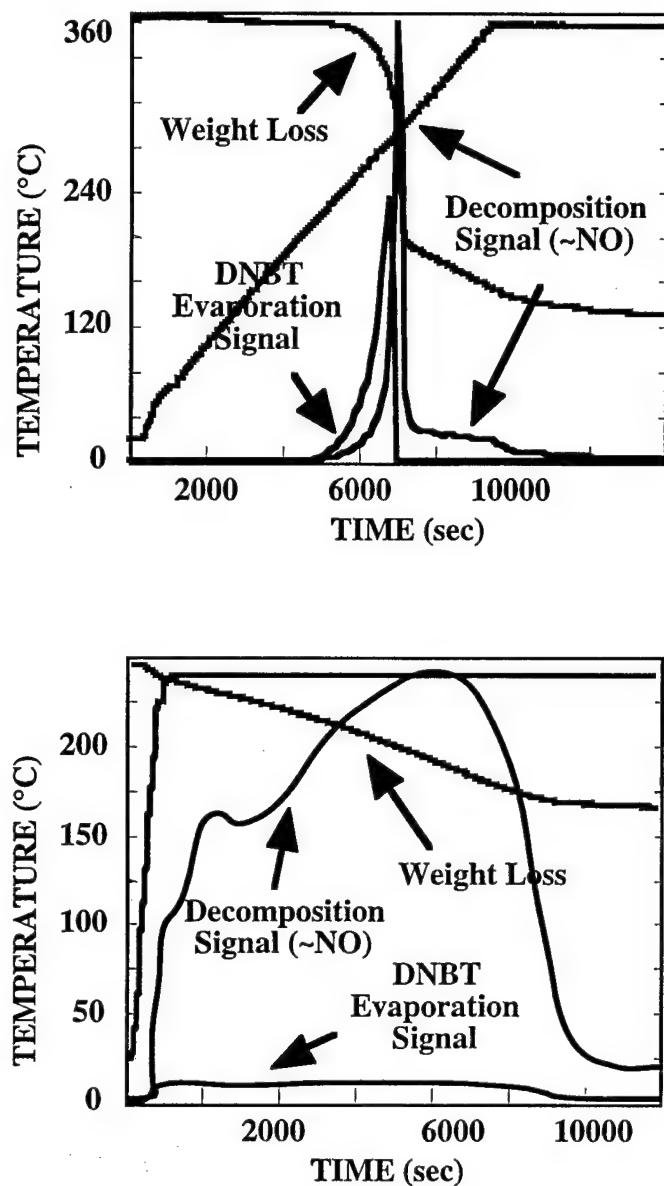


Figure 7. (Top) Heating DNBТ with a $\sim 500\ \mu\text{m}$ orifice results in rapid weight loss due to evaporation of DNBТ and decomposition, represented by $m/z\ 30$ (mostly NO). About 34% of initial weight is left as nonvolatile residue. (Bottom) Heating DNBТ at 240°C with a $25\ \mu\text{m}$ orifice results in gradual decomposition and leaves $\sim 66\%$ of the initial weight as nonvolatile residue. (The weight loss curve is normalized so the Y-scale is 100 % of the initial weight. The evaporation and decomposition signals are on the same scale in arbitrary units).

this period, and the amount of nonvolatile residue generated, it is evident that both compounds undergo decomposition and evaporation at 195°C, a dramatically lower temperature than either compound in the pure state. Furthermore, in the complex, ANTA as well as DNBT decompose when unconfined, and therefore must be decomposing in the condensed phase. Because ANTA is 53% of the complex by weight, and its signal ends at 44% weight loss, at least 17% of the ANTA decomposes. A second experiment with the same orifice size but at a constant temperature of 185°C lost 45% of its initial weight in the first period, 35% in the gradual period, and left 20% as nonvolatile residue. Therefore, decomposition at higher temperatures produces more nonvolatile residue and less gaseous products. The dominant product m/z values in the gradual decomposition period, their probable identities, and approximate order of importance are: 44 ($\text{N}_2\text{O}, \text{CO}_2$), 30 ($\text{NO}, \text{CH}_2\text{O}$), 28 (N_2, CO), 18 (H_2O), 43, 27 (HCN), 42, and 29 (CHO). Most of the signal at m/z 30 is due to NO , with the rest due to CH_2O .

Heating the DNBT•2ANTA complex with a small (25 μm) orifice at an isotherm of 190°C (Fig. 8B) resulted in an initial rapid weight loss (40% of initial weight) due mostly to decomposition, followed by a gradual weight loss period (6%) and leaving a significant amount of nonvolatile residue (54% of initial weight). The dominant product m/z values in the rapid decomposition period, their probable identities, and approximate order of importance are: 18 (H_2O), 28 (N_2, CO), 44 ($\text{N}_2\text{O}, \text{CO}_2$), 27 (HCN), 43, 30 ($\text{NO}, \text{CH}_2\text{O}$), 46 (NO_2), 45, 29 (CHO), and 42. Approximately 75% of the signal at m/z 30 is due to NO , with the rest due to CH_2O . The dominant product m/z values in the gradual decomposition period and their probable identities in approximate order of importance are: 18 (H_2O), 44 ($\text{N}_2\text{O}, \text{CO}_2$), 28 (N_2, CO), 30 ($\text{NO}, \text{CH}_2\text{O}$), 43, 27 (HCN), 46 (NO_2), 45, 42 and 29 (CHO). At least 90% of the signal at m/z 30 is due to NO , with the rest due to CH_2O .

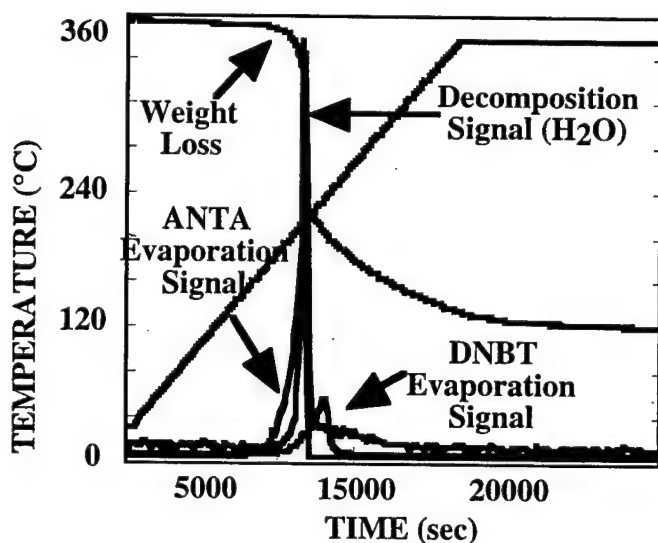


Figure 8A. Heating DNBT•2ANTA with a ~500 μm orifice results in rapid weight loss due to evaporation and decomposition of both components. About 28% of initial weight is left as nonvolatile residue. (The weight loss curve is normalized so the Y-scale is 100 % of the initial weight. The evaporation and decomposition signals are on the same scale in arbitrary units).

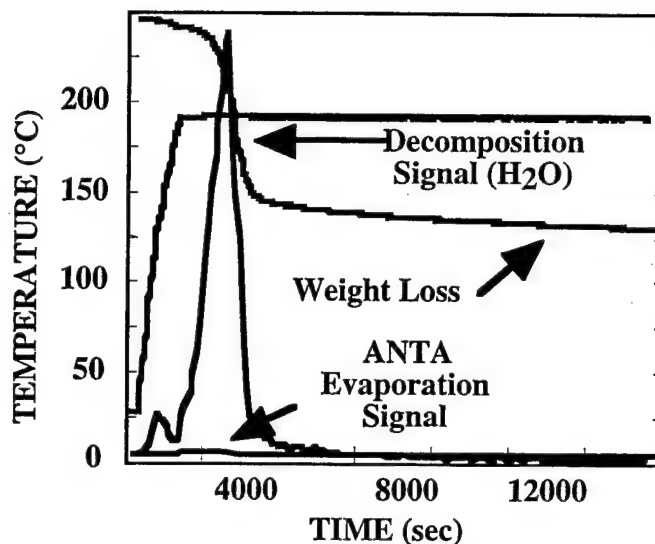


Figure 8B. Heating DNBt·2ANTA at 190°C with a 25 μ m orifice results in rapid decomposition but very little evaporation (no DNBt is observed) and leaves ~54 % of the initial weight as nonvolatile residue. (The weight loss curve is normalized so the Y-scale is 100 % of the initial weight. The evaporation and decomposition signals are on the same scale in arbitrary units).

Publications and Technical Reports

- R. Behrens and S. Bulusu, "Thermal Decomposition Studies of 1,3,3-Trinitroazetidine (TNAZ) and 1-nitroso-3,3-dinitroazetidine (NDNAZ) by Simultaneous Thermogravimetric Modulated Beam Mass Spectroscopy", Proceedings of the 32 JANNAF Combustion Meeting, Huntsville, Alabama, October, Vol. 638, pp. 1 – 11, 1995
- Behrens, R. and S. Bulusu, "Thermal Decomposition of HMX: Low Temperature Reaction Kinetics and their Use for Assessing Response in Abnormal Thermal Environments and Implications for Long-Term Aging. Decomposition, Combustion and Detonation Chemistry of Energetic Materials", ed. T.B. Brill, et al. Vol. 418. 1996, Material Research Society: Boston, MA. 119 - 126.
- L. Minier, R. Behrens, and S. Bulusu, "Solid-phase Thermal Decomposition of 2,4-Dinitroimidazole (2,4-DNI)", Material Research Society Symposium Proceedings, Vol. 418, pp. 111 – 117, 1996.
- S. Bulusu and R. Behrens, Jr., "A Review of the Thermal Decomposition Pathways in RDX, HMX and Other Closely Related Cyclic Nitramines", Defence Science Journal, Vol. 46, pp. 346-360, 1996.

R. Behrens, Jr. and S. Bulusu, "Thermal Decomposition Studies of a New, gem-Dinitroalkyl Nitramine 1,3,3-Trinitroazetidine (TNAZ)", *Defence Science Journal*, Vol. 46, pp. 361- 396, 1996.

Behrens, R. and S. Bulusu, The Importance of Mononitroso Analogues of Cyclic Nitramines to the Assessment and the Safety of HMX-Based Propellants and Explosives, in *Challenges in Propellants and Combustion 100 Years after Nobel*, K.K. Kuo, Editor. 1997, Begell House, Inc.: New York. p. 275 - 289.

Behrens, R., L. Minier, and S. Bulusu. "Coupling Experimental Data and a Prototype Model to Probe the Physical and Chemical Processes of 2,4-Dinitroimidazole Solid-Phase Thermal Decomposition." in *JANNAF Combustion Sciences Subcommittee Meeting*. 1997. West Palm Beach, FL: Chemical Propulsion Information Agency, . CPIA Pub. 662, pp. 549 - 567, 1997.

Anderson, K., et al. Mechanistic and Kinetic Studies of the Thermal Decomposition of TNAZ and NDNAZ. in *JANNAF*. 1997. West Palm Beach, FL: Chemical Propulsion Information Agency, CPIA Pub. 662, pp. 569 - 576, 1997.

Scientific Personnel

Richard Behrens, Ph.D.
Leanna Minier, Ph.D.
Kraig Anderson, Ph.D.
Jason Homsy, summer student intern
Sabrina Mack, student intern
Jeanette Wood, student intern
Timothy Buckley, summer student intern

Inventions: none

Bibliography

¹R. Behrens, "Thermal Decomposition of Energetic Materials: Temporal Behaviors of the Rates of Formation of Gaseous Pyrolysis Products from Condensed-Phase Decomposition of Octahydro-1,3,5,7-tetranitro-1,3,5,7-tetrazocine," *Journal of Physical Chemistry* **94**, 6706 (1990).

²Richard Behrens, Jr. and Suryanarayana Bulusu, "Thermal Decomposition of Energetic Materials. 2. Deuterium Isotope Effects and Isotopic Scrambling in Condensed-Phase Decomposition of Octahydro-1,3,5,7-tetranitro-1,3,5,7-tetrazocine," *Journal of Physical Chemistry* **95**, 5838-5845 (1991).

³Richard Behrens and Suryanarayana Bulusu, "Thermal Decomposition of HMX: Low Temperature Reaction Kinetics and their Use for Assessing Response in Abnormal Thermal Environments and Implications for Long-Term Aging," in *Decomposition, Combustion and Detonation Chemistry of Energetic Materials*, edited by T.B. Brill, T.P. Russel, W.C. Tao *et al.* (Material Research Society, Boston, MA, 1996), Vol. 418, pp. 119 - 126.

- ⁴Richard Behrens, Jr. and Suryanarayana Bulusu, "Thermal Decomposition of Energetic Materials 3. Temporal Behaviors of The Rates of Formation of the Gaseous Pyrolysis Products from Condensed-Phase Decomposition of 1,3,5-Trinitrohexahydro-s-triazine," *Journal of Physical Chemistry* **96** (22), 8877 - 8891 (1992).
- ⁵Richard Behrens, Jr. and Suryanarayana Bulusu, "Thermal Decomposition of Energetic Materials. 4. Deuterium Isotope Effects and Isotopic Scrambling (H/D, $^{13}\text{C}/^{18}\text{O}$, $^{14}\text{N}/^{15}\text{N}$) in Condensed-Phase Decomposition of 1,3,5-Trinitrohexahydro-s-triazine," *Journal of Physical Chemistry* **96** (22), 8891-8897 (1992).
- ⁶Richard Behrens, Jr., "Thermal Decomposition of Energetic Materials: Temporal Behaviors of the Rates of Formation of Gaseous Pyrolysis Products from Condensed-Phase Decomposition of Octahydro-1,3,5,7-tetranitro-1,3,5,7-tetrazocine," *Journal of Physical Chemistry* **94**, 6706-6718 (1990).
- ⁷Richard Behrens, Jr., Terry A. Land, and Suryanarayana Bulusu, Report No. CPIA-PUB-606-VOL-II, 1993.
- ⁸R. Behrens and S. Bulusu, "The Importance of Mononitroso Analogues of Cyclic Nitramines to the Assessment and the Safety of HMX-Based Propellants and Explosives," in *Challenges in Propellants and Combustion 100 Years after Nobel*, edited by Kenneth K. Kuo (Begell House, Inc., New York, 1997), pp. 275 - 289.
- ⁹Richard Behrens, Leanna Minier, and Suryanarayana Bulusu, Report No. CPIA Pub. 662, 1997.
- ¹⁰R. Behrens and S. Bulusu, Report No. CPIA Pub. 638, 1995.
- ¹¹R. Behrens and S. Bulusu, "Thermal Decomposition Studies of a New, gem-Dinitroalkyl Nitramine 1,3,3-Trinitroazetidine (TNAZ)," *Defence Science Journal (India)* **46** (5), 361 - 369 (1996).
- ¹²Kraig Anderson, Jason Homsy, Richard Behrens *et al.*, Report No. CPIA Pub. 662, 1997.

Appendix

Coupling Experimental Data and a Prototype Model to Probe the Physical and Chemical Processes of 2,4-Dinitroimidazole Solid-Phase Thermal Decomposition

Richard Behrens and Leanna Minier
Combustion Research Facility
Sandia National Laboratories
Livermore, CA 94551

Suryanarayana Bulusu[†]
Energetic Materials Division
U.S. Army Armament Research, Development and Engineering Center
Dover, NJ 07801-5001

ABSTRACT

The time-dependent, solid-phase thermal decomposition behavior of 2,4-dinitroimidazole (2,4-DNI) has been measured utilizing simultaneous thermogravimetric modulated beam mass spectrometry (STMBMS) methods. The decomposition products consist of gaseous and non-volatile polymeric products. The temporal behavior of the gas formation rates of the identified products indicate that the overall thermal decomposition process is complex. In isothermal experiments with 2,4-DNI in the solid phase, four distinguishing features are observed: 1) elevated rates of gas formation are observed during the early stages of the decomposition, which appear to be correlated to the presence of exogenous water in the sample; 2) this is followed by a period of relatively constant rates of gas formation; 3) next, the rates of gas formation accelerate, characteristic of an autocatalytic reaction; 4) finally, the 2,4-DNI is depleted and gaseous decomposition products continue to evolve at a decreasing rate.

A physicochemical and mathematical model of the decomposition of 2,4-DNI has been developed and applied to the experimental results. The first generation of this model is described in this paper. In this model, decomposition of 2,4-DNI and evolution of gaseous products is controlled by at least six basic processes. These processes include: 1) sublimation and decomposition in the gas phase (small contribution), 2) decomposition in a reactive shell on the surface of the particles, 3) enhancement of the reaction rates and reduction of the 2,4-DNI sticking coefficient due to absorbed exogenous water and impurities in the 2,4-DNI sample, 4) the growth of polymeric reactive nuclei in the reactive shell, 5) adsorption of 2,4-DNI on the surface of the reactive nuclei, followed by reaction of the 2,4-DNI on the surface to release gaseous products and add to the polymer, and 6) transformation of the polymer formed by the initial reaction with 2,4-DNI to a more thermally stable polymer, releasing gas in the process. The combination of processes four through six characterize the autocatalytic nature of the 2,4-DNI decomposition. Global reaction chemistry is currently used to characterize each of the basic decomposition processes. The development of the model is presented along with examples of the model applied to experiments conducted under a range of different conditions. Differences between the first generation of the model and the experimental data collected under different conditions suggest refinements for the next generation of the model.

INTRODUCTION

There is an ongoing desire in the propulsion community to develop the capability to predict the response of propulsion systems in abnormal environments, which may be encountered during their deployment, transport or storage. Exposure to elevated temperatures is one of the higher probability abnormal events. This type of situation may arise due to inadvertent exposure to fire or the storage at unusually high temperatures. To characterize the response of propulsion systems to situations in which elevated temperatures are present requires the ability to predict the time to ignition, caused by the elevated temperature, and the violence of the ensuing event, as determined by the likelihood to transition from a steady-state deflagration to an explosion or detonation.

* Approved for public release; distribution is unlimited.

† Work supported by the Army Research Office, a Memorandum of Understanding between the U.S. Department of Energy and the Office of Munitions and by the U.S. Department of Energy under contract DE-AC04-94AL85000.

† Deceased.

Empirical models of laboratory scale experiments have been successfully used in 3-dimensional codes to predict both the location and time to ignition. However, a lack of understanding of the processes that control the combustion in a bed of thermally degraded propellant has prevented meaningful predictions of the degree of violence. To overcome this limitation requires developing a better understanding of the combustion processes in thermally degraded propellants. This requires major advances in two areas. First, the morphological and chemical changes in the propellant must be understood as a function of the extent of thermal degradation. Second, the combustive behavior of thermally degraded propellants must be understood. This implies that conductive and convective burning in porous propellants with substantially higher surface areas must be understood.

Our work addresses the first issue. As propellants are slowly heated, the rising temperature leads to changes in the morphology of the propellant, as the various ingredients undergo phase changes. Accompanying these changes in morphology are chemical changes caused by the thermal decomposition processes in the various ingredients. The accumulative effect of morphological and chemical changes in the propellant will determine the state of the propellant at any given time. The challenge is to understand the mechanisms that lead to both the morphological and chemical changes, and to quantitatively predict the extent of these changes as a function of time and temperature. This is a difficult problem, but one that may now be addressed with new experimental and computational capabilities.

This paper addresses one specific aspect of the problem, the thermal decomposition processes of energetic ingredients used in propellants. More specifically, this paper addresses the issues associated with both morphological and chemical changes that occur in energetic materials as they are heated slowly, below their ignition point. In this regime, reactions in the condensed phase (solid phase of the reactant or solid/solution phase of reactant and decomposition products) dominate the thermal decomposition processes. Typical thermal analysis techniques such as differential scanning calorimetry (DSC), thermogravimetric analysis (TGA), or one-dimensional time to explosion (ODTX) methods give information on heat generation, mass loss, and time to ignition, respectively. While this information is useful for determining the temperature range in which significant events occur in the materials, and possibly determining the temperature dependence of the overall process, they do not provide information on the physical and chemical processes that underlie the overall process. Thus, one is not able to extract information from this data that will allow one to predict the state of the material as a function of time and temperature.

In our work over the last twelve years, we have conducted experiments on various energetic materials with the goal of understanding the physicochemical processes that control their decomposition behavior. One universal conclusion of this work is that there is always more than one process that contributes to control the rate of decomposition, and that these processes are almost always coupled with each other. This implies that the application of a unimolecular decomposition model, in which the weakest bond in the molecule determines the rate of decomposition, provides an inadequate framework with which to characterize the decomposition processes. We have also found that profound changes in the morphological features of the material often accompany the chemical changes.

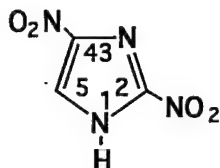
In our past work on the decomposition of energetic materials, we have uncovered many of the underlying processes that control their rates of decomposition. We have published work on the decomposition of cyclic nitramines, (HMX,¹⁻³ RDX,³⁻⁵ the mononitroso analogue of RDX,⁶ TNAZ,⁷ TNCHP and K6⁸), several azoles (14DNI,⁹ 24DNI,¹⁰ and NTO¹¹), and ammonium perchlorate (AP) and AP-based propellants.¹² In addition to providing new insight into the underlying decomposition processes, we have obtained extensive quantitative data on the rates of formation of the gaseous products formed during the decomposition processes. We continue with new experiments to add to our knowledge of these materials.

Currently, we are extending our methods to new levels, by developing procedures to create mathematical models of the physicochemical processes that occur during the thermal decomposition of energetic materials from the data measured in our experiments. The ultimate goal of this effort is to create mathematical models of the decomposition processes that can account for the following types of changes in an energetic material as it decomposes:

1. Identities and rates of formation of the gaseous and condensed-phase products.
2. Changes in particle morphology and surface area of particles in propellant.
3. Changes in porosity, hardness, strength of the propellant.

4. Energy content of remaining material
-- in reactant
-- in gaseous decomposition products.

This paper illustrates our efforts to develop procedures for creating mathematical models of the physicochemical processes that occur during the slow decomposition of energetic materials. Our desire is to create models of the thermal decomposition of HMX, RDX and AP-based composite propellants, but we begin here with development of a model for 2,4-DNI, which we believe is an easier starting point (although not that easy as we believe the reader will recognize by the conclusion of the paper).



I 2,4-DNI

The 2,4-dinitroimidazole (2,4-DNI; I), is a C-nitro heterocycle compound, that has been shown ¹³ to be a low cost, thermally stable, and impact insensitive energetic material. Under shock loading, it has been shown to be less shock sensitive than other conventional bonded explosives, with the exception of TATB-based materials.¹⁴ It also significantly outperforms TNT. Several features of the 2,4-DNI decomposition make it attractive to model. We have thoroughly studied its thermal decomposition utilizing STMBMS methods. The data show that 2,4-DNI has several interesting decomposition features. These include: competition between formation of polymeric and gaseous products, creation of new reaction pathways through nucleation processes, and the creation of a decomposition product that acts as an autocatalyst. Similar processes occur in other energetic compounds we are studying. Therefore, the model for 2,4-DNI thermal decomposition can be modified, expanded and applied to other compounds with similar behaviors.

EXPERIMENTAL

INSTRUMENTATION AND METHODS

The design and operation of the STMBMS apparatus and the basic data analysis procedures have been described previously.¹⁵⁻¹⁷ The data from this instrument provides the identities and temporal dependence of the gas formation rates of the thermal decomposition products formed as a sample decomposes. The exhaust rate of gases from the reaction cell is controlled by changing the diameter of the orifice in the reaction cell, which allows gases to escape from the cell into a vacuum. This feature is used for altering the reaction conditions in two ways. First, as the diameter of the orifice is decreased, the pressure of the gaseous decomposition products in the cell increases. For compounds in which reactions between the gaseous decomposition products and the reactant occur, this allows the contribution of this pathway to be identified and separated from other competing pathways. Second, as the diameter of the orifice is increased, the fraction of the sample that sublims, without reacting, increases. For studying reactions in the solid phase this allows one to vary the fraction of nearest neighbors in the sample that decompose. Thus, it is possible to sort out reactions in the solid phase that depend on interactions with nearest neighbors from those that do not. The use of these features will be illustrated with the results on 2,4-DNI and the accompanying model of its decomposition.

Several changes in the experimental methods have been made since earlier publications. First, the cap in the reaction cell is now sealed using vacuum grease and a viton o-ring between the taper plug and the gold foil pinhole orifice. The results from decomposition experiments presented in this paper utilize a gold foil with a 25 μ m- and 50 μ m-diameter orifices. Second, the data presented in this paper for the rate of generation of gaseous products is the rate of their exhaust from the reaction cell, as compared to the rate of their formation within the cell as was presented in our previous papers. This change allows direct comparison between the experimental results and the model.

MATERIALS

Unlabeled 2,4-DNI (98 \pm 1% purity) samples were obtained from Dr. Phil Pagoria at LLNL and used as received. The major impurities in the 2,4-DNI samples are water and the synthetic starting material, 4-nitroimidazole (4-NI).

RESULTS AND DISCUSSION

CHARACTERISTICS OF SOLID-PHASE THERMAL DECOMPOSITION

Our experiments show that neat 2,4-DNI undergoes substantial thermal decomposition in the solid phase between 200°C and 255°C. The identities of the pyrolysis products in the temperature range studied, have been reported previously.¹⁸ Between 200°C and 255°C, 2,4-DNI undergoes simultaneous sublimation and decomposition. The major products consist of low-molecular weight gases (NO, CO₂, H₂O, HNCO, CO, N₂ and HCN), and a non-volatile, polymeric residue. The temporal behaviors of the product gas formation rates (GFRs) are similar for the entire temperature range studied. The results from a typical experiment are represented by the GFR data of the major gaseous products formed at 235°C, shown in Figure 1. There are several interesting features of the temporal behaviors of the GFRs of the various products.

1. As the sample approaches its isothermal temperature, water appears early and is correlated with an increase in the vaporization rate of 2,4-DNI and an increase in the GFRs of the decomposition products.
2. After these initial GFRs decrease, there is a period of relatively constant GFRs for all major products.
3. Following the period of relatively constant GFRs, there is an accelerating rate of increase in the GFRs, typical of an autocatalytic process. The rate of increase continues to accelerate until the 2,4-DNI is depleted at approximately 38000 seconds.
4. Decomposition products continue to evolve after the 2,4-DNI is depleted. At the completion of the experiment, approximately 40% of the 2,4-DNI that has decomposed (not sublimed) remains as a nonvolatile polymeric residue.

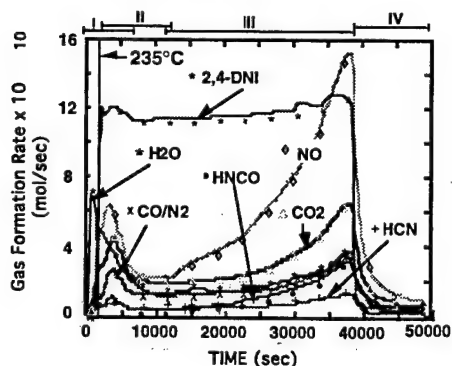


Figure 1. Gas formation rates of products from the isothermal decomposition of 10.3 mg of 2,4-DNI at 235°C in a 0.193 cc reaction cell with a 25 μ -diameter exit orifice. Isothermal 235°C is obtained at ~2300 seconds, and maintained throughout the remainder of the experiment.

The processes involved in each stage of the decomposition are better clarified by a series of three experiments, each designed to highlight the various stages of the decomposition. In the first experiment, 2,4-DNI (~10mg) is heated and maintained at 200°C for four hours. This experiment is designed to eliminate adsorbed H₂O and contaminants that may be contributing to the early decomposition stage. In the second experiment, the contents remaining in the reaction cell from the first experiment are thermally decomposed at 235°C to completion (2,4-DNI is no longer present). The second experiment is designed to observe if the early decomposition is eliminated by the previous experiment, and to observe the decomposition of neat 2,4-DNI. In the third experiment, the residue formed in the second experiment is cooled to room temperature, mixed with additional 2,4-DNI (~10mg), and decomposed to completion at 235°C. The third experiment is designed to observe if the residue is acting as an autocatalyst in the decomposition reaction. The resulting product GFRs of the three experiments are shown in Figures 2a-c.

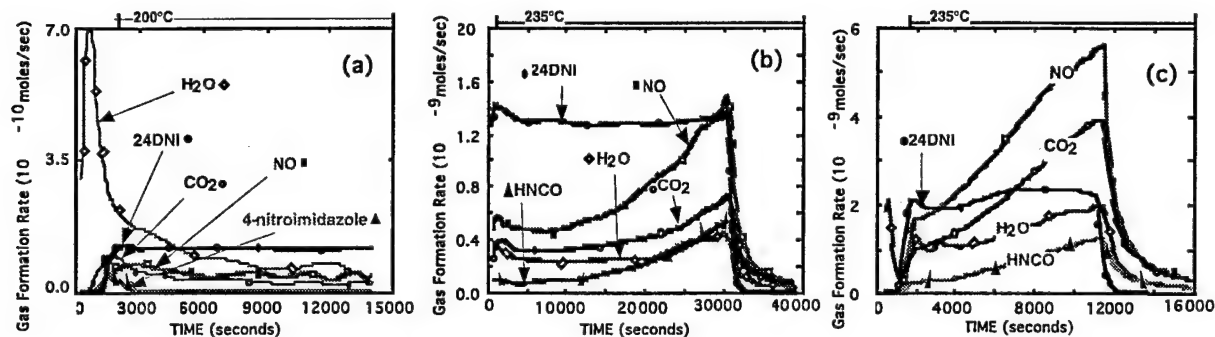


Figure 2. Gas formation rates of the products from three experiments; (a) decomposition of ~10 mg of 2,4-DNI at 200°C, (b) decomposition at 235°C of the 2,4-DNI remaining from the previous experiment and (c) decomposition at 235°C of 10 mg of fresh 2,4-DNI that is mixed with the residue from experiment (b).

Early decomposition stage. The dominant process during this stage is desorption of the water from the surface layers of the 2,4-DNI particles as 2,4-DNI sublimates, and the loss of impurities remaining from the synthesis, such as 4-NI. The GFRs of the species that evolve as 2,4-DNI is taken and held at 200°C are shown in Figure 2a. There is an onset of decomposition that occurs near the time when 2,4-DNI begins to sublime. Water is the most abundant evolving gas, obtaining a maximum GFR as 200°C is approached, and then decaying with time. Studies with deuterium labeled 2,4-DNI- D_2 have shown that most of the H_2O that evolves during this time is from an exogenous source and is not a decomposition product. The desorption of water correlates with increased reaction rates during the early decomposition process of 2,4-DNI. Further support for the presence of water altering the early decomposition process is the observed decrease in the extent of the early decomposition when the sample is heated from 200°C to the next isothermal temperature of 235°C (Fig. 2b). The extent of the increase in the GFRs of the decomposition products during the early decomposition period of mostly-dehydrated 2,4-DNI (Fig.2b), is substantially less than observed during the early decomposition stage of hydrated 2,4-DNI (Fig.1).

Induction and accelerating-rate stages. Two processes dominate the decomposition of 2,4-DNI during the induction and accelerating stages. One process involves either gas-phase reactions within the reaction cell or reactions on the surface of the 2,4-DNI particles. This process forms the observed gaseous products and must lead to the development of the second process. The second process involves reaction between 2,4-DNI and the reactive intermediates formed during the induction stage. As the second process evolves the rate of reaction must increase, suggesting that this process itself accelerates the rate of this process. The temporal behaviors of the GFRs of products formed during each stage is illustrated by the data in Figure 2b. The induction stage is characterized by the behavior of the product GFRs up to approximately 8000 sec, at which point the GFRs start to gradually increase and the accelerating rate stage commences.

Decay stage. This stage is characterized by the evolution of gaseous products formed after the reactant is depleted. The products that evolve during this stage are formed from the decomposition of the secondary nonvolatile products formed during the earlier stages of the decomposition. During this stage of reaction, the processes associated with the direct decomposition of 2,4-DNI have stopped and only products originating from the decomposition of secondary products are observed.

These four stages of the reaction provide the basis for our model of the decomposition of 2,4-DNI.

PROTOTYPE MODEL FOR THE THERMAL DECOMPOSITION OF 2,4-DNI

A first-generation model to characterize the thermal decomposition processes of 2,4-DNI has recently been developed. The important features of the model are derived from the physical parameters of conducting an experiment in the reaction cell, the temporal behaviors of the GFRs of the gaseous decomposition products, visual observations of the decomposition process, microscopy of the reactant and residual products, and IR spectra of the non-volatile decomposition products. These features are illustrated in Figures 3 and 4. Details of the visual observations, microscopy, and infrared measurements will be included in a future publication. As illustrated in Fig. 3, when the sample is first heated to its isothermal temperature, a quasi-equilibrium is established between the rate of

vaporization (k_v) and rate of condensation (k_c) of 2,4-DNI, which essentially maintains 2,4-DNI in the gas phase near its equilibrium vapor pressure. The rate of evolution of 2,4-DNI from the reaction cell is determined by the number density of 2,4-DNI in the reaction cell and the flow characteristics (k_e) of gas through the reaction cell orifice. The 2,4-DNI contained in the reaction cell undergoes several different reaction processes (which will be described in more detail below). The gaseous products exit through the reaction cell orifice, their rates also being determined by the flow characteristics of the orifice (k_e). As the 2,4-DNI contained in the reaction cell nears depletion, the observed gaseous products evolve solely from a polymeric residue formed during the decomposition.

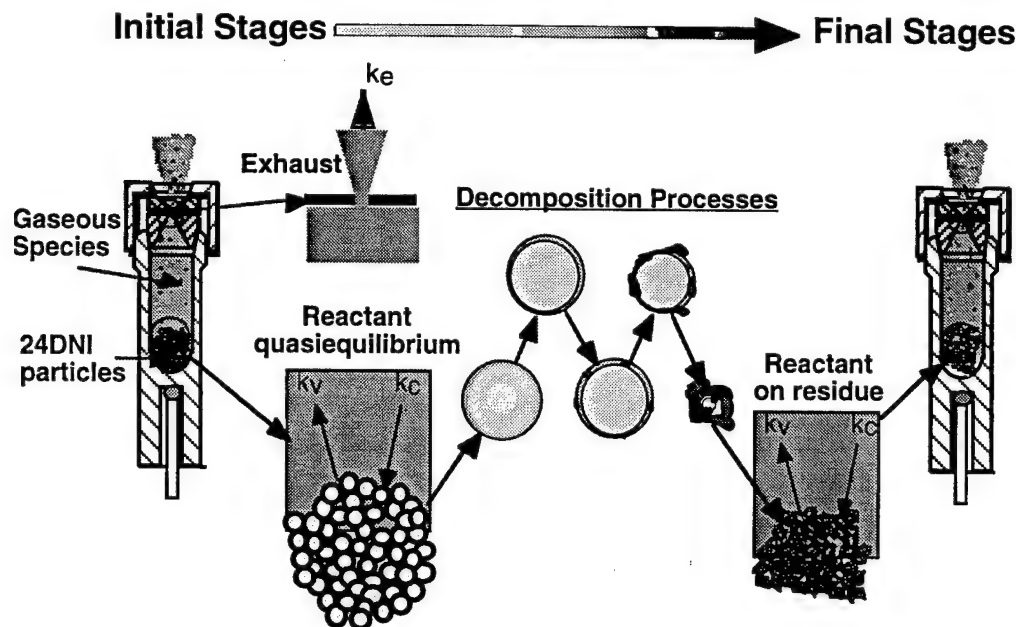


Figure 3. Schematic representation of 2,4-DNI decomposition in a reaction cell.

The general features of the reaction model for the processes that control 2,4-DNI decomposition are illustrated in Figure 4. In this model, 2,4-DNI in the gas phase may decompose within the reaction cell (step 1). The first stages of the decomposition are affected by the presence of water absorbed in the outer layers of the particle (step 2). As the 2,4-DNI begins to decompose, reactions occur in a surface layer on the particle (step 3), and gaseous products evolve. As the 2,4-DNI decomposes in this surface shell, a portion of each molecule remains behind in the shell. The fragments of each decomposed 2,4-DNI molecule remaining in the reactive shell combine to form larger polymeric nuclei (step 4). When these nuclei reach a critical size, they undergo direct reaction with 2,4-DNI. The reaction between the 2,4-DNI and the polymer (A) is then controlled by the transport rate of 2,4-DNI to the polymer surface (A) (step 5) where reaction occurs at the interface between 2,4-DNI and polymer (A) (step 6). Reaction between polymer (A) and 2,4-DNI leads to release of gaseous products and growth of polymer A. As the reactions continue, polymer (A) decomposes, releasing gaseous products and forming a new polymer (B) (step 7). Polymer (B) under the normal course of decomposition can still react with 2,4-DNI, leading to further growth of the polymer. At the model's present state of development, global chemistry is used to represent the various chemical reactions that occur during each of the processes just described. Differences between the rates of gas formation predicted by the model and the measured data will be used to generate a second-generation model of the 2,4-DNI decomposition processes that include more details on the individual chemical reactions involved in each process. Eventually, individual reaction mechanisms will be formulated to characterize each step of the process.

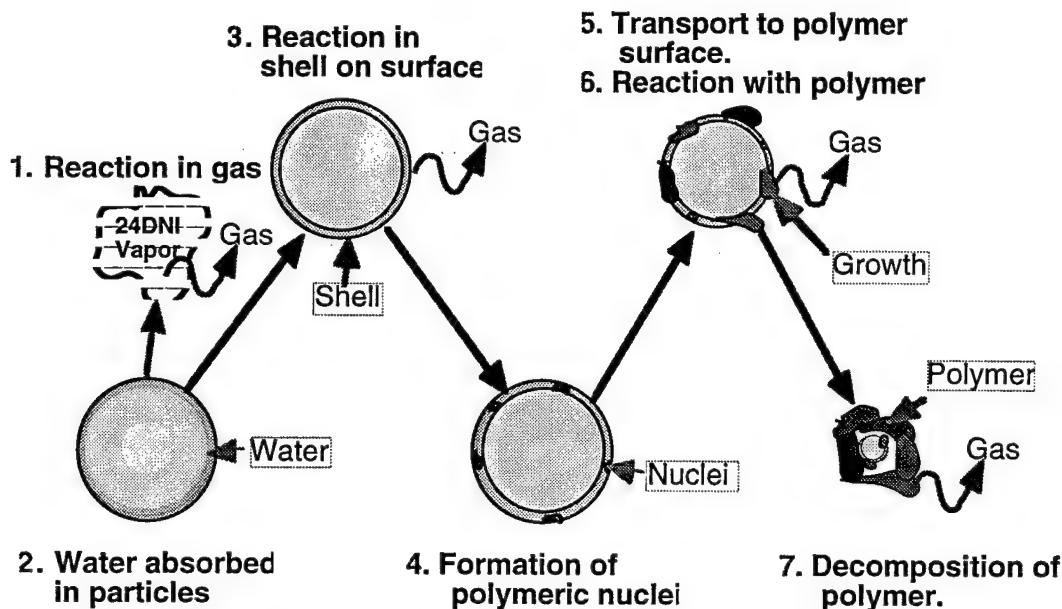
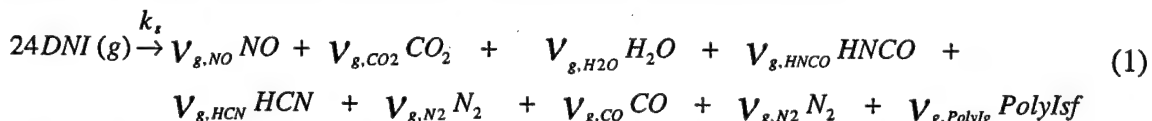
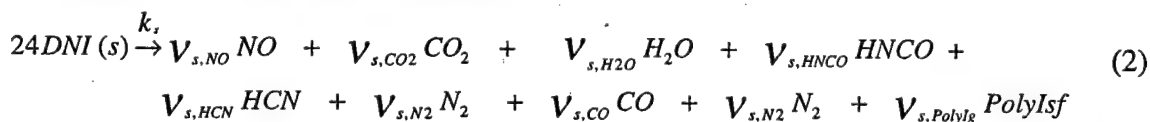


Figure 4. Schematic representation of 2,4-DNI decomposition processes in the solid phase.

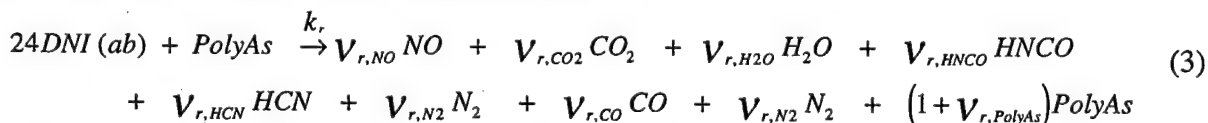
The global reaction chemistry for the main decomposition processes of 2,4-DNI is captured by fitting the reaction model to our data. The reaction chemistry for the gas phase is characterized by



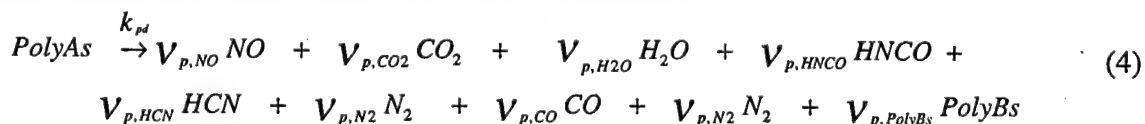
where k_g is the rate constant for this reaction and $v_{g,xxx}$ is the global stoichiometric coefficient for species xxx in this reaction. The reaction in the surface shell is characterized by



where k_s is the rate constant for this reaction and $v_{s,xxx}$ is the global stoichiometric coefficient for species xxx in this reaction. This reaction leads to the formation of the species, PolyIsf, that form nucleation centers which react directly with 2,4-DNI after they grow to some critical size. The reaction between the adsorbed 2,4-DNI on the surface of the reactive polymer PolyAs, is characterized by



where k_r is the rate constant for this reaction and $v_{r,xxx}$ is the global stoichiometric coefficient for species xxx in this reaction. Note that this reactions leads to the growth of PolyAs. PolyAs then decomposes, releasing gases and forming a second polymeric species, PolyBs. This reaction is characterized by



where k_{pd} is the rate constant for this reaction and $v_{p,xxx}$ is the global stoichiometric coefficient for species xxx in this reaction.

The mathematical model of 2,4-DNI thermal decomposition is described by a set of time-dependent, first order differential equations representing the physical processes and the evolution of gaseous products. For example, the rate of change of 2,4-DNI in the solid phase during the course of a decomposition experiment is described by

$$\frac{d24DNI_{(s)}(t)}{dt} = asurf1(t) * [-ks1(t) * xreact(t) + kc1(t) * stick(t) * 24DNI_{(g)}(t)] - ks * nshell(t) \quad (5)$$

where $asurf1(t)$ is the surface area of 2,4-DNI particles, $ks1(t)$ is the sublimation rate constant, $kc1(t)$ is the gas kinetic collision rate of 2,4-DNI with the particle surfaces, $xreact(t)$ is the modification of the reactivity of the surface due to water absorbed in the particles, $stick(t)$ is the 2,4-DNI sticking probability on the particle surfaces, $24DNI_{(g)}(t)$ is the concentration of 2,4-DNI in the gas phase, ks is the rate constant for reaction in the surface shell, and $nshell(t)$ is the amount of material in the reactive shells of the particles. An example of a rate expression characterizing the time-dependent behavior of the gaseous product concentrations within the cell is given by the expression for the time-dependent rate of change of NO within the cell,

$$\frac{dNO(t)}{dt} = \frac{1}{v_{cell}} * [kg * v_{cell} * v_{g,NO} * 24DNI_{(g)}(t) + ks(t) * v_{s,NO} * nshell(t) + kr * v_{r,NO} * 24DNI_{(ads)}(t) + kpd * v_{p,NO} * PolyAs(t)] - ke1(t) * NO(t) \quad (6)$$

where v_{cell} is the free volume of the reaction cell, kg is the rate constant for reaction in the gas phase, kr is the rate constant for reaction between the polymer and 2,4-DNI adsorbed on the polymer surface, $24DNI_{(ads)}(t)$, kpd is the rate of decomposition of the polymer, $PolyAs$ to $PolyBs$, $ke1(t)$ is the constant that characterizes the rate of exhaust from the cell, and $NO(t)$ is the concentration of NO in the cell. The other parameters are defined above.

The rate expression characterizing the time-dependent behavior of water within the cell must also account for the evolution of water that is absorbed in the sample. Thus, the time-dependent concentration of water in the reaction cell is given by

$$H_2O_T(t) = H_2O_R(t) + H_2O_A(t) \quad (7)$$

where $H_2O_T(t)$ is the total concentration of water in the cell, $H_2O_R(t)$ is the concentration of water originating from the decomposition of 2,4-DNI and $H_2O_A(t)$ is concentration of water originating from the absorbed water in the particles. The time-dependent rate of change of the concentration of water originating from absorbed water in the particles is given by

$$\frac{dH_2O_A(t)}{dt} = \frac{1}{v_{cell}} \left(ks1(t) * xwater(t) * asurf(t) - ke1(t) * H_2O_A(t) - asurf(t) * kc1(t) * H_2O_A(t) \right) \quad (8)$$

where $xwater(t)$ is the mole fraction of water at the surface of the particle at time t and the other parameters are described above.

The rate of growth of the nuclei in the reactive shell on the 2,4-DNI particles is given by

$$\frac{d \text{ nuclei}(t)}{dt} = knuc * polyIsf(t) \quad (9)$$

where $knuc$ is the rate constant for nucleation and $PolyIsf$ is the concentration of the fragments formed from the decomposition of 2,4-DNI in the shell on the surface of the 2,4-DNI particles. When the nuclei reach some critical size they can then undergo reaction directly with 24DNI that is absorbed on their surface.

The rate of growth of polymer, $PolyAs$, is given by

$$\frac{dPolyAs(t)}{dt} = kr(t) * aads(t) - kpd(t) * PolyAs(t) \quad (10)$$

where PolyAs(t) is the monomer unit from each 2,4-DNI molecule that adds to the polymer during the reaction, aads(t) is the amount of 2,4-DNI absorbed on the surface of the polymer, kr(t) is the rate constant for the reaction of 2,4-DNI absorbed on the surface of the polymer, and kpd(t) is rate of decomposition of the polymer formed from PolyAs to a different polymer, PolyBs. The stoichiometry of the PolyAs monomer unit is the difference between the stoichiometry of 2,4-DNI and the stoichiometry of the gases lost in the reaction between 2,4-DNI and polymer PolyAs.

The rate of formation of the PolyBs polymer is given by

$$\frac{d \text{PolyBs}(t)}{dt} = kpd(t) * \text{PolyAs}(t) \quad (11)$$

The stoichiometry of the PolyBs monomer unit is the difference between the stoichiometry of the PolyAs monomer and the stoichiometry of the gases lost as the PolyAs polymer decomposes to the PolyBs polymer.

ILLUSTRATION OF THE MODEL

Basis Experiment. An illustration of the application of the model to the results from a decomposition experiment conducted at 235°C is shown in Figure 5. The set of time-dependent first order differential equations representing the model are solved numerically. The rate constants and stoichiometric coefficients are determined from fits of the model to the measured data. The data in Fig. 5 shows a number of features of the decomposition process. The plots with only species labels show the data (solid lines) and the results of the calculation from the model (dashed line). The plots labeled as "species channels" show the contribution of each decomposition pathway to the rate of formation of each decomposition product. The plot labeled "reaction shell" shows the amount of 2,4-DNI in the reaction shell. For results from all of the calculations involving the reaction shell shown in this paper, the particle size of 2,4-DNI was estimated to be 10 µm and the thickness of the reactive shell was assumed to be 10 nm. Thus, a combination of the particle diameter, the thickness of the reaction shell and the rate constant, ks, are coupled parameters in the model. In this case, we held the particle diameter and reaction shell thickness constant and varied ks to fit the data. Figure 5 also shows one plot of the amount of each polymer and another plot of the surface area of the polymer that is available for reaction with 2,4-DNI. For the polymers, polyIsf represents the amount of monomer, formed from reaction in the shell, that is not incorporated into critical size nuclei. Nuclei(t) represents the amount of polyIsf monomers that have been incorporated into nuclei of a critical size that can react with 2,4-DNI absorbed on their surface. PolymerA represents the PolyAs product and PolymerB represents the PolyBs product.

In this first generation of the model, several assumptions have been made with regard to the polymers. First, the size of the critical size nuclei is an unknown value. In these calculations, we have assumed the nuclei to be spherical and chosen to be a diameter that is some fraction of the 2,4-DNI particle diameter. We have used a value of 1/10th of the 2,4-DNI particle diameter in this paper. Better estimates of this parameter will be made in the future from microscopy measurements. Second, 2,4-DNI is assumed to cover the surface of PolyAs with one monolayer of 2,4-DNI. The gas kinetic collision rate of 2,4-DNI with the surface, under the conditions of these experiments, will easily maintain a coating of 2,4-DNI on the surface of the polymer. Build up of more than one layer of 2,4-DNI on the surface of the polymer probably occurs, but inclusion of this behavior in the model would not add any new features to the process and would increase the complexity of the model. The surface concentration of 2,4-DNI on the polymer is determined by assuming the 2,4-DNI are spherical molecules and estimating the diameter of the individual molecules from the density of 2,4-DNI. Finally, the surface area of the polymer is determined by calculating the amount of decomposed 2,4-DNI that resides in the polymer, calculating the volume occupied by the polymer from estimates of its density, and then distributing the total volume of polymer over the number of critical size nuclei formed up the current point in time. The density of the polymer is assumed to be ~ 1.4 gm/cm³. This value is based on infrared spectra suggesting the polymer has a polyamide-like functionality and using an average density of several different amino acids. The parameters of the polymer discussed here along with the rate constant kr form another set of coupled parameters in the model. All of the parameters are kept constant, except for kr, which is varied to fit the data.

The fraction of water absorbed in the particles, xwater(t), is determined from the measurements. The distribution of the water beneath the surface of the particle at time t=0 is also determined from the experimental data. In addition, exchange of hydrogen with deuterium on at the labile 2-position of the 2,4-DNI molecule in a deuterium

labeled 2,4-DNI sample is also used to determine the distribution of the water that has diffused into the 2,4-DNI particles. The details of these measurements will be described in a later publication.

The method used to determine the parameters in the model is as follows:

1. The calculated rate of evolution of 2,4-DNI from the reaction cell is compared to the data. Slight adjustments ($< 5\%$) are made to the diameter of the orifice to approximately match the initial measured evolution rate of 2,4-DNI.
2. Initial guesses for the stoichiometric coefficients of several products are made.
3. The rate constants, k_s , k_{nuc} , and k_r are varied to match the temporal behavior of the gas evolution rates, and more importantly, are varied such that the calculated time for depletion of the 2,4-DNI matches the data.
4. The rate constant k_{pd} is varied to match the gas evolution rates after the 2,4-DNI is depleted.
5. The calculated rates of gas evolution for each product are compared to the measured rates. The stoichiometric coefficients are renormalized to obtain the best fit.
6. Steps 3 and 4 are repeated with the new stoichiometric coefficients.
7. The stoichiometric coefficients associated with each process are checked to determine if they appear to be plausible reactions.

For each process, the coupled parameters, the rate constant and stoichiometric factors, can be varied dependently to obtain the same gas evolution rates of the products. However, this variation will require a correlated variation in the other processes to maintain the same length of time for depletion of the sample. Thus, only certain combinations of rate constants and stoichiometric coefficients are allowed. This criteria will be used in future analysis of this data to obtain the most chemically plausible reaction pathways that are consistent with the data.

This data analysis method has been applied to the data set shown in Figure 5. A comparison of the calculated fits with the data shows that the model captures most features of the data. Several interesting features are worth noting. The contribution of the absorbed water (H_2O_{abs}) matches the data quite well. The enhancement in the reaction rates caused by the presence of water is also captured by the model. The origin of some products, such as H_2O and CO_2 , is greater from reaction in the shell. Whereas, the origin of other products, such as HCN and HNCO, is greater from reaction between the polymer and the adsorbed 2,4-DNI. Further examination of the origins of the HCN and HNCO show that HNCO is more likely to originate from the direct reaction of 2,4-DNI with the polymer and less likely to originate from the subsequent decomposition of the polymer while the opposite is true for HCN. The contribution from decomposition in the gas phase is almost zero compared to the other channels. The reason for this situation in the model will become apparent when the results from decomposition in a larger volume reaction cell are discussed below. The final aspect to discuss briefly is the relative amount of the different species associated with nucleation and growth of the polymers. A comparison of the amount of polyIsf monomer, that has been incorporated into an active nucleation site (nuclei), to the amount of polyIsf that remains free of active sites (polyIsf), shows that the fraction of polyIsf in the active nuclei during the early stages of the experiment are small. After a small number of nuclei are formed the total amount of polymer available for reaction, the sum of Polymer A and Polymer B, is formed predominantly by reaction of 2,4-DNI with the polymer. While this nucleation model provides the correct delay for onset of the growth of the polymer, whether or not the nucleation process used here properly characterizes the actual nucleation process in 2,4-DNI will require further experiments.

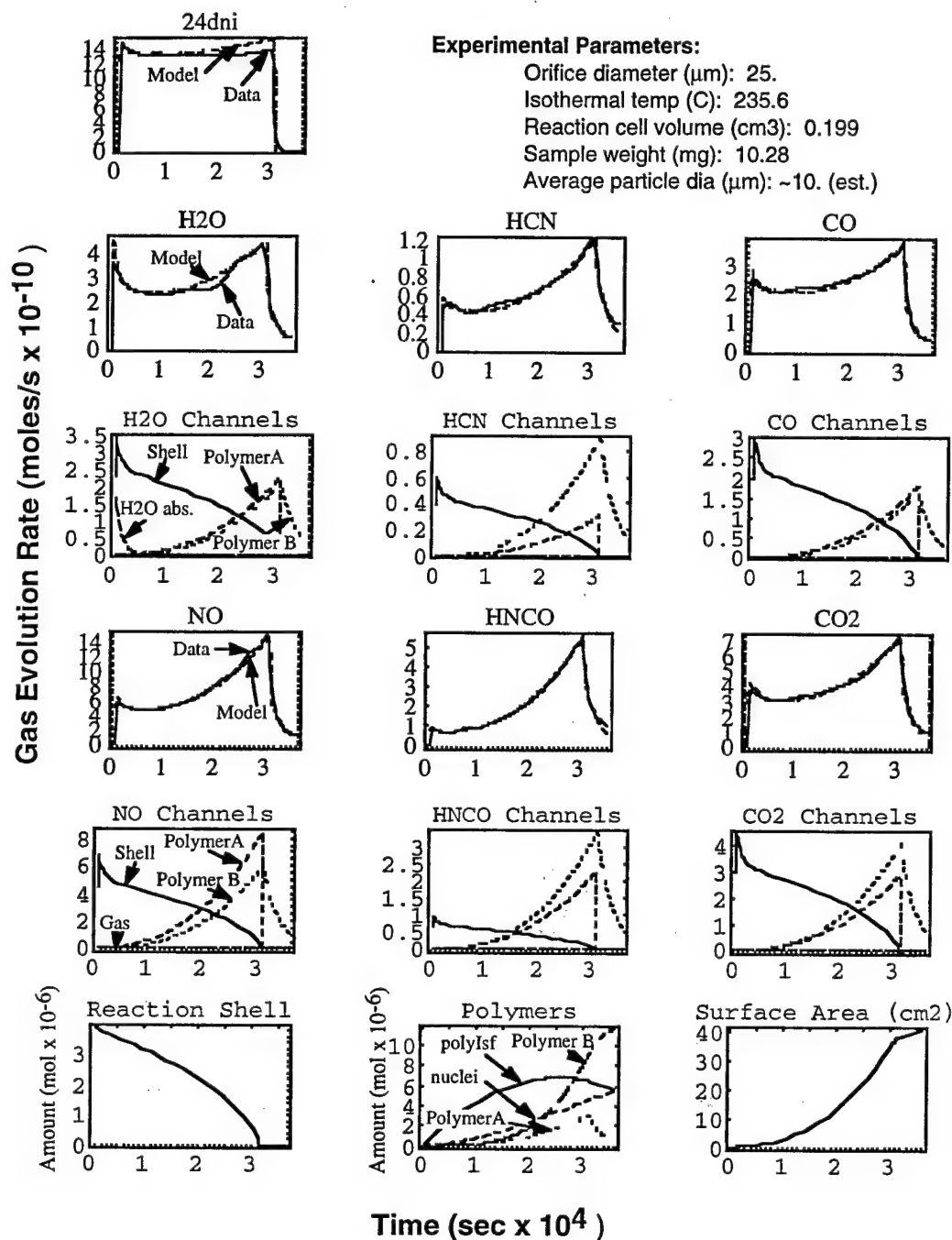


Figure 5. The evolution rates of gaseous products from the decomposition of 2,4-DNI at 235°C in a reaction cell with a 25 μm diameter orifice are shown along with the results from a model of the decomposition process. Plots with only product labels show the measured rate of gas evolution from the reaction cell (solid line) and the resulting fit of the model (dashed line) for each product. Plots of the product channels show the contribution of each channel described in the model to the overall evolution of each decomposition product. The legend for each type of plot is shown in the first plot in each row.

Catalysis Experiment. The next experiment assessed the catalytic activity of the polymer formed during the decomposition of 2,4-DNI. In this experiment, 10.32 mg of 2,4-DNI was added to the residue remaining from the previous experiment in the manner described above. The data and the results from the model are shown in Fig. 6.

The number of parameters in the model, which were varied for this experiment and the remainder of the experiments described in this paper, were significantly reduced from the first experiment. The reason for this is twofold. First, we wanted to determine how well the parameters from one experiment would fit another. Second, we wanted to identify the variations between the predictions of our model and the data so that we could develop further insights into the processes controlling the decomposition of 2,4-DNI. For the case of the calculation shown in Fig. 6, no parameters in the model were changed from the model calculation used for the experiment shown in Figure 5. The only difference in this model calculation was that the starting values for polyIsf, nuclei, PolyAs and PolyBs were set to their final values from the calculation for the previous experiment.

Comparison of the results of the calculation with the data show many consistencies between the model and the data. First, the rate of decomposition of 2,4-DNI is correctly predicted. Note that the length of time for ~ 10 mg of 2,4-DNI to decompose in this experiment is ~10,000 seconds compared to ~ 31,000 seconds for the same amount of material in the previous experiment with no added residue. Thus, the model appears to be a good representation of the autocatalytic process. Closer examination of the gas evolution rates show that the calculated rates for H₂O, HCN, NO and CO₂ compare quite closely with the data. However, there are larger discrepancies between the calculated and measured gas evolution rates for CO and HNCO. The origin of these differences will be considered in the future and a better understanding of the process will be incorporated into the next generation of the model.

Gas-phase decomposition. To assess the extent of decomposition of 2,4-DNI in the gas phase, an experiment was carried out in a reaction cell with a volume seven times greater than used in the standard experiments. This increases the fraction of the sample in the gas phase seven-fold. Thus, if the reaction during the early stages of decomposition occur solely in the gas phase, a seven-fold increase in the rate of formation of the decomposition products would be expected. As the results show in Figure 7, for the experiment with the larger volume reaction cell, this is not the case. When the same parameters are used in the model as were used to fit the basis experiment, and the gas-phase rate constant is set to zero, the model provides a good fit to the data (the short dashed line). This indicates that decomposition in the gas phase is not a large contributor to the overall reaction process. This fact led to our development of the reactive shell process as one of the primary decomposition pathways.

To evaluate how decomposition in the gas phase may contribute to the overall rates of evolution of the various products, the rate constant for the gas-phase reaction, k_g , was set equal to the rate constant for reaction in the shell, k_s , and the calculation was repeated. The results of the calculation are represented by the long dashed line in Figure 7. A slight increase in the rates of gas formation of the various products is observed. In light of the fact that we are assuming that the decomposition of 2,4-DNI in the reactive shell is undergoing a unimolecular decomposition in the model, it is reasonable to assume that the rate constant for 2,4-DNI in the gas phase would be similar. Given these assumptions, comparing the results of the two calculations to the data, and realizing that the relative contributions of decomposition in the shell and decomposition in the gas phase are proportional to the amount of 2,4-DNI available to react in each process, it appears that our estimation of the amount of material available for reaction in the shell is approximately correct. For example, if we assumed that the thickness of the reactive shell was 1 nm instead of 10 nm, then the contribution from gas-phase reactions in the larger cell would have been ten times larger and running the experiment in the larger volume reaction cell would have had significantly different results from our basis experiment. On the other hand, if we assumed the thickness of the reactive shell was 100 nm, then the contribution of gas-phase reactions would be even less. Given the differences between the calculated rates from the model and the data, when the gas-phase rate constant is set to zero, it is difficult to determine whether the slightly better fits to several of the gas evolution rates when the gas-phase rate constant is set equal to k_s is actually due to the gas phase contributions or some other aspect of the decomposition process. Thus, the certainty for an estimated value of the maximum thickness of the reactive shell is low.

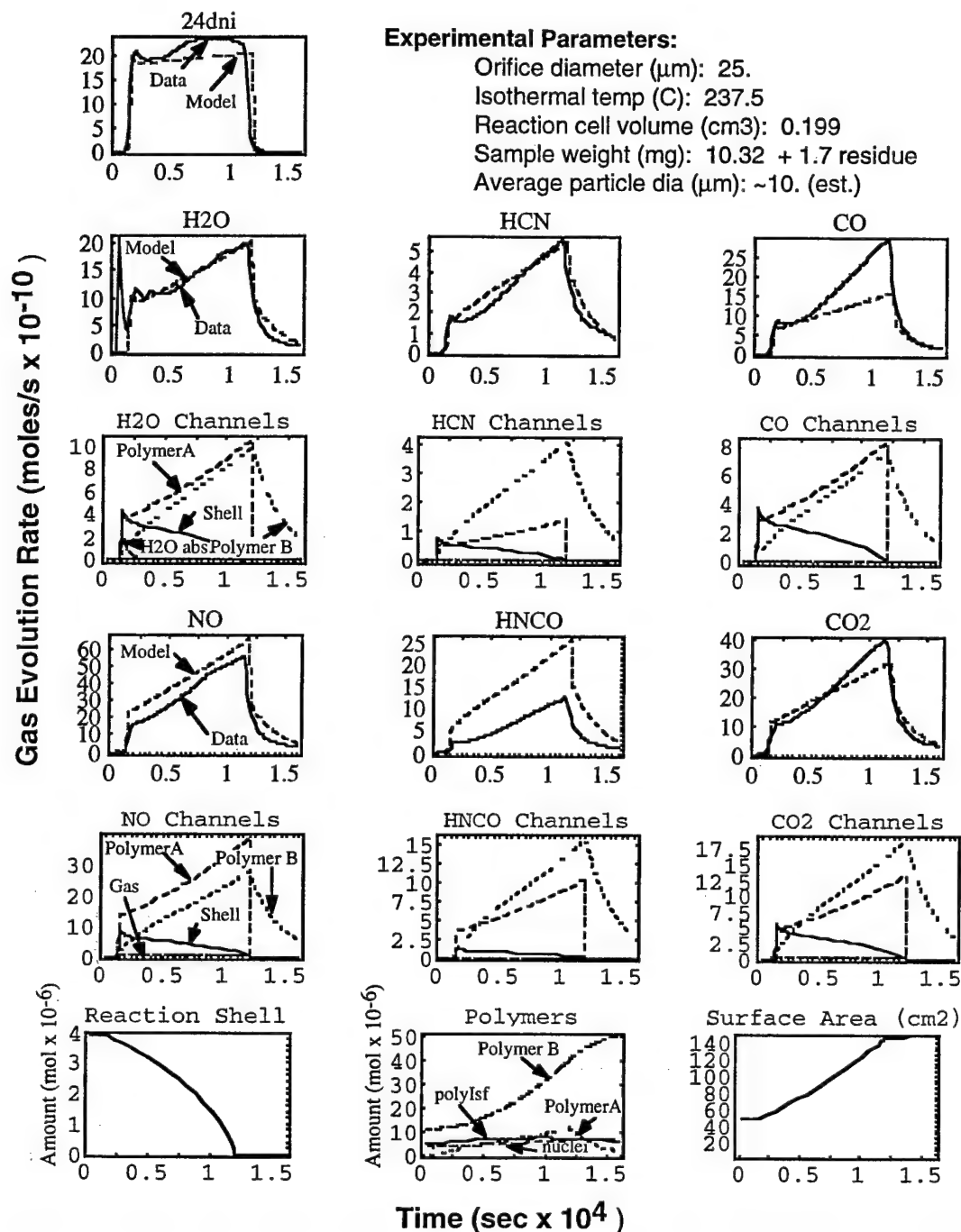


Figure 6. The evolution rates of gaseous products, resulting from the decomposition of 2,4-DNI mixed with a residue from a previous experiment, are shown along with the results from a model of the decomposition process. Plots with only product labels show the measured rate of gas evolution from the reaction cell (solid line) and the resulting fit of the model (dashed line) for each product. Plots of the product channels show the contribution of each channel described in the model to the overall evolution of each decomposition product. The legend for each type of plot is shown in the first plot in each row.

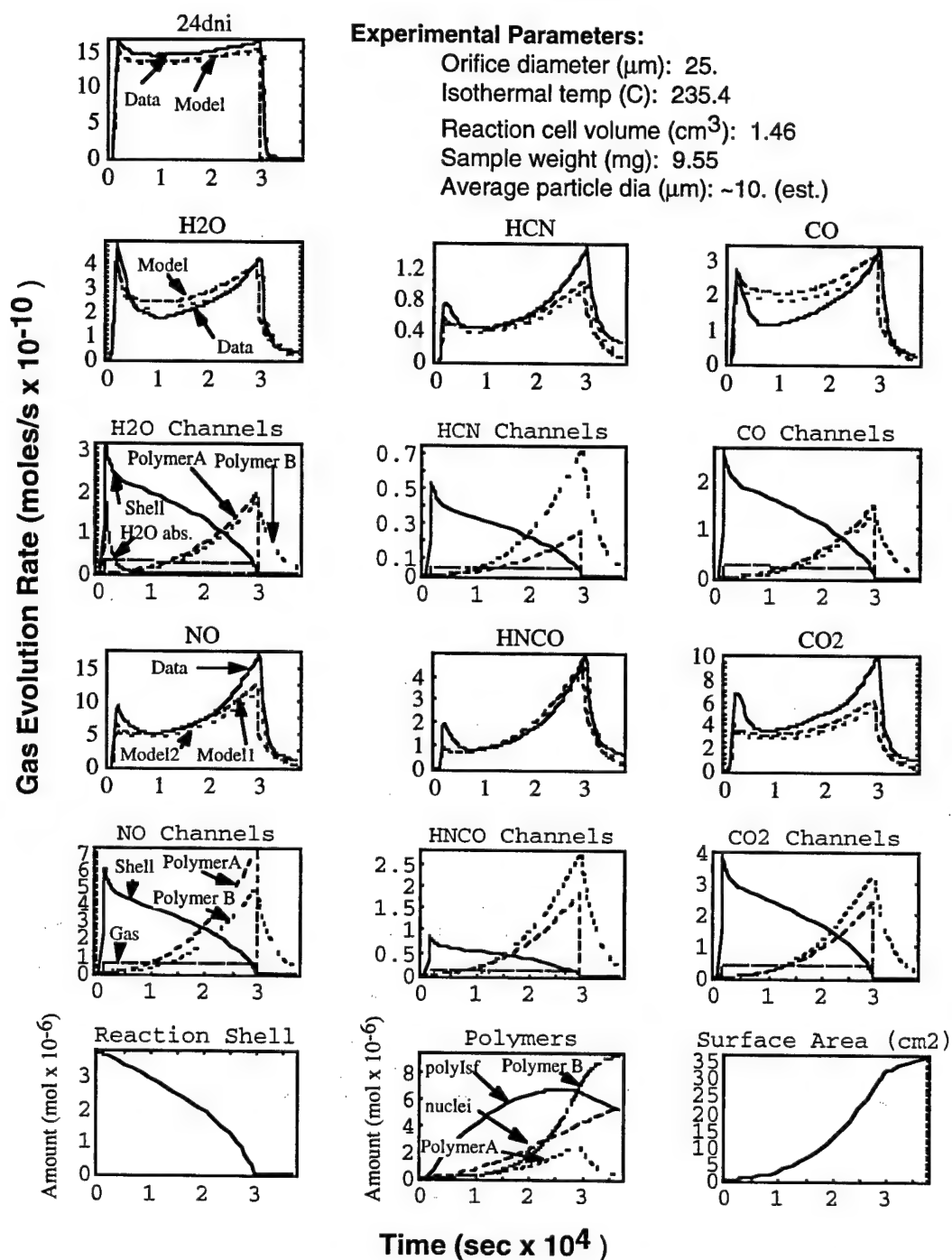


Figure 7. The evolution rates of gaseous products from the decomposition of 2,4-DNI in a larger volume reaction cell (1.46 cm^3) is shown along with the results from a model of the decomposition process. Plots with only product labels show the measured rate of gas evolution from the reaction cell (solid line) and the results of two different calculations with the model. One calculation with the model includes no contributions from gas-phase reactions (short dashes) while the other calculation does include gas-phase contributions (long dash). Plots of the product channels show the contribution of each channel described in the model to the overall evolution of each decomposition product. The legend for each type of plot is shown on the first plot in each row.

Temperature dependence. The temperature dependence of the processes is incorporated into the model by optimizing the rate constants to fit the data collected in experiments at several different isothermal temperatures. An example of a fit to one set of data collected in an experiment at 244.3°C is shown in Figure 8. The four rate constants, k_s , k_{nuc} , k_r and k_{pd} , were the only parameters adjusted to fit the data. The stoichiometric coefficients and all other parameters are the same as those used in fitting the basis experiment. The procedure for optimizing the coefficients by comparison to the data is the same method used for the basis experiment.

The results of the optimization procedure show the rate constants have been optimized to correctly predict the depletion time of the sample, and thus, the correct amount of 2,4-DNI decomposed. A comparison of the measured gas evolution rates with corresponding calculated rates from the model are for the most part in good agreement. However, close inspection shows that there are several differences. For example the model predicts higher gas evolution rates for NO and H₂O, in the final stages of the decomposition, than actually measured. The model also predicts a lower rate of CO₂ evolution than measured. We suspect these deviations arise from our oversimplification of the global reaction chemistry used for each process. These deviations will be used to create a more accurate representation of the reaction chemistry in the next generation of the model.

Comparison of the relative contributions to the gas evolution rates of the individual species from each decomposition process shows that in the higher temperature experiment more of the products are formed from reaction between the 2,4-DNI and the polymer than from decomposition in the reactive shell.

Extent of decomposition. For the experiments discussed to this point, the ratio of the undecomposed 2,4-DNI to the decomposed 2,4-DNI has ranged from 0.45 for reaction with residue from a previous experiment, to 0.8 for decomposition at 244°C, up to 1.8 to 2.0 for experiments at 235°C in the standard and large volume reaction cells. In the results from the experiment presented in Figure 9, the orifice diameter used in the reaction cell for the experiment was increased from 25 μ m to 50 μ m. The ratio of undecomposed to decomposed 2,4-DNI in this experiment was 12.5. Thus, only one out of twelve 2,4-DNI molecules underwent decomposition.

The results differ quite dramatically from the previous experiments, in which a larger fraction of the sample decomposed. The two most notable differences are the lack of a significant contribution from reaction between the 2,4-DNI and the polymer, and the larger increase in the rates of gas evolution due to the exogenous water absorbed in the sample. The larger rates of gas evolution due to exogenous water are most likely due to slightly different conditions used for this experiment. In this experiment the 2,4-DNI was held at ~121°C for 10,000 seconds whereas in the previous experiments it was held at 200°C for 15,000 seconds. This suggests that this experiment contained more exogenous water when it reached 235°C, increasing the reaction rates to higher levels during the early stages of the reaction compared to the basis experiment.

The more interesting difference is in the limited extent of contribution of the autocatalytic process between 2,4-DNI and the polymer. This is consistent with the model for two reasons. First, the rate of formation of the critical size nuclei are dependent on the concentration of 2,4-DNI in the volume of the reactive shell. The lower concentration leads to a lower rate of formation of critical size nuclei. Second, since the exhaust rate of 2,4-DNI from the reaction cell is greater, the sample is depleted in a shorter period of time and the process involving the growth of the polymer is shortened.

The most significant difference between the measured data and the calculated rates is in the values for the NO gas evolution rate. The measured rate of NO evolution is 3 times greater than the rate predicted by the model. This discrepancy suggests that either the decomposition mechanism of 2,4-DNI is significantly different at lower extents of decomposition or that there is a possible error in the experiment. These issues are being considered in the next generation of the model.

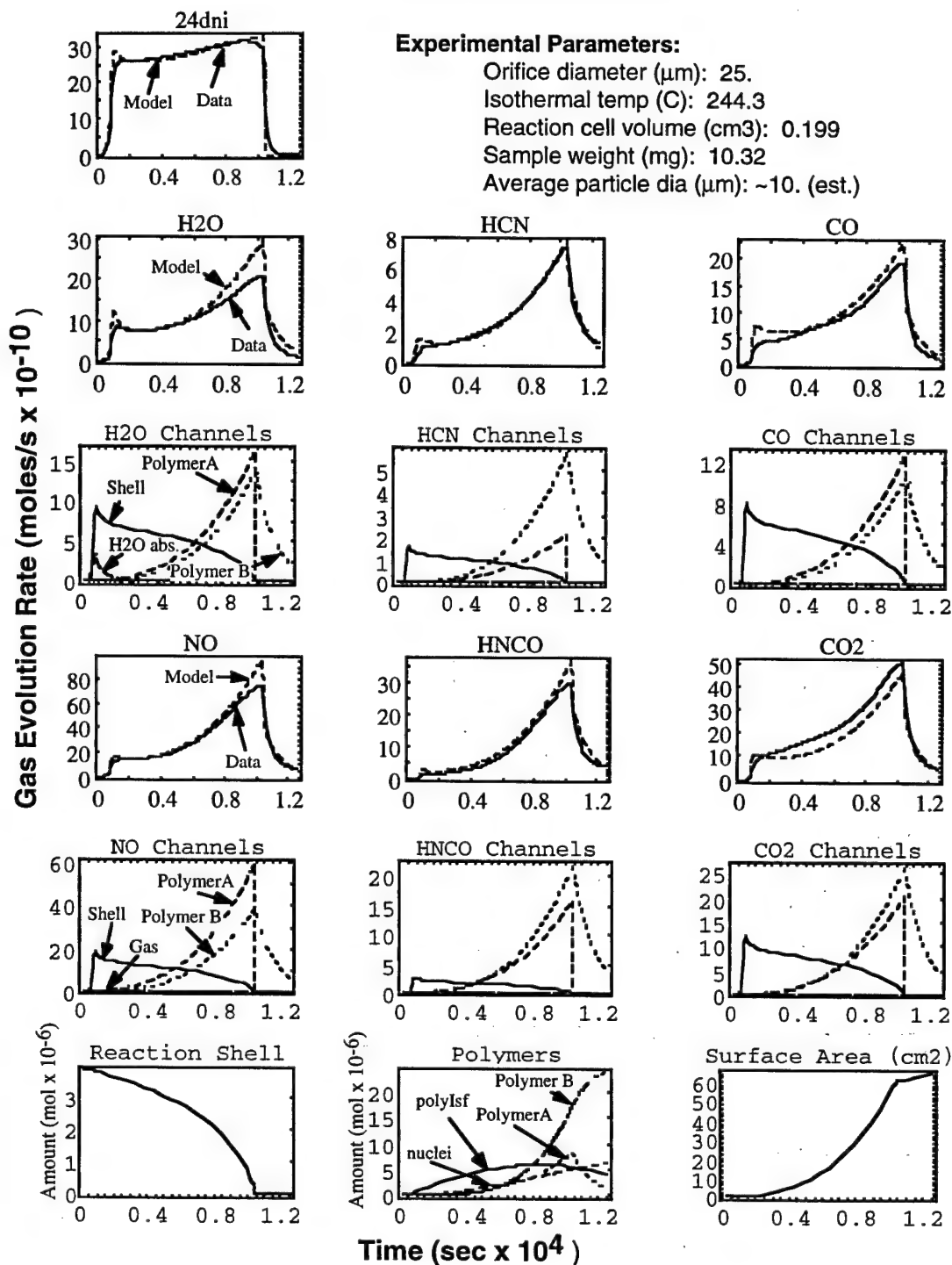


Figure 8. The evolution rates of gaseous products from the decomposition of 2,4-DNI at a higher temperature (244°C) are shown along with the results from a model of the decomposition process. Plots with only product labels show the measured rate of gas evolution from the reaction cell (solid line) and the resulting fit of the model (dashed line) for each product. Plots of the product channels show the contribution of each channel described in the model to the overall evolution of each decomposition product. The legend for each type of plot is shown on the first plot in each row.

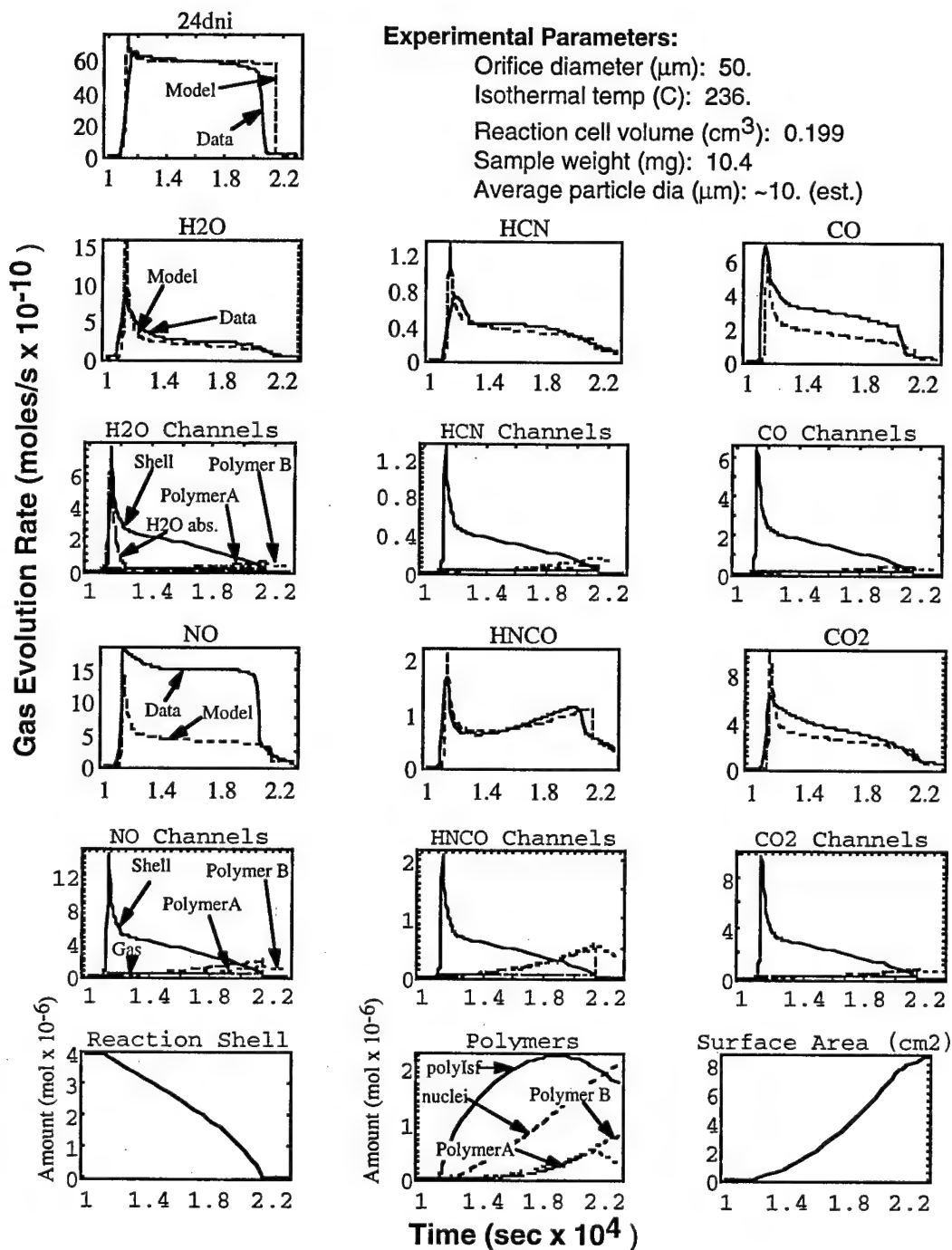


Figure 9. The evolution rates of gaseous products from the decomposition of 2,4-DNI using a larger diameter orifice ($50\mu\text{m}$) are shown along with the results from a model of the decomposition process. Plots with only product labels show the measured rate of gas evolution from the reaction cell (solid line) and the resulting fit of the model (dashed line) for each product. Plots of the product channels show the contribution of each channel described in the model to the overall evolution of each decomposition product. The legend for each type of plot is shown on the first plot in each row.

Outstanding issues. The following outstanding issues are being addressed in the next generation of the reaction model:

1. The details of the reaction chemistry will be developed. New reactions will be formulated from differences between the gas evolution rates for the various products predicted by the model, and the measured data collected in experiments spanning the temperature range of the process (200°C to 255°C).
2. Information derived from results of infrared, microscopic, and mass spectrometric analysis of the residue will be incorporated into the model.
3. Better characterization of the sample morphology will be made.
4. The effects of containment of gaseous products and the extent of reaction will be evaluated using results from experiments conducted using smaller diameter reaction cell orifices.
5. The effects of sample size will be evaluated.

SUMMARY

Our study of the solid-phase thermal decomposition behavior of 2,4-DNI has shown that the decomposition behavior is complex, and not defined by a single dominant process that can be accurately represented with a simple analysis of the quantified results. The decomposition products consist of several different gases and a polymeric residue that accounts for ~40% of the total decomposition product weight. A first-generation model has been developed to describe the solid-phase pyrolysis of 2,4-DNI, that is based on the temporal behaviors of the gas-evolution rates of the gaseous products of decomposing 2,4-DNI under various conditions. The results of the model show that the decomposition of 2,4-DNI and evolution of gaseous products is controlled by at least six basic processes. These processes include: 1) sublimation and decomposition in the gas phase (small contribution), 2) decomposition in a reactive shell on the surface of the particles, 3) enhancement of the reaction rates and reduction of the 2,4-DNI sticking coefficient due to absorbed exogenous water and impurities in the 2,4-DNI sample, 4) the growth of polymeric reactive nuclei in the reactive shell, 5) adsorption of 2,4-DNI on the surface of the reactive nuclei, followed by reaction of the 2,4-DNI on the surface to release gaseous products and add to the polymer, and 6) transformation of the polymer formed by the initial reaction with 2,4-DNI to a more thermally stable polymer, releasing gas in the process. The combination of processes four through six characterize the autocatalytic nature of the 2,4-DNI decomposition. Global reaction chemistry has been used to characterize each of the basic decomposition processes in the first generation of the model. At the model's present state of development, global chemistry is used to represent the various chemical reactions that occur during each of the processes just described. Differences between the rates of gas formation predicted by the model and the measured data will be used to generate a second-generation model of the 2,4-DNI decomposition processes that include more details on the individual chemical reactions involved in each process.

ACKNOWLEDGMENTS

The authors thank Mr. D.M. Puckett for collecting the mass spectrometry data and to Dr. Phil Pagoria for providing the 2,4-DNI sample. Work is supported by the Army Research Office, a Memorandum of Understanding between the DoD Office of Munitions and the Department of Energy under Contract DE-AC04-94AL85000, and by the U.S. Army, ARDEC.

REFERENCES

- 1 R. Behrens, Jr., *Journal of Physical Chemistry* **94**, 6706-6718 (1990).
- 2 R. Behrens, Jr. and S. Bulusu, *Journal of Physical Chemistry* **95**, 5838-5845 (1991).
- 3 S. Bulusu and R. Behrens, *Defence Science Journal (India)* **46**, 347 - 360 (1996).
- 4 R. Behrens, Jr. and S. Bulusu, *Journal of Physical Chemistry* **96**, 8877-8891 (1992).
- 5 R. Behrens, Jr. and S. Bulusu, *Journal of Physical Chemistry* **96**, 8891-8897 (1992).
- 6 R. Behrens, Jr., T. A. Land, and S. Bulusu, in *30th JANNAF Combustion Meeting* (Chemical Propulsion Information Agency, Monterey, California, 1993).

- 7 R. Behrens and S. Bulusu, in *32nd JANNAF Combustion Subcommittee Meeting* (CPIA Publication #638, Huntsville, AL, 1995), Vol. 1, p. 1 - 11.
- 8 R. Behrens, Jr. and S. Bulusu, in *Fall 1992 Meeting of the Materials Research Society*, edited by R. W. Armstrong, J. J. Gilman and D. H. Liebenberg (Material Research Society, Boston, Mass., 1992), Vol. 296, p. 13 - 24.
- 9 S. Bulusu, R. Damavarapu, J. R. Autera, *et al.*, *Journal of Physical Chemistry* **99**, 5009-5015 (1995).
- 10 L. Minier, R. Behrens, and S. Bulusu, in *1995 JANNAF 32nd Combustion Subcommittee* (CPIA, Huntsville, Alabama, 1995).
- 11 L. Minier, R. Behrens, and T. J. Burkey, in *33rd JANNAF Combustion Meeting* (CPIA Publication # 653, Monterey, CA, 1996), Vol. 2, p. 427 - 437.
- 12 R. Behrens and L. Minier, in *33rd JANNAF Combustion Meeting* (CPIA Publication # 653, Monterey, CA, 1996), Vol. 2, p. 1-19.
- 13 K. Jayasuriya, R. Damavarapu, R. L. Simpson, *et al.*, (Lawrence Livermore National Laboratory, 1993).
- 14 R. L. Simpson, C. L. Coon, M. F. Foltz, *et al.*, (Lawrence Livermore National Laboratory, 1993).
- 15 R. Behrens, Jr., *Review of Scientific Instruments* **58**, 451 (1986).
- 16 R. Behrens, Jr., *International Journal of Chemical Kinetics* **22**, 135-157 (1990).
- 17 R. Behrens, Jr., *International Journal of Chemical Kinetics* **22**, 159 (1990).
- 18 L. Minier, R. Behrens, and S. Bulusu, in *Decomposition, Combustion and Detonation Chemistry of Energetic Materials*, edited by T. B. Brill, T. P. Russel, W. C. Tao and R. B. Wardle (Material Research Society, Boston, MA, 1996), Vol. 418, p. 111 - 117.

The Importance of Mononitroso Analogues of Cyclic Nitramines to the Assessment of the Safety of Propellants and Explosives

Richard Behrens
Sandia National Laboratories
Combustion Research Facility
Livermore, California

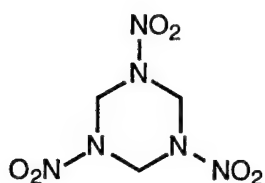
Suryanarayana Bulusu
U.S. Army, ARDEC
Dover, New Jersey

Abstract

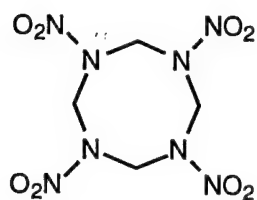
A summary of the thermal decomposition behaviors of HMX, RDX and 1-nitroso-3,5-dinitro-s-triazine (ONDNTA) as determined from simultaneous thermogravimetric modulated beam mass spectrometry (STMBMS) measurements is presented. A qualitative model of the physical and chemical processes that control decomposition of HMX in the solid phase, based on results from all three compounds, is described. Its implications for the response of systems containing these materials to abnormal thermal environments, such as fire, is discussed.

Introduction

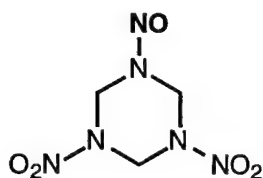
Cyclic nitramines, such as RDX (I) and HMX (II), are high energy containing compounds that are used extensively in both propellant and explosive formulations. These formulations are found in devices ranging from rocket motors to explosives. Typically, these devices are not used for long periods of time after they are initially manufactured and in many cases they are destroyed or recycled before ever being used. During the life of these devices, they are transported and stored in different environments. It is important that these devices remain safe throughout this life cycle. To assess the safety of these devices during the life cycle, it is necessary to understand how they will respond to their environment. In this regard, two main areas are of interest. First, how will the device respond in an abnormal environment, such as a fire? Second, what effect does aging in the various environments have on the properties and behavior of the device? For example, does the thermal, impact, or shock sensitivity increase with age? To address these issues from a scientific point of view requires an increased understanding of the chemical and physical processes that occur in the energetic materials found in these devices.



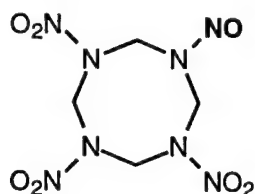
RDX (I)



HMX (II)



ONDNTA (III)



ONTNTA (IV)

Recent efforts to develop models, that will describe the response of a munition in a "slow-cockoff" situation, associated with a fire, strive to use a fundamental understanding of the chemical and physical processes that occur in energetic materials to predict the time to ignition of the event and the degree of violence after ignition. (HOBBS, BAER***) Significant success has been obtained in predicting the time to ignition but less success has been achieved in predicting the degree of violence. The degree of violence may be characterized by relatively benign event, such as a deflagration, or a more serious event, characterized by an explosion or detonation. The success achieved in modeling the time to ignition arises, in part, from the empirical characterization of one-dimensional time-to-explosion data collected on various energetic materials.¹ However, predicting the degree of violence of the event requires a more in depth understanding of the processes that control the reaction of the material after ignition. The degree of violence of this event will be controlled by the combustion process and the interaction of the combustion process with the extent of confinement of the reacting material. For example, with higher degrees of confinement the pressure at which the combustion occurs will be higher, and thus, the burn rates should be higher.

Measurement of the pressure dependence of burn rates of energetic materials associated with propellants has been done extensively in pressure ranges associated with both rocket motors and guns. Modeling these processes in an empirical fashion has been quite successful² and more recent modeling on a molecular level in the gas phase and to a lesser extent in the condensed phase have had good success. However, little work has been done on burn rates under highly confined conditions, although several recent measurements have been made on burn rates of energetic materials between 200 and 400 MPa.³ (Maienschein)

Characterizing the response of a munition in a 'slow-cockoff' situation poses a more difficult problem than that associated with the confined combustion problem. This increased difficulty is due to the degradation of the material prior to ignition. This degradation process can lead to the formation of both gaseous and condensed phase products that are not present under normal conditions. As these products are produced in the decomposition process, they may lead to the formation of bubbles and pores within the energetic material or possibly form solutions between the normal material and its decomposition products. Basically this changes the physical and chemical characteristics of the bed of energetic material. The extent of change of the chemical and physical properties is dependent on both time and temperature field within the material prior to ignition.

Therefore, developing models for predicting the response of a munition in a "slow-cookoff" situation, or even developing experiments to characterize the combustion process requires a good understanding of the decomposition process. Ultimately, one should understand both the chemical and physical changes that occur in the materials, where they occur within the materials and how fast they occur. In this paper we address the decomposition chemistry associated with two materials used extensively in propellants and explosives, RDX and HMX.

Over the past ten years we have conducted extensive thermal decomposition studies on HMX^{4,5} and RDX^{6,7} and several less extensive studies on other cyclic nitramines having five-, six- and seven-member rings. In all of these studies we have found that the mononitroso analogue of the parent compound is formed in the decomposition process. The identity and relative amounts of the gaseous decomposition products (i.e., NO₂, HCN, N₂O, CH₂O, NO, H₂O, CO) depends on whether these products are formed directly from the cyclic nitramine or through the mononitroso intermediate. We have also found that the mononitroso intermediate plays a significant role in the decomposition of HMX and RDX in the solid phase. As a consequence of our findings on the decomposition of HMX and RDX, we have undertaken a study of the decomposition of the independently synthesized mononitroso analogue of RDX, 1-nitroso-3,5-dinitro-s-triazine (ONDNTA).⁸

From our STMBMS measurements on ONDNTA, we have found that its decomposition is quite complex. It decomposes in two different temperature regimes and its decomposition rate and mechanism are very sensitive to the extent of interaction between ONDNTA and its decomposition products. The higher temperature decomposition regime commences at approximately 170 C, the melting point of ONDNTA and is autocatalytic in nature. The lower temperature regime occurs up to ~ 140 C and the extent of decomposition in this regime is very sensitive to interaction with product gases.

The highlights of our experiments that led to our current understanding of the decomposition mechanisms of RDX and HMX along with implications for possible changes in the sensitivity of RDX and HMX will be discussed in this paper.

Experimental

Instrument Description. Thermal decomposition measurements of energetic materials are carried out on 2 to 10 mg samples using the STMBMS apparatus, which has been described in detail, previously.⁹ This instrument allows the gas phase species to be identified and their rates of formation to be measured as a function of time. The decomposition is carried out in a specially designed alumina reaction cell in which the gaseous decomposition products may exit only through an orifice whose size ranges from 2.5 μm to 1000 μm depending on the degree of confinement of the decomposition products desired. The molecules exit the cell into a high vacuum environment ($\sim 10^{-6}$ torr), are formed into a modulated molecular beam, and pass directly through the electron-bombardment ionizer of a quadrupole mass spectrometer without undergoing any further collisions with background molecules or walls of the vacuum chamber. The force due to the gas within and exiting the reaction cell (thrust and mass loss) is measured simultaneously with the mass spectra of the evolving gases. The gases are identified from the m/z values of temporally correlated groups of ion signals, from the molecular weight of the neutral molecules evolving from the cell as determined from time-of-flight velocity spectra, and by use of isotopically tagged analogues of the molecules being studied. The rates of gas formation are determined in an analysis procedure that utilizes the ion signals

measured with the mass spectrometer, the force measured by the microbalance and the flow characteristics of the reaction cell orifice. The end result of the experiments and the data analysis procedure is the rate of gas formation of each species formed during the thermal decomposition as a function of time and of pressure of the contained gases. From this information, insight into the reaction mechanisms that control the decomposition process and the kinetic rate parameters associated with the rate controlling reaction mechanisms is obtained.

Sample Preparation. The syntheses of RDX(I), HMX(II) and their isotopic analogues were described in previous papers⁴⁻⁷. ONDNTA (III) and deuterium labeled, ONDNTA-d₆, which are intermediates in the decomposition of RDX and RDX-d₆ respectively, were prepared according to previously known methods¹⁰ starting with the corresponding hexahydro-1,3,5-s-triazine analogue. The deuterated version of the hexahydro-1,3,5-s-triazine was prepared by the base catalyzed deuterium exchange method described in an earlier paper⁷. The ONDNTA samples were characterized by NMR and IR measurements that their mass spectra indicated a purity greater than 99% with ~0.25% RDX contamination. The samples melt between 165 and 170°C.

RDX and HMX decomposition.

The decomposition of both RDX and HMX is by a complex process that is controlled by multiple reaction pathways whose behavior depends on both the individual properties of the molecules themselves, as well as the physical state of the sample. The global chemical reaction pathways that control the decomposition process in the liquid phase are shown in Figure 1 for the case of RDX. Important physical processes in the decomposition of material in the solid phase are illustrated in Figure 2 for the case of HMX.

Four primary reaction pathways control the decomposition of RDX in the liquid phase between 200 and 215°C (Fig. 1). Two pathways are first order reactions solely in RDX. One of these produces predominantly OST, NO, and H₂O and accounts for approximately 30% of the decomposed RDX and the other produces predominantly N₂O and CH₂O with smaller amounts of NO₂, CO, and NH₂CHO and accounts for 10% of the decomposed RDX. The third pathway consists of formation of ONDNTA by reaction between NO and RDX, followed by the decomposition of ONDNTA to predominantly CH₂O and N₂O. The nature of the fourth reaction pathway is less certain. From our original experiments on RDX, we proposed that in the fourth pathway RDX decomposes through reaction with a catalyst that is formed from the decomposition products of previously decomposed RDX. This was based on the temporal behaviors of the gas formation rates of the decomposition products. However, from more recent experiments with the independently synthesized mononitroso analogue of RDX, ONDNTA, it appears that this fourth channel may also involve the ONDNTA intermediate. The third and fourth reaction channels each account for approximately 30% of the decomposed RDX.

Experiments with solid-phase RDX have shown that its decomposition rate is very much slower than that of liquid phase RDX. ONDNTA is the only product that appears to be formed during the early stages of the decomposition of RDX in the solid phase. As the solid-phase decomposition progresses, N₂O and lesser amounts of CH₂O start to evolve and their rates of evolution increase until products associated with the liquid-phase RDX decomposition appear and the rates of gas formation of all products rapidly increase. This behavior strongly suggests that the decomposition of solid RDX occurs through formation of ONDNTA within the lattice. Its subsequent decomposition within the lattice to N₂O and CH₂O, followed by the dispersion of CH₂O in the RDX, leads to the eventual liquefaction

of the remaining RDX and the onset of the associated liquid-phase decomposition reactions.

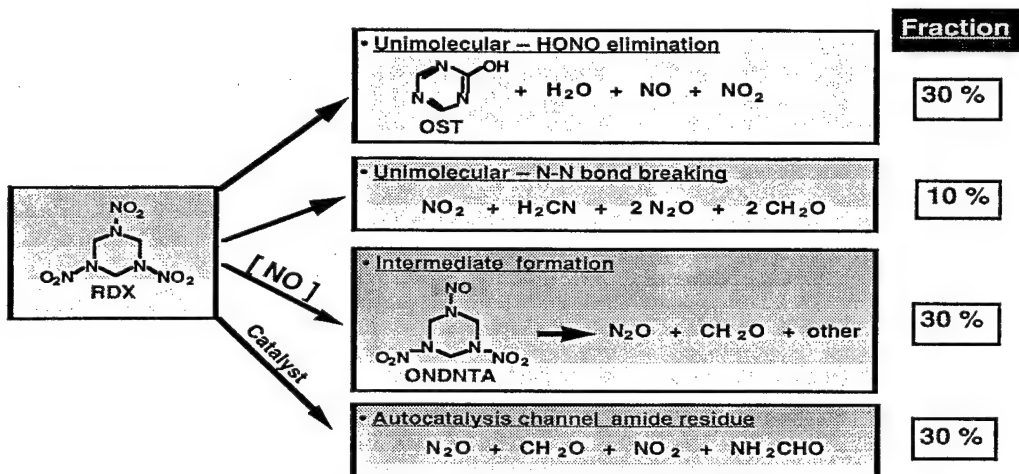


Figure 2. Decomposition pathways for RDX in the liquid phase. (Data from Ref. 6)

Physical processes also play a role in controlling the rates of thermal decomposition for HMX and RDX. A model of these physical processes, based on the identities of the decomposition products and the temporal behaviors of their gas formation rates as determined from our experiments with HMX and RDX, is illustrated in Fig. 2. An illustration of the typical observed data from the decomposition of HMX below its melting point is shown in Figure 3.

The first step in the decomposition of HMX in the solid phase is illustrated in Figure 2. As the solid HMX is heated, a quasi-equilibrium is established between the gas and solid phase HMX. During the initial period, decomposition of HMX in the gas phase occurs and the decomposition products are observed directly as the gas exits the reaction cell. Concurrently, decomposition of HMX occurs in the solid phase, first forming the mononitroso analogue of HMX, ONTNTA (IV), which then decomposes to lower molecular weight decomposition products. Both the ONTNTA and its decomposition products remain trapped within the HMX particles during the initial stages of the decomposition. These processes are illustrated in the first two diagrams in Fig. 2. These aspects of the model are based on the following results:

- 1) Gas-phase decomposition contributes to the decomposition products as can be seen from the gas formation rates of CD₂O and N₂O, shown in Fig. 3b, which are constant and proportional to the vapor pressure of HMX. The duration of the constant gas formation rate of N₂O is referred to as the induction period.
- 2) During the decomposition of RDX in the solid phase only ONDNTA and its decomposition products are observed.

HMX continues to decompose in the solid phase through the mononitroso intermediate. Decomposition of the mononitroso intermediate produces low molecular weight products, such as N₂O and CH₂O, and a polymeric product. The low molecular weight products move within and interact with the surrounding HMX lattice, to form bubbles, containing primarily N₂O, and solutions between the HMX and CH₂O, which may be localized in the volumes surrounding the bubbles. A polymeric product is also formed in the region of the bubbles and itself undergoes a thermal decomposition process yielding both lower molecular weight decomposition products and other polymeric products. Eventually, the

size and pressure within the bubbles grows, leading to cracking of the HMX particles and release of the trapped products. These aspects of the model are based on the following results:

- 1) At the end of the induction period there is a rapid rise in the rate of release from the solid of N_2O followed some time later by a rise in the rate of release of formaldehyde (CD_2O in Fig. 3). This along with similar results for decomposition of RDX in the solid phase and the fact that the mononitroso analogue of RDX forms mostly N_2O and CH_2O when decomposed under high confinement (see ONDNTA results below) strongly supports this mechanism.
- 2) At the completion of a decomposition experiment, at isothermal temperatures below the melting point of HMX, an orange-brown residue remains that retains the same shape as the original HMX particles and upon examination with transmission electron microscopy was found to be composed of broken spherical shaped shells ranging in size from $\sim 0.1 \mu m$ to $\sim 5 \mu m$. This residue is a form of polyamide that decomposes to formamide, N-methylformamide, and N,N-dimethylformamide, as well as several other lower molecular upon further heating. This supports the idea of bubble formation as well as polymerization in the decomposition process.
- 3) The fact that only 25% of the ONTNTA formed in the decomposition of HMX in the solid phase undergoes scrambling of the N-NO bond (Ref. 5) compared to 100 % of the ONDNTA in the decomposition of RDX in the liquid phase (Ref. 7) suggests that decomposition of ONTNTA in the solid phase occurs at individual sites in the lattice. After the ONTNTA decomposes at the lattice site, the lower molecular weight products disperse in the lattice to expand existing bubble sites or create new nucleation centers.
- 4) The observation of the formation of dimethylnitrosamine, $(CH_3)_2NNO$, from the decomposition of HMX in the solid phase as well as from the unusual decomposition process of ONDNTA under high confinement (see below) suggests that the mononitroso analogue of HMX plays a very important role in its decomposition in the solid phase.

The rise in the rate of decomposition after the induction period suggests an autocatalytic process, as can be seen from Fig. 3. The processes that occur in the early stages of decomposition continue but now the decomposition process is affected by the reaction of gaseous decomposition products with the remaining HMX. This effect can be seen from a comparison of the rate of decomposition, as characterized by the rate of formation of N_2O , from experiments in which the pressure of the decomposition products was varied by using reaction cell orifices with diameters of 5 and 100 μm as can be seen from the results in Figure 4. The higher pressure of contained gaseous products in the experiment with the 5 μm diameter orifice increases the rate of decomposition of the HMX sample.

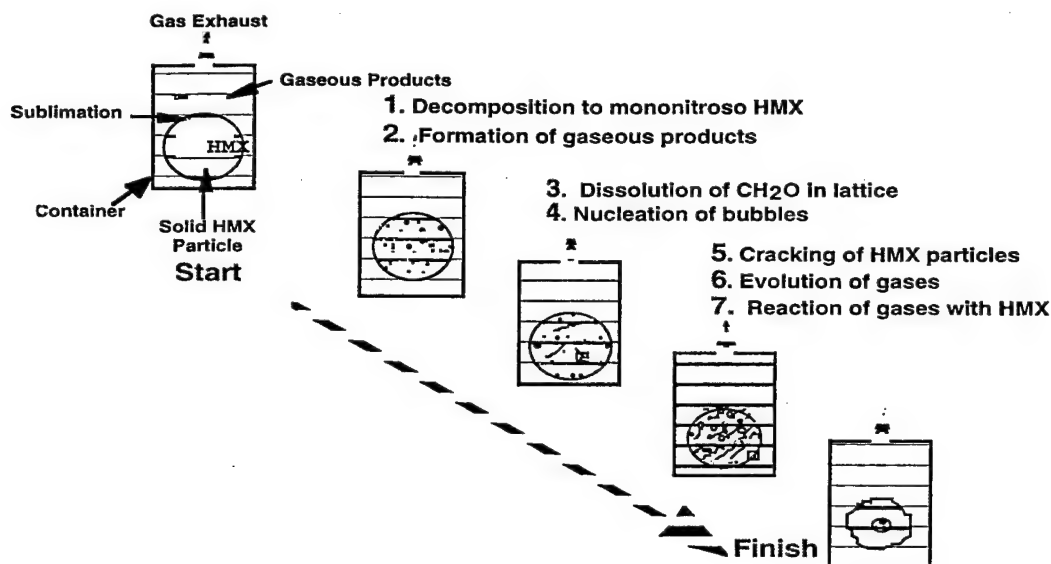


Figure 2. Schematic representation of the processes involved in the decomposition of a particle of HMX. The particle is in a container that is representative of the reaction cell used in the STMBMS thermal decomposition experiments.

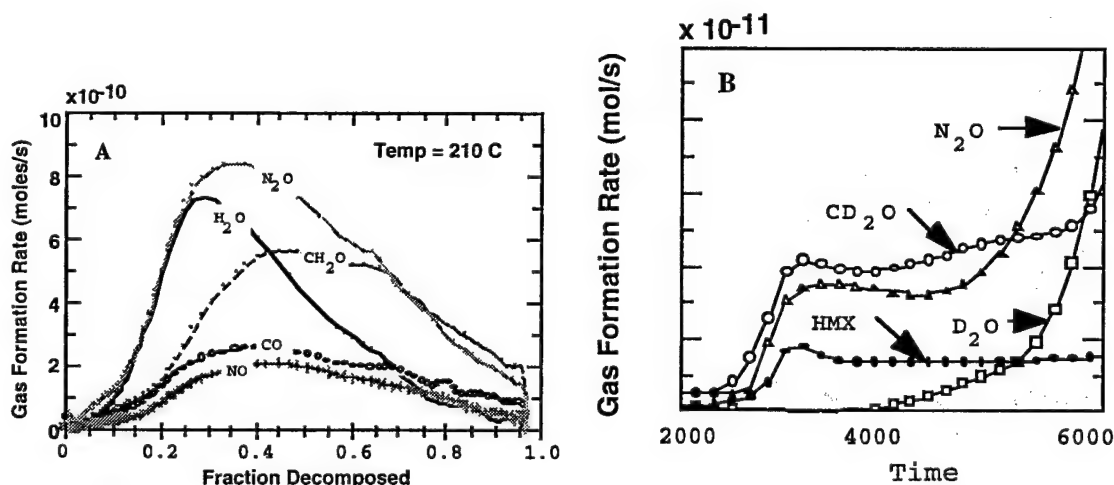


Figure 3. a) Gas formation rates of the products from the thermal decomposition of HMX at 210°C. The duration of the decomposition process is about 37000 seconds. b) Gas formation rates of thermal decomposition products from HMX-d8 during the induction period and first stage of the acceleratory period.

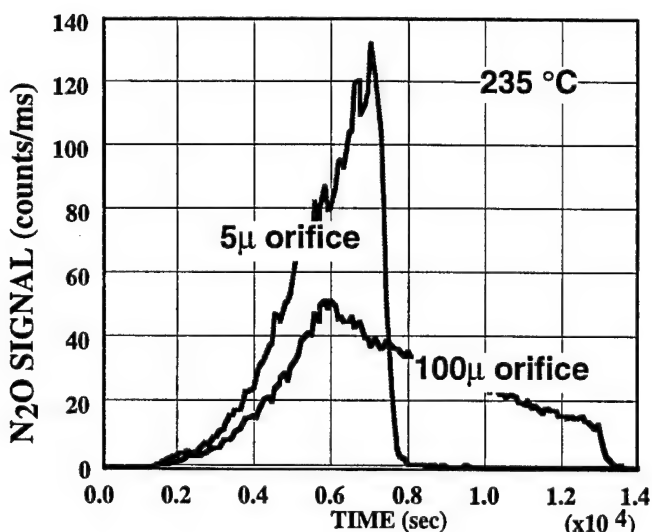


Figure 4. The effect of containment of gaseous decomposition products on the decomposition of HMX in the solid phase is illustrated with the ion signals associated with the rate of formation of N_2O formed during the decomposition in two different experiments with HMX at 235 °C and using orifice diameters of 100 μm and 5 μm .

ONDNTA decomposition

In the case of the intermediate in RDX decomposition, ONDNTA, we have been able to independently synthesize it and study its decomposition mechanisms separately.⁸ Analysis of the details of its decomposition behavior are currently underway and only a brief summary of the results are presented here. This nitramine decomposes in two separate temperature regions sequentially, one between 95 and 145 °C and the other between 155 and 210 °C. An illustration of this behavior is shown in Figure 5 for the decomposition of ONDNTA in a reaction cell with a 50 μm diameter orifice and held at two different isothermal temperatures. The major decomposition products are N_2O , CH_2O , CO/N_2 and NO_2 and the minor decomposition products include several formamides and dimethylnitrosamine, $(\text{CH}_3)_2\text{NNO}$. The products obtained from both regions are very similar to those obtained from the decomposition of HMX and RDX in the solid phase with some variation between the two channels of decomposition. Careful examination of the ONDNTA sample by IR, NMR and mass spectrometry show no evidence of any major impurity that would account for the decomposition products observed in the lower temperature channel of the decomposition. Furthermore, examination of samples that were held at temperatures associated with the lower temperature decomposition region stopped producing decomposition products and when the remaining sample was evaporated only the reactant, ONDNTA, was detected with the STMBMS. It is not understood why the decomposition stops in the intermediate temperature region. However, it is surmised that in this temperature region there is a competition between two competing processes. One is an autocatalytic process in which contained gas-phase decomposition products accelerate the decomposition process and the second is some undetectable phase transition that leads to a more stable phase of ONDNTA that is not susceptible to autocatalysis. This behavior is illustrated quite dramatically by the data shown in Figure 6 for the decomposition of ONDNTA in reaction cells with two different orifice diameters. Decomposition of ONDNTA in the experiment conducted in a reaction cell with a 5 μm diameter orifice occurs much more rapidly than in a reaction cell with a 50 μm diameter orifice. With the 5

μm diameter orifice the ONDNTA decomposes approximately 100 times as fast and the entire sample is consumed in the low temperature channel. Details of this unusual behavior of the sample and the kinetics of the decomposition will be the subject of another paper.

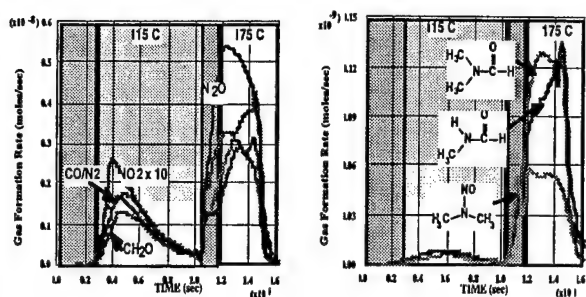


Figure 5. Gas formation rates of decomposition products from the thermal decomposition of ONDNTA in a reaction cell with a $50 \mu\text{m}$ orifice at isothermal temperatures of 115 C and 175 C .

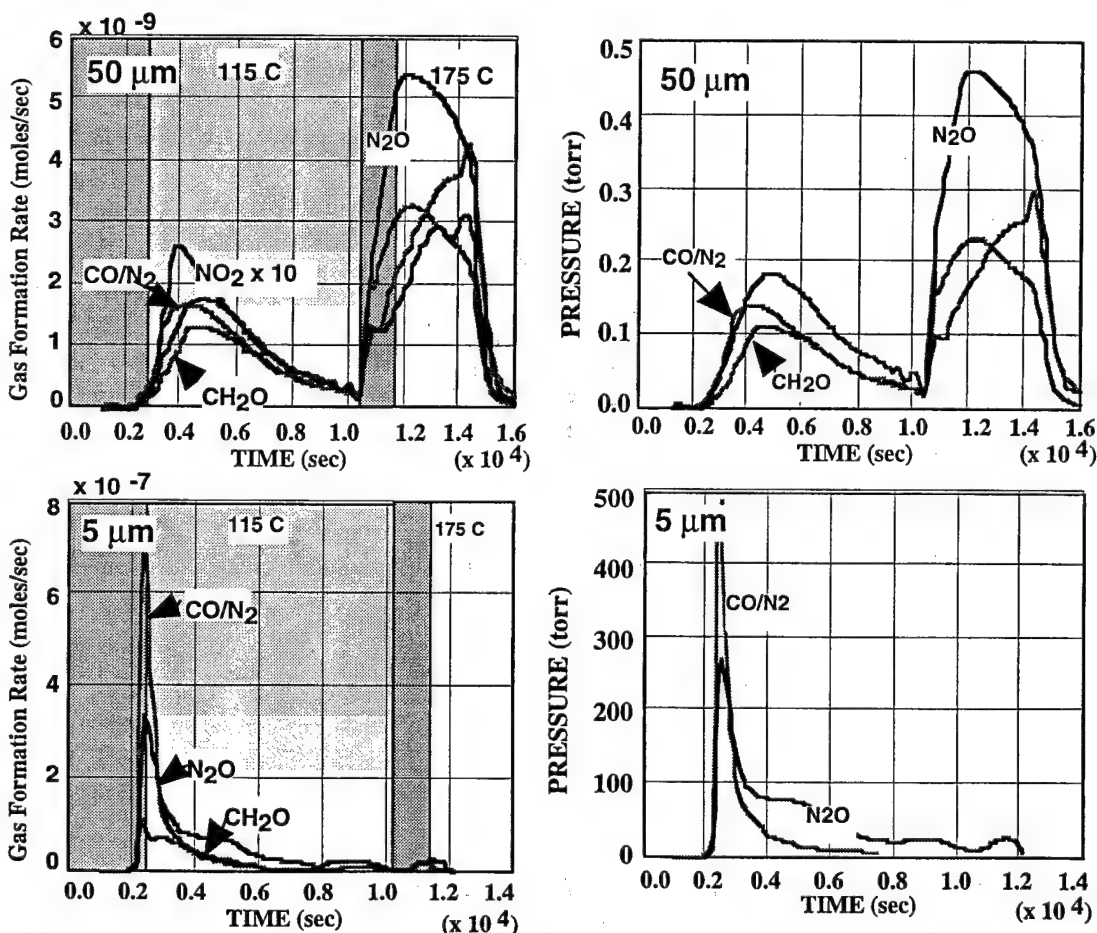


Figure 6. Comparison of the gas formation rates and partial pressures of the decomposition products formed during the thermal decomposition of ONDNTA in reaction cells with orifice diameters of $50 \mu\text{m}$ and $5 \mu\text{m}$ at isothermal temperatures of 115 C and 175 C .

175 C. The increased containment of the gaseous decomposition products in the experiment with the 5 μm diameter orifice leads to an increase in the gas formation rate of approximately 100 compared to the rates with the 50 μm orifice.

The steps in the decomposition process of ONDNTA under high confinement are apparent from the identities of thermal decomposition products and the sequence of their formation as illustrated by the data in Fig. 7. The temporal behavior of the rate of formation of the gaseous thermal decomposition products is characterized by two regions. The first region starts at approximately 110 and peaks at 125 C. The second region starts at approximately 140 and peaks at 145 C. A similar temporal behavior is observed during the decomposition of ONDNTA at isothermal temperatures in the 110 to 150 C range. Thus, it appears that the observed gaseous thermal decomposition products are formed in a series of steps and it is not necessary to increase the temperature as was done in the experiment shown in Fig. 7. The first step in the process leads to the release of CO/N_2 and NO_2 as can be seen from these signals in Fig. 7b. These two signals rise and fall sharply. The N_2O and CH_2O signals also rise sharply but decline much more gradually as can be seen from Fig. 7a. At 140 C, after approximately 70 % of the sample has decomposed, there is a rapid rise in the rate of formation of a new set of decomposition products as shown in Fig. 7c and 7d. These products include H_2O , N-methylformamide, N,N-dimethylformamide and dimethylnitrosamine. After the sample stops losing gaseous products between 5 and 10 % of the sample remains as a residue.

These results indicate that as ONDNTA decomposes it releases gaseous products and also forms a nonvolatile compound (possibly polymeric) that is relatively stable. The first step in the process may be scission of the N- NO_2 bond as evidenced by the NO_2 signal, followed immediately by loss of CO/N_2 , N_2O and CH_2O as indicated by the simultaneous rapid rise in these signals. Two different explanations may be made for the sharper decrease in the CO/N_2 and NO_2 signals compared to the N_2O and CH_2O signals. The first explanation is that the ONDNTA sample is rapidly converted to a nonvolatile product (the rate of conversion is characterized by the NO_2 or CO/N_2 signals) that then undergoes a slower decomposition to form N_2O and CH_2O . The second possible explanation is that the nonvolatile decomposition product interacts with the remaining ONDNTA, thus providing another decomposition pathway that leads to the release of N_2O and CH_2O . The fact that there is an abrupt appearance of a new set of decomposition products later in the process suggests that the first explanation may be more likely. This is based on the fact that the abrupt appearance of these new products occurs in both the thermal ramp and isothermal experiments. It suggests that the nonvolatile product formed in the initial decomposition of ONDNTA itself decomposes, releasing N_2O and CH_2O until it reaches a point at which the nonvolatile product becomes sufficiently unstable that it starts to decompose more rapidly into water, dimethylnitrosamine and the formamides. This process is quite consistent with the observed data. A discussion of details of this process will be presented in a future paper.

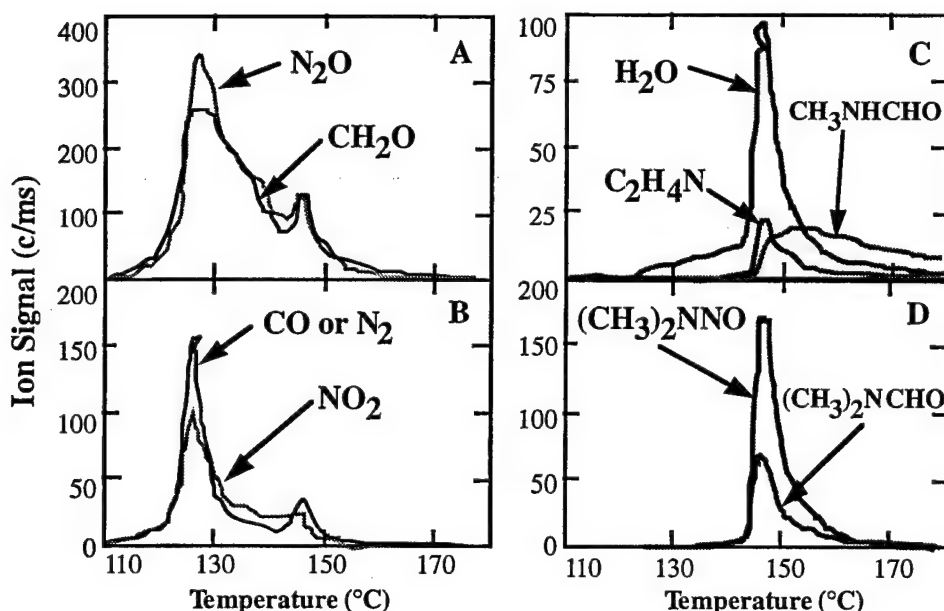


Figure 7. Ion signals formed in the mass spectrometer from thermal decomposition products from ONDNTA under conditions of high confinement. The heating rate is $2^{\circ}\text{C}/\text{min}$.

Implications of the Results from HMX, RDX and ONDNTA on the HMX Decomposition Process

The similarities between the products and their sequence of formation in the thermal decomposition of ONDNTA under high confinement conditions and the products observed in the decomposition of HMX in the solid phase are quite striking. First, the major products formed in the decomposition are the same, namely N_2O , CH_2O and CO/N_2 . Second, the products that originate from the decomposition of the nonvolatile product formed in the decomposition of ONDNTA are the same as those observed in the decomposition of HMX in the solid phase (H_2O , $(\text{CH}_3)_2\text{NNO}$, CH_3NHCHO , and $(\text{CH}_3)_2\text{NCHO}$). Third, a stable residue remains after the decomposition of both materials. One notable difference between the decomposition of these two materials is the observation of NO_2 during the decomposition of ONDNTA and the absence of NO_2 as an observed product during the decomposition of HMX. However, since HMX decomposes at higher temperatures and the process occurs within the HMX particles it is quite likely that the NO_2 reacts within the HMX particles to form NO and thus is not observed in our experiments with HMX. One other difference between the decomposition of ONDNTA and HMX is the presence of HCN in the decomposition of HMX and its absence in the decomposition of ONDNTA. Although HCN is not one of the more abundant products observed in the solid phase decomposition of HMX, its presence indicates that a pathway similar to the OST pathway observed in the liquid phase decomposition occurs during the decomposition of HMX, but with only a minor contribution. This behavior is also supported by our previous work on decomposition of HMX in the liquid phase¹¹ in which OST and products similar to OST that upon further decomposition would form HCN were observed.

From this qualitative description of the decomposition of HMX, RDX and ONDNTA, the following model of the decomposition of HMX in the solid phase can be constructed.

- 1) HMX decomposes to its mononitroso analogue at individual lattice sites within the particles.
- 2) The mononitroso analogue decomposes to gaseous products (CO/N_2 , N_2O and $\text{CH}_2\text{O}, \dots$).
- 3) The gaseous products move within and interact with the lattice. Initially the CO/N_2 and N_2O coalescing to form bubbles and the CH_2O dissolving in the HMX lattice.
- 4) Weakening of the HMX lattice due to dissolved CH_2O allows dissociation associated with liquid-phase decomposition to occur. This leads to the formation of HCN from the ring and HONO and its decomposition products, H_2O , NO and NO_2 .
- 5) Formation of the HMX mononitroso analogue, ONTNTA, and its subsequent decomposition continues. The ONTNTA now decomposes to CO/N_2 , N_2O and CH_2O and a nonvolatile product that may be polymeric. This nonvolatile product itself undergoes decomposition to CH_2O and N_2O and eventually becomes unstable and decomposes to formamides and dimethylnitrosamine. This nonvolatile product may be a catalyst for the decomposition.
- 6) The size and gas pressure within the bubbles grow eventually leading to cracking of the HMX particles and release of the gaseous products.
- 7) The gaseous products interact with the remaining HMX sample to accelerate its decomposition. The reactions responsible for this aspect of the process have not yet been determined.
- 8) Finally the HMX is depleted and a residue with polyamide characteristics remains.

This model summarizes the global chemical reaction pathways and physical processes that we believe control the decomposition of HMX in the solid phase. Clearly more work needs to be done to probe aspects of both the chemical reaction pathways, such as catalysis by gaseous decomposition products, and the physical processes, such as bubble growth and gas release from the particles. In addition, we need to develop models to accurately represent these processes so that these results may be used in models addressing issues of long-term aging and response of these materials in abnormal environments such as fires.

Summary and implications for cookoff response.

Understanding the physical and chemical changes that occur prior to ignition in energetic materials in munitions that are subjected to abnormal thermal environments is important for developing reliable models for characterizing the violence of the resulting event. Although HMX and RDX are usually but one ingredient in a propellant or explosive formulation, the results of our work on these materials indicates that several of the decomposition processes occur within the solid particles and thus should not be significantly influenced by other ingredients in the formulation. However, other aspects of the results suggest that interactions with other ingredients may be important.

The important aspects of the decomposition of HMX that may be independent of other ingredients involve the formation and decomposition of the mononitroso analogue of HMX. The formation of ONTNTA in the lattice of HMX and its subsequent decomposition to gaseous products will create more localized defects within the HMX particles, thus increasing the density of potential "hot spots" and possibly increasing the

shock or impact sensitivity. Further degradation of HMX within the particles leads to formation of bubbles within the particles and eventual fracture of the particles, creating smaller particles with more edges. This may also increase the impact or shock sensitivity of the material. As the decomposition progresses the material becomes porous as the HMX decomposes. Its pores being filled by its thermal decomposition products (i.e., N_2O , CH_2O , etc.), which still contain a large fraction of the energy originally stored in the HMX. Ignition of the material in this porous condition may lead to a more violent event.

The important aspects of the decomposition of HMX that may be dependent on other ingredients in a formulation are associated with the influence of thermal decomposition products on the rate of decomposition of HMX in an autocatalytic manner. This interaction may manifest itself by either an increase or a decrease in the rate of decomposition of HMX depending on whether the other ingredients increase or decrease the amount of the species responsible for autocatalysis. Neither the identity of the autocatalyst nor how it may interact with other components in a formulation are known at present.

Future work in this area involves developing models to represent the decomposition processes outlined in this paper and investigating the role of autocatalysis by the gaseous decomposition products.

ACKNOWLEDGMENTS

The authors wish to thank D.M. Puckett for assistance in collecting the mass spectrometry data. This work was supported by the Memorandum of Understanding between the Office of Munitions and the U.S. DOE, the U.S. Department of Energy under Contract DE-AC04-94AL85000, the U.S. Army, ARDEC, and the U.S. Army Research Office under contract 33655-CH***.

¹ McGuire, R. R. and Tarver, C.M., Seventh Symposium (International) on Detonation, NSWC MP 82-334, Annapolis, Maryland, 56 (1981).

² "Fundamentals of Solid-Propellant Combustion," Kuo, K. K. and M. Summerfield eds.; Progress in Astronautics and Aeronautics Vol. 90., p. 121, AIAA Inc., New York, NY, 1984.

³ Maienschein ***

⁴ R. Behrens, Jr.; J. Phys. Chem. **94**, 6706-6718, 1990.

⁵ R. Behrens, Jr. and S. Bulusu; J. Phys. Chem. **95**, 5838-5845, 1991.

⁶ R. Behrens, Jr. and S. Bulusu; J. Phys. Chem. **96**, 8877-8891, 1992.

⁷ R. Behrens, Jr. and S. Bulusu; J. Phys. Chem. **96**, 8891-8897, 1992.

⁸ Behrens, R. Jr., Land, T., Bulusu, S., *Proceedings of the 30th JANNAF Combustion Meeting*, Monterey, CA., November 1993.

⁹ a) Behrens, Jr., R., *Rev. Sci. Instrum.*, **1986**, 58, 451; b) Behrens, Jr. R., "The Application of Simultaneous Thermogravimetric Modulated Beam Mass Spectrometry and Time-of-Flight Velocity Spectra Measurements to the Study of the Pyrolysis of Energetic Materials." In *"Chemistry and Physics of Energetic Materials"*, Bulusu, S.N., Ed.; Proceedings of the NATO Advanced Study Institute, Vol. 309, Kluwer Academic Publishers, Netherlands, **1990**, p. 327; c) Behrens, Jr., R., *Int. J. Chem. Kinetics*, **1990**, 22, 135.

¹⁰ Brockman, F. J., Downing, D. C. and Wright, G. F., *Canadian J. of Research*, **1949**, 27B, 469.

¹¹ MRS meeting 1st

Mechanistic and Kinetic Studies of the Thermal Decomposition of TNAZ and NDNAZ*†

Kraig Anderson, Jason Homsy, and Richard Behrens
Combustion Research Facility
Sandia National Laboratories
Livermore, CA 94551

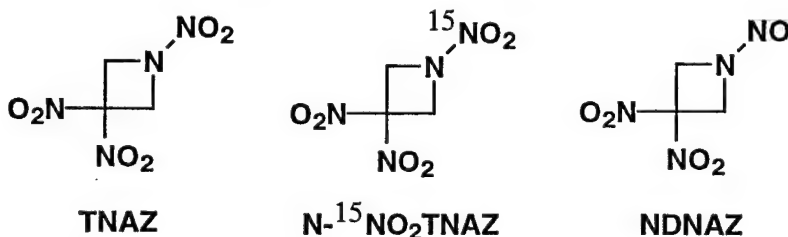
Suryanarayana Bulusu‡
Energetic Materials Division
U.S. Army Armament Research, Development and Engineering Center
Dover, NJ 07801-5001

ABSTRACT

We have studied the mechanism and detailed reaction kinetics of the thermal decomposition of 1,3,3-trinitroazetidine (TNAZ), and separately, its key decomposition intermediate, 1-nitroso-3,3-dinitroazetidine (NDNAZ), using a simultaneous thermogravimetric modulated beam mass spectrometer (STMBMS). These decompositions were conducted in a sealed alumina cell with a 2.5 μm orifice, at varying temperatures and at a range of isothermal temperatures (at 10°C intervals from 120-160°C for NDNAZ and 160-210°C for TNAZ). The gaseous products have been identified and their rates of formation have been measured as a function of time, temperature, and pressure. This system is complex, with TNAZ decomposing by four separate routes, one of which leads to NDNAZ, which itself decomposes by at least two distinct routes.

INTRODUCTION

The new energetic material TNAZ (1,3,3-trinitroazetidine),¹ alone and as a eutectic with the closely related NDNAZ (1-nitroso-3,3-dinitroazetidine), has been under serious consideration as a relatively insensitive, high energy, melt castable replacement for HMX and TNT. We therefore began a detailed analysis of the kinetics and mechanisms of their thermal decomposition behaviors in order to develop a predictive model which will be useful in planning appropriate processing, storage, and usage conditions for these new materials. Additionally, we have a great deal of interest in TNAZ as a cyclic nitramine arising from our past detailed work on RDX and HMX.²⁻¹⁶



Previous work by other groups examined TNAZ decomposition in the condensed phase, by rapid-scan Fourier transform infrared spectroscopy (RSFTIR),¹⁷ and in a molecular beam, by infrared multiphoton dissociation (IRMPD).¹⁸ Both studies showed NO₂ loss by cleavage of either the nitramine or a nitroalkane group. The condensed-phase work also indicated HNO₂ elimination and nitro-nitrite rearrangement of the nitroalkane groups. The molecular beam work suggested that the initial NO₂ cleavage was followed by ring-opening, additional NO₂ loss and then decomposition to N₂O₂ and C₃H₄. Neither study determined which, or if both, of the nitramine and nitroalkane groups were responsible for the initial NO₂ cleavage. It is unclear whether the unimolecular processes operant in the molecular beam environment also control decomposition in higher pressure environments, or if bimolecular processes are important. Also, in the condensed phase study, the existence of the nitro-nitrite rearrangement was uncertain, and the observation of HONO suggested the possibility of an alternative decomposition pathway to NO₂ cleavage.

* Approved for public release; distribution is unlimited.

† Work supported by the Army Research Office, a Memorandum of Understanding between the U.S. Department of Energy and the Office of Munitions and by the U.S. Department of Energy under contract DE-AC04-94AL85000.

‡ Deceased.

In preliminary work reported previously,^{19, 20} we identified the major liquid/gas phase thermal decomposition products of TNAZ. One important new product we observed is its nitroso analog, NDNAZ, which we anticipated based on our previous observations of nitroso analogs formed in the decomposition of other cyclic nitramines such as HMX and RDX. We also reported the major thermal decomposition products of independently-synthesized NDNAZ, and, using N-¹⁵NO₂ labelled TNAZ, showed that NO₂ loss occurs at both possible sites with cleavage of the weaker nitramine bond preceding that of the gem-dinitroalkane group. Here we report additional mechanistic details, improved experimental techniques, gas formation rates of major decomposition species versus time, and a novel autocatalytic behavior displayed by a polymeric decomposition residue.

EXPERIMENTAL

The experiments for this report were conducted using our Simultaneous Thermogravimetric Modulated Beam Mass Spectrometer (STMBMS), which we have described in detail previously.²¹⁻²³ Briefly, samples of energetic material (ca. 5-15 mg) are loaded into an alumina reaction cell (internal volume ~ 0.25 cc) containing a "splash" baffle and capped with a supported gold foil disk with a small orifice. The orifice size can be varied to choose the amount of containment of evaporated TNAZ/NDNAZ and evolved gaseous decomposition products. The cell is loaded onto a thermocouple probe attached to the arm of a microbalance. The reaction cell is surrounded by a tubular alumina furnace shell wrapped with a bifilar-wound tungsten wire heating element. During an experiment, the chamber is evacuated to ~1 X 10⁻⁶ Torr. The effluent from the cell undergoes an isentropic expansion, passes through two beam-defining orifices located in a differentially-pumped vacuum chamber, and is chopped by a rotating, toothed wheel. This modulated beam enters a quadrupole mass spectrometer, which gains a considerable improvement in the signal-to-noise ratio by subtracting the background signal from the signal of the free beam. Ions are generated in the mass spectrometer by electron impact at an energy of ~20 eV, less than the typical ~70 eV in order to reduce the contribution of ion fragmentation due to electron impact. Mass spectra, weight loss, and temperature data are collected versus time. By correlating the ion signals with the force measured by the microbalance, the concentration and formation rate of each gaseous decomposition product can be determined.

We have made several improvements in our experimental design. We have extended the range of gas containment, going down to orifice sizes as small as 2.5 μm. The gold orifice disk is compressed on top of an O-ring residing in a recessed groove in the tapered alumina cap, and a light coat of silicone vacuum grease seals the tapered joint between the cap and the cell; no significant weight loss or ion signal contribution due to the silicone grease is observed in the temperature range of this study. Under these conditions pressures exceeding 1000 Torr can be achieved during a NDNAZ or TNAZ experiment.

The flow through such small, irregularly shaped channels is not amenable to an analytic description. We have dealt with this in the past for larger orifices by calibrating the weight loss and ion signal of a naphthalene evaporation experiment to literature vapor pressure data. These calibrations, however, are time consuming and thus impractical for continuing surveillance of orifice flow characteristics which can change dramatically upon deposition of a miniscule amount of material. Therefore, we devised a rapid flow test, separate from the STMBMS, consisting of a measured, minimum volume, stainless steel dummy cell equipped with a pressure transducer and appropriate valving. A known amount of N₂ is applied to one side of the orifice and an active vacuum to the other. The pressure drop as the N₂ flows through the orifice is measured versus time. From this, the relationship between flow rate and pressure is determined, and furthermore, the question of whether the flow characteristics of a particular orifice have changed after an experiment can be answered. One naphthalene calibration experiment is run for each 2.5 μm orifice and is assumed valid as long as the N₂ flow tests for that orifice do not vary significantly.

The extent of gas containment is determined by the flow characteristics of the orifice (which vary among orifices of the same nominal size), the free volume of the cell (fixed in this study), and the leak rate of the cell. For 2.5 μm experiments, we demand the leak rate at a cell pressure of 1000 Torr, measured before and after the experiment with a helium leak detector, be less than 1% of the flow rate through the orifice. Typical flow rates at 1000 Torr for nominally 2.5 μm orifices range from 4.0-9.0 X 10⁻⁸ mol/s. Cell leak rates of 2.0 X 10⁻¹⁰ mol/s are routinely achievable and cells with a carefully matched cap can have rates as low as 5 X 10⁻¹² mol/s. These rates are usually the same or smaller after an experiment; in rare cases where the cell seal fails, there are obvious residue streaks around the cap.

Successful use of the 2.5 μm orifices is quite challenging. They are actually channels rather than point orifices (the gold foil is 25 μm thick), and are quite rough compared to their diameter (Figure 1). Because the volume of the orifice channel is only $\sim 5 \times 10^{-10} \text{ cm}^3$, full obstruction of the orifice would require only a few picomoles or roughly $1/10^7$ of a typical sample! Considering that most of the materials we study are prone to forming intractable polymeric residues, it is quite remarkable these orifices are useful at all.

Syntheses of TNAZ and $^{15}\text{NO}_2$ -TNAZ have been previously described.^{19, 20} Samples of NDNaz were obtained from M. Hiskey at Los Alamos National Laboratory. A final purification to remove adsorbed water and small amounts of other volatile impurities was performed by holding the reactions at an initial isotherm of 100°C for 3000-5000 seconds.

Data analysis and quantification techniques have been described in detail elsewhere.²¹⁻²³ In our earlier report, we described preliminary decomposition experiments primarily conducted with a linear heating ramp and a few high temperature, isothermal experiments. The interpretations were based on the raw ion signal data, which can be misleading because the absolute ion signals depend on the ion formation probabilities of the parent molecules. Here we present data from isothermal experiments conducted at 10°C increments spanning 120-160°C for NDNaz and 160-210°C for TNAZ. The raw data have been corrected to reflect the relative ion formation probabilities of the species measured.

RESULTS AND DISCUSSION

TNAZ DECOMPOSITION

Previously we reported the major decomposition products of TNAZ were NO and NO_2 , based on ion signal intensities. We find that NO and NO_2 are still major decomposition products after adjusting for relative ion formation probabilities, although the latter's importance is substantially reduced, especially at higher temperatures. This adjustment also reveals a more significant role for products such as H_2O and CO/N_2 , and to a lesser extent $\text{CO}_2/\text{N}_2\text{O}$, HCN, and CH_2O . At low temperatures, the major initial product is NO_2 (Figure 2). At higher temperatures, the relative amount of NO_2 is decreased and the relative amount of NO is increased. At higher temperatures, H_2O , CO/N_2 , $\text{CO}_2/\text{N}_2\text{O}$, and HCN also become more important (not shown). A smaller, yet significant product is the N-nitroso analog of TNAZ, NDNaz (Figure 3). On increasing temperature, its amount and gas formation rate decrease relative to the other products, which is reasonable since it decomposes much more readily than TNAZ. The time evolution changes, however, with the initial gas formation rate rising earlier with increasing temperature, following the increase in NO. Also notable are small increases in the gas formation rates of several decomposition products following the increase in NDNaz, which correspond to products of its decomposition.

Experiments using N- $^{15}\text{NO}_2$ labeled TNAZ show both isotopes are represented in NO and NO_2 , proving they are from both the nitramine and the gem-dinitroalkane sites (Figure 2). Because their gas formation rates, though similar at low temperatures, are not perfectly correlated and diverge further with increasing temperature, they must be generated by different reaction pathways. The relative gas formation rates of $^{15}\text{NO}_2$ are much greater than for $^{14}\text{NO}_2$, starting at a ratio of approximately 16:1 at 160°C and decreasing to about 6:1 at 210°C. As this ratio decreases with elevated temperature, the gas formation rate of ^{15}NO increases, particularly the initial rate. At low temperatures, the ^{14}NO gas formation rate is about 20% greater than for ^{15}NO over the course of the decomposition, with similar (though not perfectly correlated) time evolutions for each showing a gradual decline from the initial peak rate. At 210°C, the initial formation rate of ^{15}NO is nearly double that of ^{14}NO but decreases fairly rapidly, contrary to the ^{14}NO rate which increases more slowly and holds relatively constant for some time after reaching its peak. These behaviors indicate the first decomposition step is cleavage of the nitramine $^{15}\text{NO}_2$ group. This is followed by a temperature sensitive decomposition of the free $^{15}\text{NO}_2$, generating most or all of the observed ^{15}NO . In contrast, relatively little $^{14}\text{NO}_2$ arises from the gem-dinitroalkane group at any temperature. Because there is still a considerable amount of ^{14}NO , however, it must be produced by mechanisms other than free $^{14}\text{NO}_2$ decomposition. The primary mechanism is probably nitro-nitrite rearrangement of the gem-dinitroalkane followed by decomposition to ^{14}NO , CO_2 , and other fragments.

Also interesting is the lack of correlation between the ^{15}NO -NDNAZ and ^{14}NO -NDNAZ (Figure 3). These are somewhat similar at low temperatures, but at higher temperatures they become quite different, with the ^{15}NO -NDNAZ formation rate rising significantly earlier in the course of the decomposition. The difference is not as great as that between ^{14}NO and ^{15}NO but the two sets of products do compare. Because the ^{15}NO -NDNAZ rate decreases as ^{15}NO decreases while the ^{14}NO -NDNAZ drops when the TNAZ signal drops, we surmise that NDNAZ formation is dependent on NO concentration, and furthermore, it occurs primarily by a direct displacement of the nitramine- NO_2 group by NO.

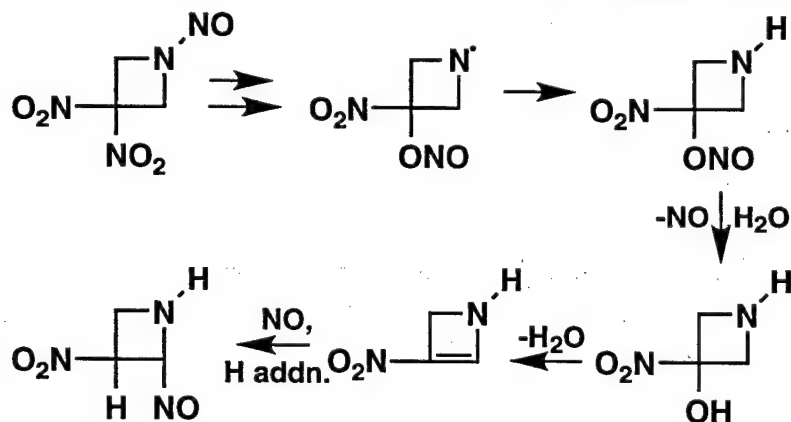
NDNAZ DECOMPOSITION

We also performed a series of experiments using independently synthesized NDNAZ. The number of pathways important in NDNAZ decomposition seems to be less than for TNAZ, though the entire process is still complex. The product mix is substantially different, however, and the decomposition, which proceeds more readily, also exhibits a dramatic autocatalytic effect.

The major product is again NO, which must come from both the nitrosamine and the gem-dinitroalkane sites because more than one equivalent of NO is released (Figure 4). Although we have not examined labeled NDNAZ, several observations point to nitrosamine cleavage as the likely dominant source of NO in the initial, precatalysis phase. First, the nitrosamine bond is weaker than the gem-dinitroalkane bond. Second, simple cleavage is sufficient to release NO from the nitrosamine site, whereas a more complicated (and presumably slower) pathway is required to generate NO from the gem-dinitroalkane site. Third, low levels of NO_2 show nitroalkane cleavage followed by decomposition to NO (probably the simplest potential route to NO from the gem-dinitroalkane) is not an important reaction, which is also consistent with observations of TNAZ decomposition. Fourth, because the gas formation rate of NO is greater relative to other low molecular weight products in the initial phase, it must be dominated by a process like nitrosamine cleavage which releases NO and a high molecular weight, low volatility species.

The advent of pathways generating low molecular weight products in addition to NO are consistent with the increasing importance of low molecular weight gaseous products relative to NO in the catalysis phase. An obvious candidate is a pathway involving nitro-nitrite rearrangement as observed in TNAZ decomposition, which generates CO_2 and other products upon releasing NO.

A minor, but significant product due to its high molecular weight, is observed at m/z 131. One plausible route to a product at m/z 131 is shown in Scheme 1. Initial steps involve nitrosamine cleavage, hydrogen addition, and at least one nitro-nitrite rearrangement. The key step is the decomposition of an alkyl nitrite to NO and the corresponding alcohol in the presence of water. Elimination to the alkene is next, followed by NO addition to the double bond and another hydrogen addition to give a $m/z = 131$ species. The actual sequence of steps may vary, and there is as yet no direct proof of the structure at m/z 131. Given the the high concentrations of NO and H_2O , however, and that nitrosamine cleavage and nitro-nitrite rearrangements are already favored, we feel this scheme is reasonable. Future studies will use isotopically labeled NDNAZ to further investigate this mechanism.



Scheme 1: Possible reaction path leading to a species at m/z 131.

The key feature of NDNaz decomposition is the autocatalysis exhibited after an initial induction period. This leads to a substantial rise in gas formation rates, nearly 400% in the case of NO formation at a 150°C isotherm. We have observed similar behavior for other compounds, which like NDNaz, form polymeric residues. Proof of the catalytic activity of the polymer residue is given by an experiment (Figure 5) where fresh NDNaz was added to the residue-coated cell from a prior NDNaz decomposition. Upon heating to the same isotherm, formation rates of the decomposition products rose almost immediately to the high rates seen near the end of the catalysis phase of the previous experiment.

Is this residue a general catalyst or specific to NDNaz? The TNaz decomposition experiments show a slight rise in product formation rates near the end. This rise is due at least to NDNaz decomposition. It is possible that residue-catalyzed NDNaz and TNaz decomposition also contribute to this feature. It is also true, however, that TNaz forms much less residue than NDNaz, so there may not be enough to have a clear effect. An obvious future experiment is to add fresh TNaz to a cell coated with NDNaz residue.

In this sort of catalysis, one likely controlling feature is surface area. When we required samples of these intractable residues for elemental analysis, we tried adding clean, microscopic (~100 µm) glass beads to the reaction cell, hoping the residue would coat the beads and could then be easily removed from the cell. Although effective for its intended purpose, this also led to observable autocatalysis in *both* TNaz and NDNaz decompositions; furthermore, the effect was much more dramatic than in experiments without glass beads (Figure 6). Certainly, simply increasing available surface area can give a catalytic effect. When the rate of catalysis (in an isothermal experiment) increases with the reaction progress, however, it clearly indicates the role of an accumulating product, the definition of autocatalysis. The increase in the catalytic effect compared to experiments without beads suggests the beads serve at least to increase the surface area available for a catalytic residue, but does not rule out a participating catalytic role for the surface of the beads.

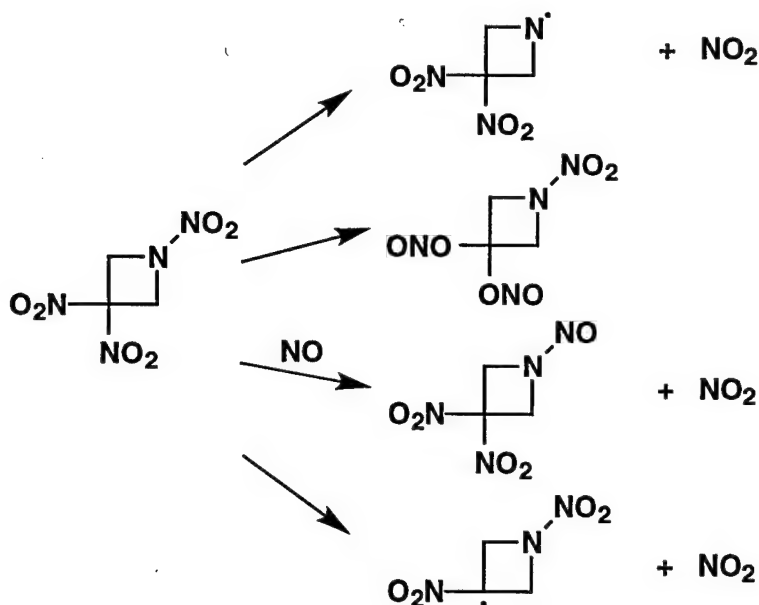
One feature shown by both TNaz and NDNaz is duration of product evolution after the parent molecule is depleted (Figure 7). At low temperatures, product evolution drops almost as soon as the parent is depleted. At higher temperatures, products continue to evolve after depletion. This indicates the formation of less volatile, higher MW products, such as the polymeric residue, or containment of volatile products within the residue. Consistent with the amount of polymeric residue formed for each material, the continued evolution of products after depletion is more important in NDNaz decomposition than in TNaz decomposition.

TNAZ DECOMPOSITION PATHWAYS

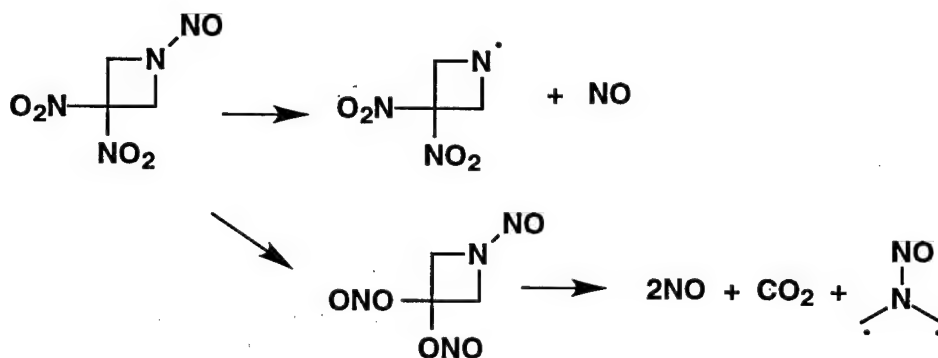
The basic framework of TNaz decomposition is shown below (Scheme 2). Clearly, the first and most important step is cleavage of the nitramine bond, releasing NO₂ and the 3,3-dinitroazetidiny radical. Cleavage of a gem-dinitroalkane occurs, but to a substantially lesser degree. Another important route is the nitro-nitrite rearrangement. All of these routes lead to NO formation, which in turn leads to a direct displacement of the nitramine NO₂ groups on remaining TNaz molecules. Another possible path is elimination of HONO/HNO₂ (not shown), but this does not seem to be an important pathway.

NDNAZ DECOMPOSITION PATHWAYS

There are two likely first steps for the decomposition of NDNaz. The first involves cleavage of the nitrosamine bond, which as discussed before, is probably the dominant process in the initial, precatalysis phase. The other likely pathway begins with the nitro-nitrite rearrangement. Because the amount of NO relative to the other decomposition products is much larger than in the TNaz decomposition, in fact larger than can be accounted for by nitrosamine cleavage, it suggests some feature of NDNaz or its decomposition environment favors the nitro-nitrite rearrangement, most likely the catalytic polymeric residue. This can be tested by decomposing fresh TNaz in the presence of the polymeric residue; if true, the relative amounts of NO production would be much higher than for TNaz decomposition alone. Other possible first steps, such as direct NO₂ cleavage or HONO/HNO₂ elimination, may be present in small amounts but are not major contributors according to the data.



Scheme 2: Major TNAZ decomposition pathways



Scheme 3: Major NDNAZ decomposition pathways

FUTURE WORK

Work continues on this system to complete collection of quantitative data and address a few more mechanistic details, such as the structure, formation, and activity of the catalytic polymer residue from NDNAZ. Time-of-flight velocity spectra will be employed to identify which minor peaks are actually products and not fragments of parent molecules created by electron impact ionization in the quadrupole mass spectrometer employed in this study. This information will be folded into a global decomposition model incorporating the different reaction pathways, the quantified data, and the gas formation rates.

SUMMARY

The major products formed in the decomposition of TNAZ are NO_2 and NO , with lesser amounts of H_2O , HCN , CO/N_2 , $\text{CO}_2/\text{N}_2\text{O}$, NDNAZ, and a small amount of polymeric residue. The results indicate four likely steps for the first step in the TNAZ decomposition. Three of these generate NO_2 , either by unimolecular cleavage of a nitramine or nitroalkane, or by displacement of the nitramine NO_2 by NO , while the fourth involves a nitro-nitrite rearrangement of the gem-dinitro group (elimination of HNO_2 occurs, but is relatively small). The unimolecular fragmentation pathways are supported because NO_2 generation is initially first order in TNAZ concentration in both liquid and gas phases (additional sources of NO_2 must exist because its signal does not decrease as TNAZ nears

depletion). Experiments using $1\text{-}^{15}\text{NO}_2\text{-TNAZ}$ show NO_2 evolution from both sites in the molecule, though occurring first at the weaker nitramine bond; and also indicate, by lack of isotopic shifts, that signals at m/z 28 and 44 are mostly CO and CO_2 rather than N_2 and N_2O . The observation that the rates of formation of NO_2 , NO, and NDNAZ increase sequentially indicates NDNAZ is formed by direct replacement of the nitramine NO_2 in TNAZ by NO. This and the nitro-nitrite pathway are also suggested because CO_2 , NO, CO/N_2 , HCN, CH_3CN , and NDNAZ do not correlate with the first-order NO_2 cleavage. Evolution of $\text{CO}_2/\text{N}_2\text{O}$, NO, HCN, and CO/N_2 after TNAZ depletion indicates they are thermal decomposition products of NDNAZ.

The decomposition of independently synthesized NDNAZ provides further clues to the overall decomposition process. The major product in the decomposition of NDNAZ is NO, followed by lesser amounts of H_2O , HCN, CO/N_2 , $\text{CO}_2/\text{N}_2\text{O}$, and a significant amount of polymeric residue, which actually catalyzes NDNAZ decomposition. While these products are similar to those formed in the TNAZ decomposition, their ratios differ significantly. There are two likely first steps for the decomposition of NDNAZ, either cleavage of the N-nitroso group to form NO and 3,3-dinitroaziridiny radical, or nitro-nitrite rearrangement of the gem-dinitro group. Because more than one equivalent of NO is evolved, a nitro-nitrite rearrangement as in the second path almost certainly occurs.

The results of our experiments confirm loss of NO_2 as one of the first steps in TNAZ decomposition, as discovered in RSFTIR and IRMPD experiments by other groups, and furthermore, show that the NO_2 arises from both possible sites. Contrary to the RSFTIR experiments, however, HNO_2 elimination is relatively unimportant. We find once again that a mononitroso analog (NDNAZ) is an important intermediate in nitramine decomposition, as we have shown previously for RDX, TNCHP, and HMX.

Several significant improvements have been made to our experimental protocol, allowing the effective use and characterization of $2.5\text{ }\mu\text{m}$ diameter orifices, despite their inherent difficulties. With these improvements, quantification of our data is more reliable. Coupled with kinetic, mechanistic, and physical information on these decompositions, this will provide the foundation to develop a detailed mathematical model of the decomposition processes of TNAZ and NDNAZ.

ACKNOWLEDGMENTS

We thank D.M. Puckett for collecting the mass spectrometry data and to Dr. Michael Hiskey for providing the 2,4-DNI sample. Work is supported by the Army Research Office, a Memorandum of Understanding between the DoD Office of Munitions and the Department of Energy under Contract DE-AC04-94AL85000, and by the U.S. Army, ARDEC.

REFERENCES

1. T. G. Archibald, R. Gilardi, K. Baum, *et al.*, *Journal of Organic Chemistry* **55**, 2920 (1990).
2. R. Behrens, Jr. and S. Bulusu, *Journal of Physical Chemistry* **96**, 8891-8897 (1992).
3. R. Behrens, Jr. and S. Bulusu, *Journal of Physical Chemistry* **96**, 8877-8891 (1992).
4. R. Behrens, Jr. and S. Bulusu, in *29th JANNAF Combustion Meeting* (Chemical Propulsion Information Agency, Langley, Virginia, 1992).
5. R. Behrens, Jr. and S. Bulusu, *Journal of Physical Chemistry* **96**, 8891-8897 (1992).
6. R. Behrens, Jr. and S. Bulusu, *Journal of Physical Chemistry* **96**, 8877 - 8891 (1992).
7. R. Behrens, Jr. and S. Bulusu, *Journal of Physical Chemistry* **95**, 5838 (1991).
8. R. Behrens, Jr. and S. Bulusu, *Journal of Physical Chemistry* **95**, 5838-5845 (1991).
9. R. Behrens, Jr., *Journal of Physical Chemistry* **94**, 6706-6718 (1990).
10. R. Behrens, Jr., *International Journal of Chemical Kinetics* **22**, 159-173 (1990).
11. R. Behrens, Jr., *International Journal of Chemical Kinetics* **22**, 135-157 (1990).

- 12 R. Behrens, in *Chemistry and Physics of Energetic Materials*, edited by S. N. Bulusu (Kluwer Academic Publishers, Dordrecht, The Netherlands, 1990), Vol. 309, p. 347.
- 13 R. Behrens, Jr., *International Journal of Chemical Kinetics* **22**, 159 (1990).
- 14 R. Behrens, Jr., in *23rd JANNAF Combustion Meeting* (Chemical Propulsion Information Agency, 1986), Vol. 457, p. 231.
- 15 R. Behrens, Jr., in *24th JANNAF Combustion Meeting* (Chemical Propulsion Information Agency, Monterey, California, 1987), Vol. 476, p. 333-342.
- 16 R. Behrens, *Journal of Physical Chemistry* **94**, 6706 (1990).
- 17 Y. Oyumi and T. B. Brill, *Combustion and Flame* **62**, 225-231 (1985).
- 18 D. S. Anex, J. C. Allman, and Y. T. Lee, in *Chemistry of Energetic Materials*, edited by G. A. Olah and D. R. Squires (Academic Press, 1991), p. 27 - 54.
- 19 R. Behrens and S. Bulusu, *Defence Science Journal (India)* **46**, 361 - 369 (1996).
- 20 R. Behrens and S. Bulusu, in *32nd JANNAF Combustion Subcommittee Meeting* (CPIA Publication #638, Huntsville, AL, 1995), Vol. 1, p. 1 - 11.
- 21 R. Behrens, Jr., *Review of Scientific Instruments* **58**, 451 (1986).
- 22 R. Behrens, Jr., *Review of Scientific Instruments* **58**, 451-461 (1987).
- 23 R. Behrens, Jr., in *Chemistry and Physics of Energetic Materials*, edited by S. N. Bulusu (Kluwer Academic Publishers, Netherlands, 1990), Vol. 309, p. 327.

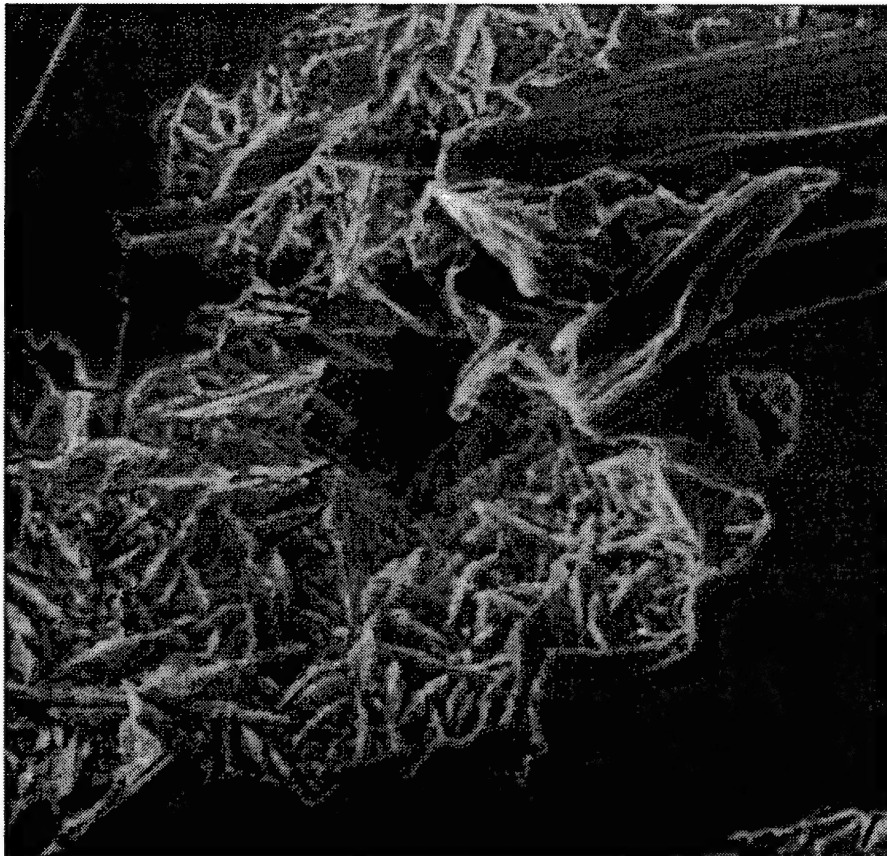
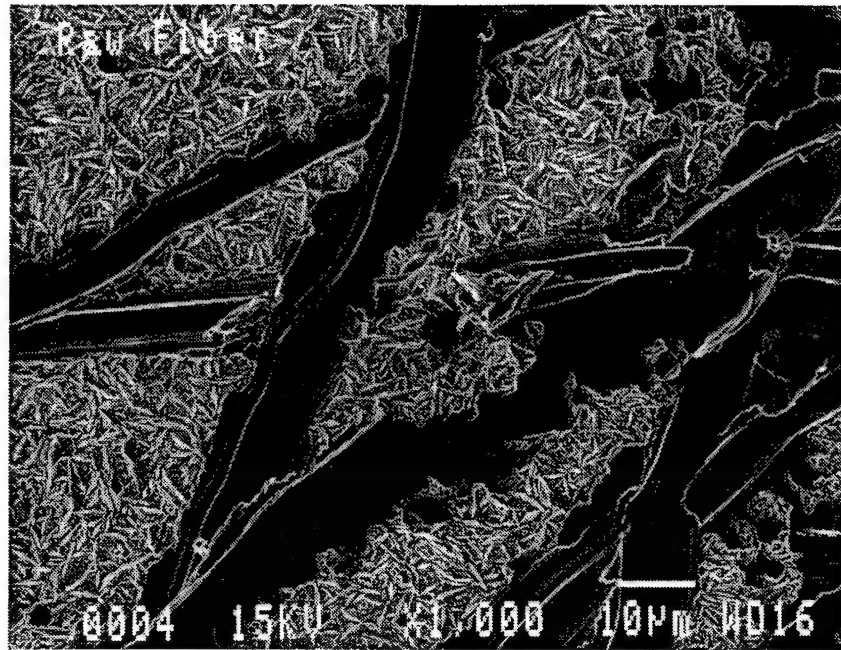


Figure 1: Electron microscope pictures of a 2.5 μm orifice disk. Top (1000X): The orifice is the dark spot in the center, framed by smooth dark bands. These bands are mechanical scratches made to assist location of the orifice under a light microscope. Bottom: Same orifice, higher magnification. The orifice is quite rough and irregular compared to its diameter. The gold in the undisturbed areas appears semicrystalline.

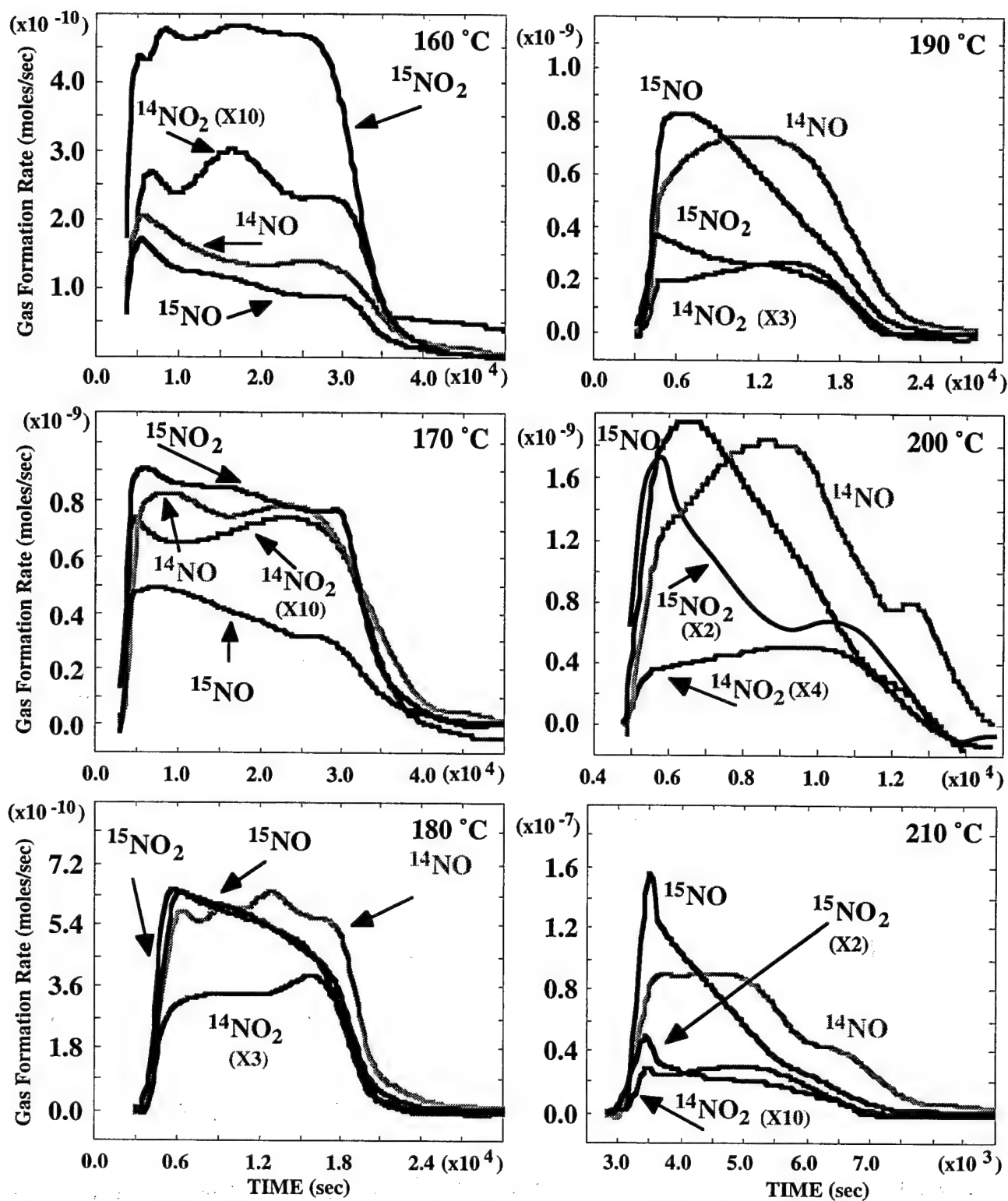


Figure 2: Gas formation rates for ^{14}NO , ^{15}NO , $^{14}\text{NO}_2$, and $^{15}\text{NO}_2$ in $\text{N-}^{15}\text{NO}_2$ labeled TNAZ at isotherms from 160-210°C. Initially, $^{15}\text{NO}_2$ dominates. Overall, $^{14}\text{NO}_2$ lags $^{15}\text{NO}_2$ slightly. At high temperature, $^{14}/^{15}\text{NO}$ dominates, with ^{15}NO significantly preceding ^{14}NO .

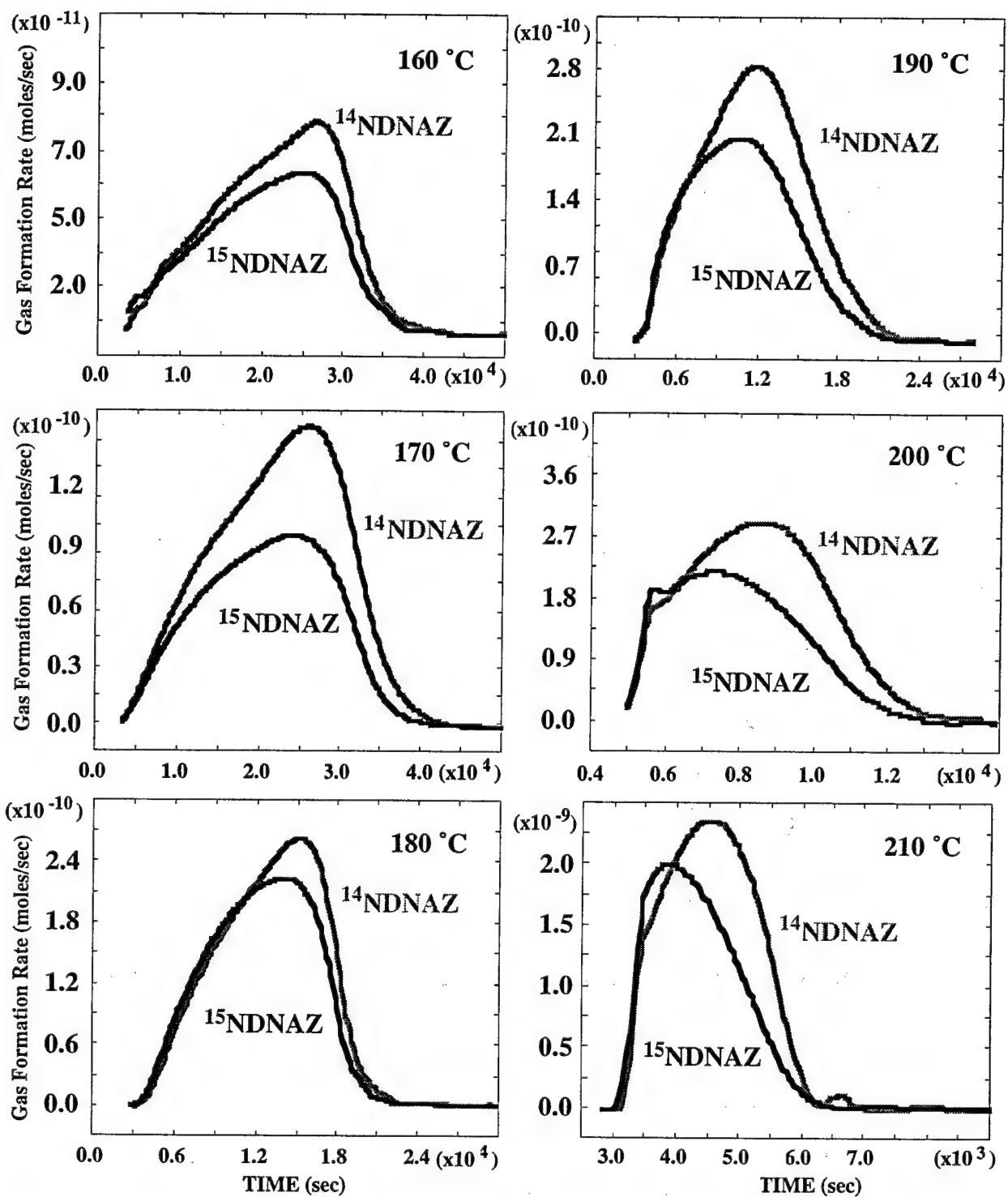


Figure 3: ¹⁵NDNAZ and ¹⁴NDNAZ formation in N-¹⁵NO₂ labeled TNAZ decomposition. Note differing time behaviors. Also, as temperature increases, ¹⁵NDNAZ formation begins to precede ¹⁴NDNAZ formation.

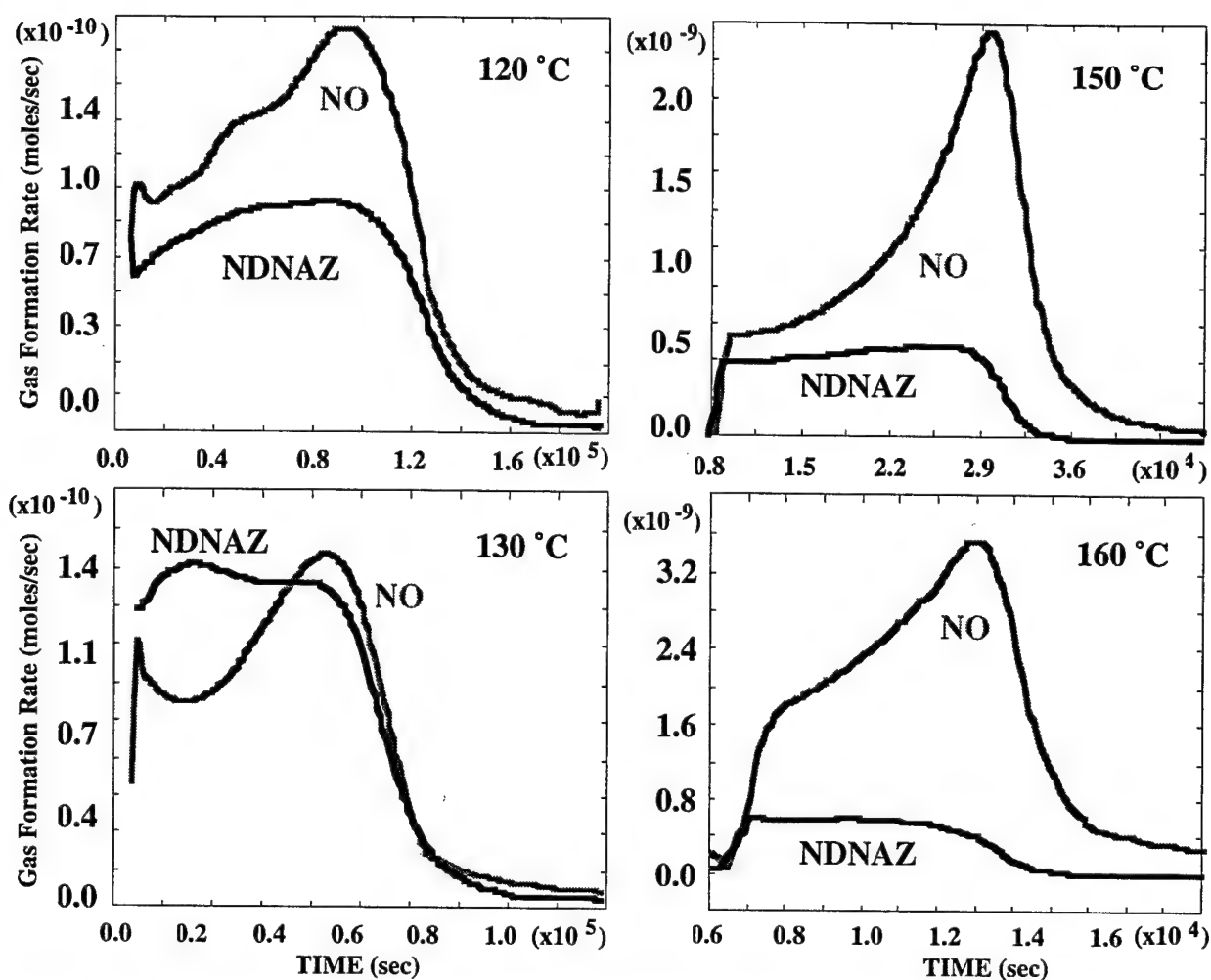


Figure 4: NO formation by decomposition of pure, independently synthesized NDNAZ. NO dominates at higher temperatures, indicating greater decomposition. The nonlinear increase in the NO rate over time is evidence of autocatalysis by the polymeric residue. More catalytic effect is evident in the 150°C experiment compared to the 160°C experiment because the 160°C sample is smaller (to avoid orifice blockage), and the NDNAZ is depleted before much residue is created.

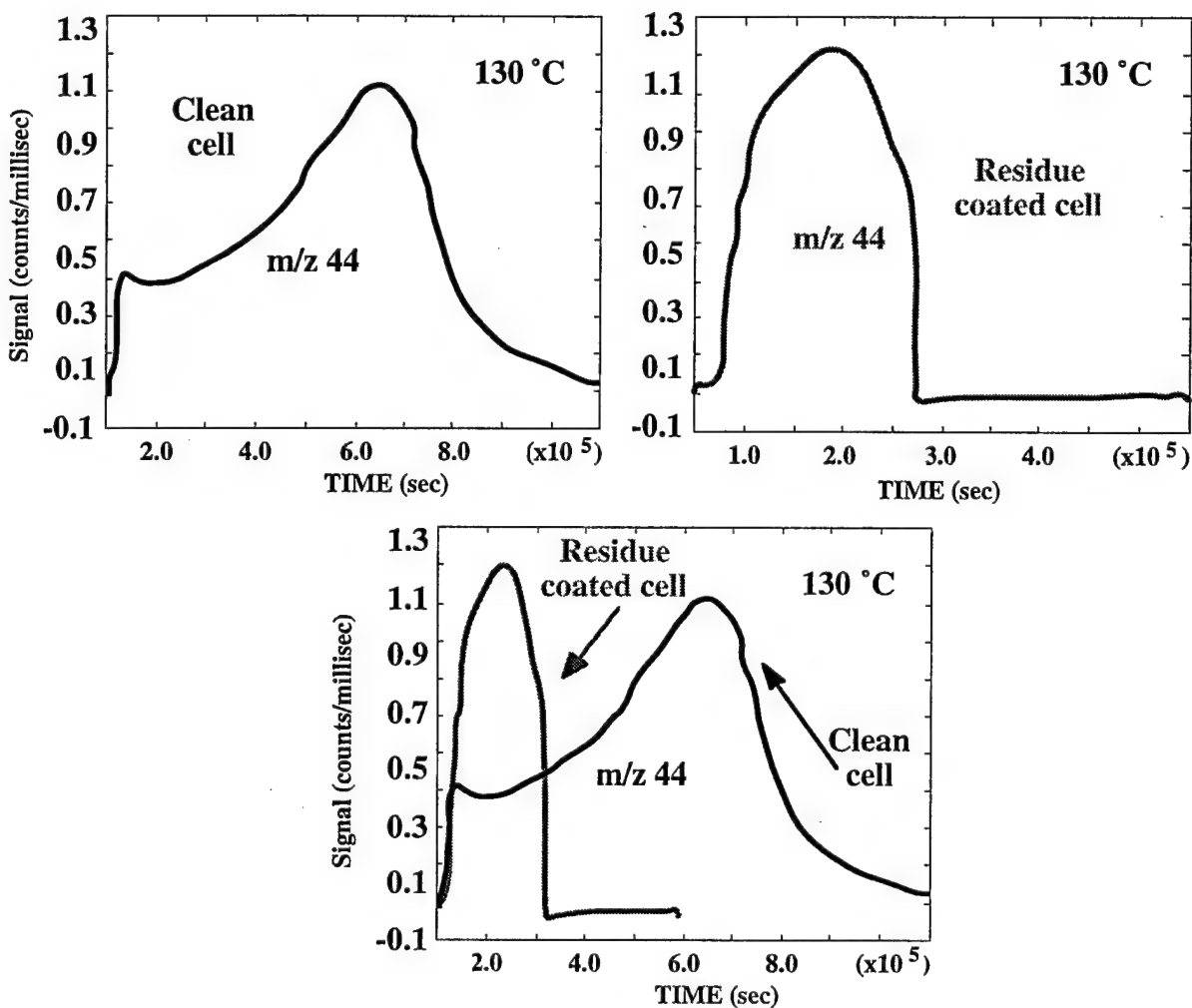


Figure 5: Proof that the autocatalytic behavior is due to the decomposition residue. Upper left, NDNaz decomposition in a clean cell as monitored by m/z 44 ($\text{CO}_2/\text{N}_2\text{O}$). Upper right, fresh NDNaz is added to the residue-coated cell and the rate of decomposition rises almost immediately to the peak rate from the previous experiment (and continues to increase). Lower middle shows the two signals superimposed at the same time scales. Note y axis here is ion signal, not gas formation rate.

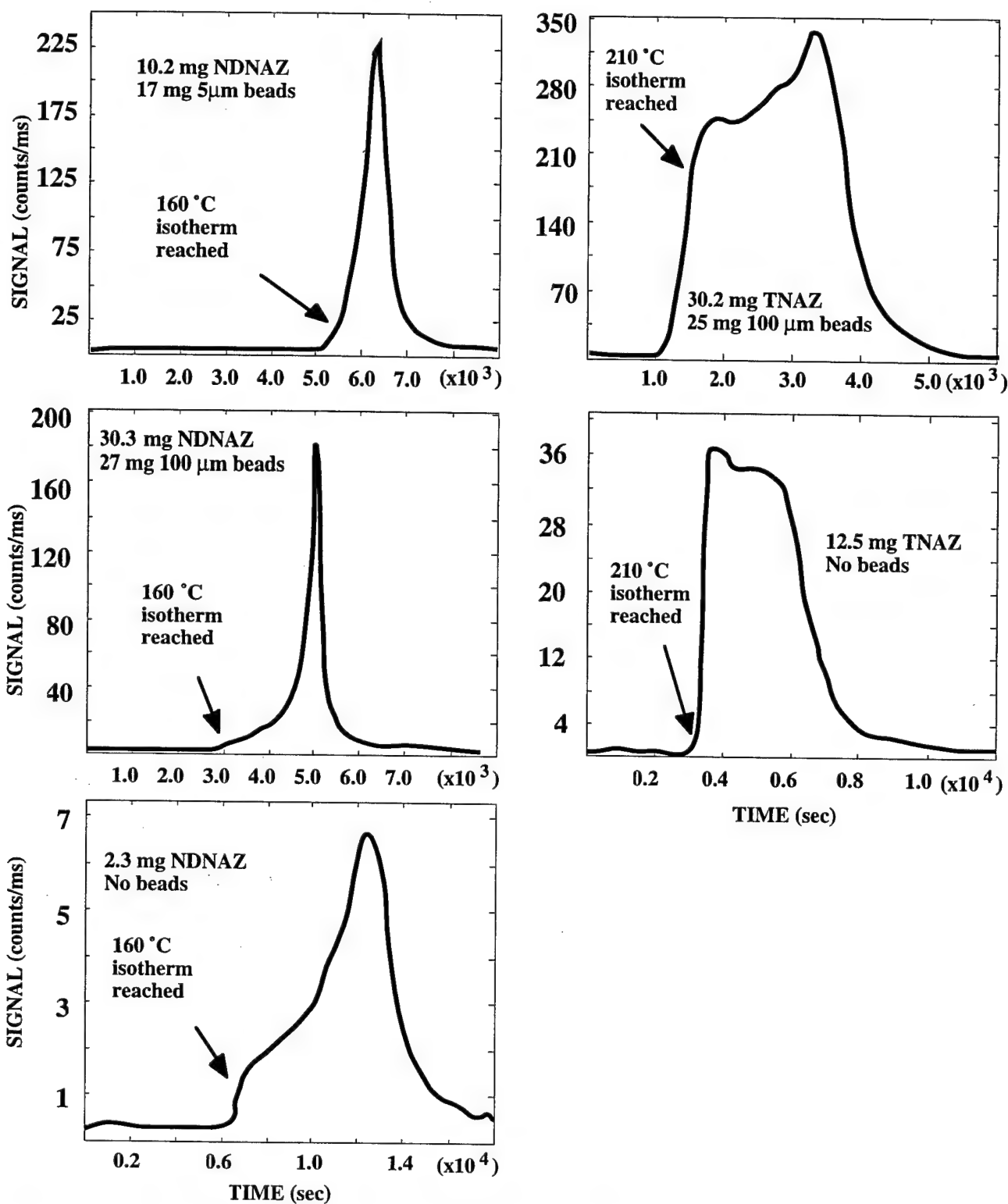


Figure 6: Higher rates of catalysis are seen in the presence of microscopic glass beads compared to normal decomposition. Left column, NDNAZ, right column, TNAZ. Note different time scales; the bead experiments for each compound are exactly half as long as the normal experiments. Also, note the > 2 order of magnitude increase in maximum ion signal with beads (again, m/z 44, $\text{CO}_2/\text{N}_2\text{O}$).

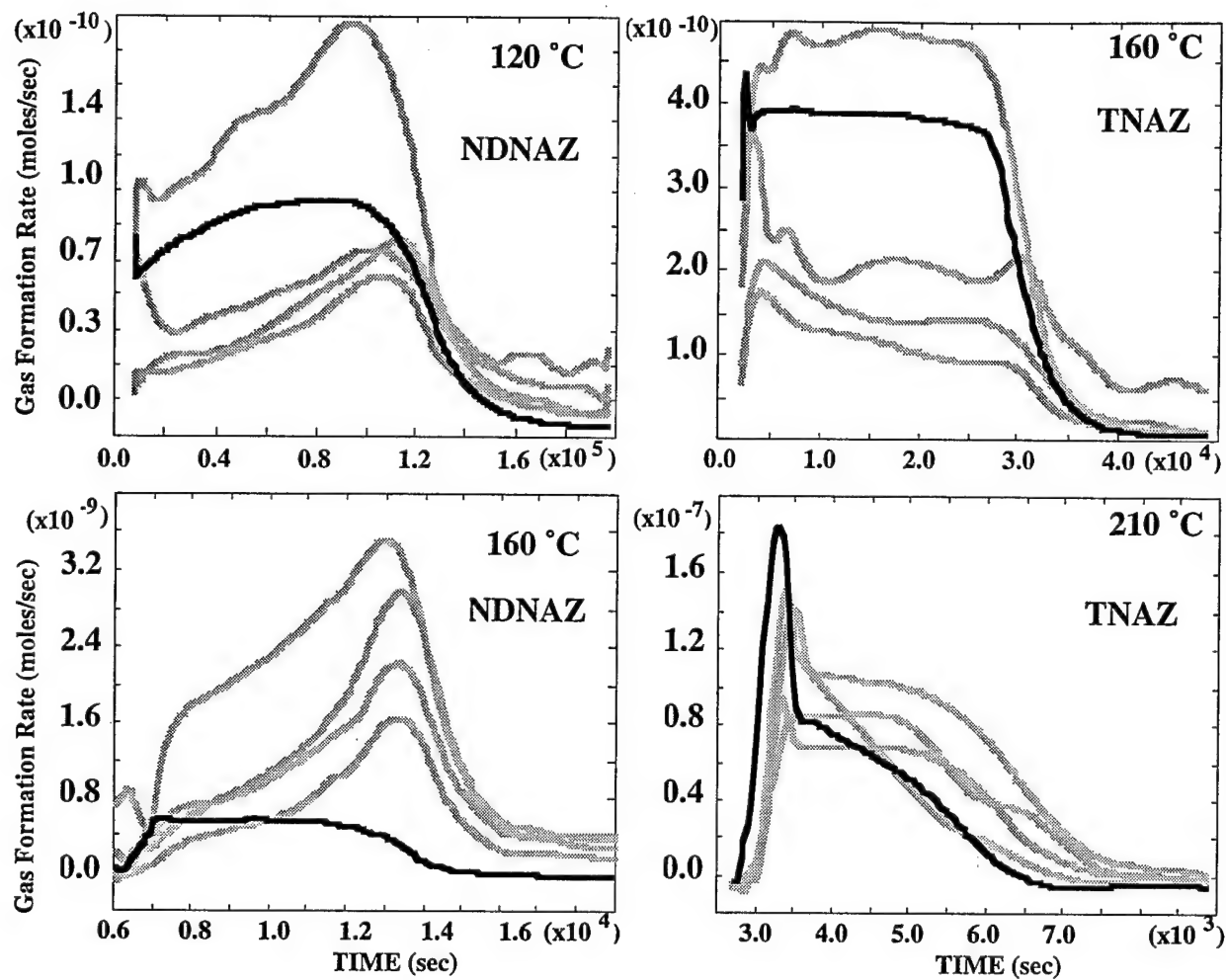


Figure 7: Evidence for less volatile intermediates and/or product trapping in polymeric residue. Dark lines represent the NDNaz or TNAz vapor formation rate, while grey lines represent various important low molecular weight products. In the top row, product evolution drops almost as soon as the parent material is depleted. At high temperature (bottom row), products continue to evolve after depletion.

A Review of the Thermal Decomposition Pathways in RDX, HMX and Other Closely Related Cyclic Nitramines.

Suryanarayana Bulusu

*US Army Armaments Research, Development and Engineering Center
Picatinny Arsenal, NJ 07806*

and

Richard Behrens, Jr.

*Combustion Research Facility, Sandia National Laboratories
Livermore, CA 94551*

ABSTRACT

Understanding the complex physicochemical processes involved in the combustion and decomposition of energetic materials is essential to the development of reliable models for the performance, stability and hazards analysis of propellants and explosives and to provide a basis for improvement of ignition and sensitivity properties of their formulations. Since the nitramines RDX and HMX are important materials as propellants and explosives, we have undertaken a comprehensive, in-depth study, over the years, of their thermal decomposition kinetics and mechanisms using unusual sophisticated techniques, namely, simultaneous thermogravimetric modulated beam mass spectrometry (STMBMS), time-of-flight velocity spectra analysis, isotope labeling (^{15}N , ^{13}C , ^2H and ^{18}O), isotope scrambling techniques and deuterium kinetic isotope effects (DKIE). In this paper, the results of the condensed and gas phase decomposition studies of RDX and HMX are reviewed in terms of the reaction pathways, bond-breaking steps and some bond-forming reactions. A comparison is made with the decomposition of six other cyclic nitramines and the common and contrasting modes of decomposition are highlighted. In particular, it is shown that the formation of a mononitroso analogue from RDX and HMX, respectively, as intermediates, represents an important thermal degradation pathway in each and probably also in four other nitramines studied. The cyclic nitramine 1,3,5-trinitro-1,3,5-triaza-cyclo-heptane exhibits the potential to be a new useful nitramine with valuable applications.

1. INTRODUCTION

The cyclic nitramines hexahydro-1,3,5-trinitro-s-triazine, RDX (I) and octahydro-1,3,5,7-tetranitro-1,3,5,7-tetraazocine, HMX (II) are high energy containing compounds that are used extensively in both propellant and explosive formulations. A thorough knowledge of the underlying complex physico-chemical processes in the combustion of these materials is essential to develop methods to modify their

formulations so as to obtain better ignition, combustion or sensitivity properties. There are several other less known cyclic nitramines also described in the literature which are structurally similar to RDX and HMX, some of which are covered in this review; Their structures are shown in Fig. 1. A detailed study of the decomposition processes of these materials serves several purposes. Firstly, in solid-propellant combustion, the decomposition processes occurring in the condensed

phase generate low molecular weight chemical species that feed the gas phase flames. These processes together control the burn rates of propellants. Secondly, in both propellants and explosives it is important to understand the mechanisms that control the stability of these materials when they are subjected to elevated temperatures, electrostatic discharge, impact or shock. The response of energetic materials to these stimuli determines their degree of safety when subjected to abnormal environments such as fires. Thirdly, a knowledge of the molecular processes that control the response of the energetic materials to abnormal environments will provide an insight into the molecular properties which control the relative stability and sensitivity of these materials. Finally, a comparison of the decomposition pathways of a variety of cyclic nitramines should shed some light on the structural factors that promote stability and other desirable properties.

Until about ten years ago there were scattered reports on investigations of the decomposition chemistry of RDX and HMX which included slow-heating rate studies,¹⁻⁴ mass spectrometry studies,⁵⁻⁹ high-heating rate studies^{10,11} and studies of shock initiated decomposition^{12,13}. These studies were recently reviewed^{14,15} in the literature. The current work in these laboratories over the last ten years being reviewed now, has utilised more sophisticated experimental techniques namely, simultaneous thermogravimetric modulated beam mass spectrometry (STMBMS)¹⁶, time-of-flight velocity spectra analysis, isotope labeling (¹⁵N, ¹³C, ²H and ¹⁸O), isotope scrambling techniques¹⁷⁻²⁰ and

deuterium kinetic isotope effects (DKIE)¹⁷⁻²⁰ to investigate the kinetics of decomposition and the initial work focussed on RDX and HMX decompositions¹⁷⁻²⁰. Following this work, less extensive investigations have been carried out on the nitramines (III) to (VIII) (Fig.1) in an effort to obtain structural correlations²¹⁻²³. The highlights of these investigations on RDX, HMX and the other cyclic nitramines in Fig. 1, are presented in this paper with the focus on the common features as well as the significant differences.

2. EXPERIMENTAL METHODS & MATERIALS

2.1 Experimental Methods

Various experimental techniques employed in obtaining the quantitative and qualitative data on the nitramine decompositions are already described in great detail in References 16 to 23. Therefore, merely a brief outline of the methods will be included here. Thermal decomposition measurements in these studies are carried out on typically 2 to 10 mg samples using the STMBMS apparatus¹⁶.

This apparatus basically consists of a thermo-balance, a specially designed alumina reaction cell in which the decomposition is carried out and a quadrupole mass spectrometer with the ionisation source vertically above the reaction cell. The molecules that exit the cell into a high vacuum environment ($\sim 10^{-6}$ to 10^{-10} torr), are formed into a modulated molecular beam and pass directly through the electron-bombardment ionizer of a quadrupole mass spectrometer without undergoing any further collisions with background

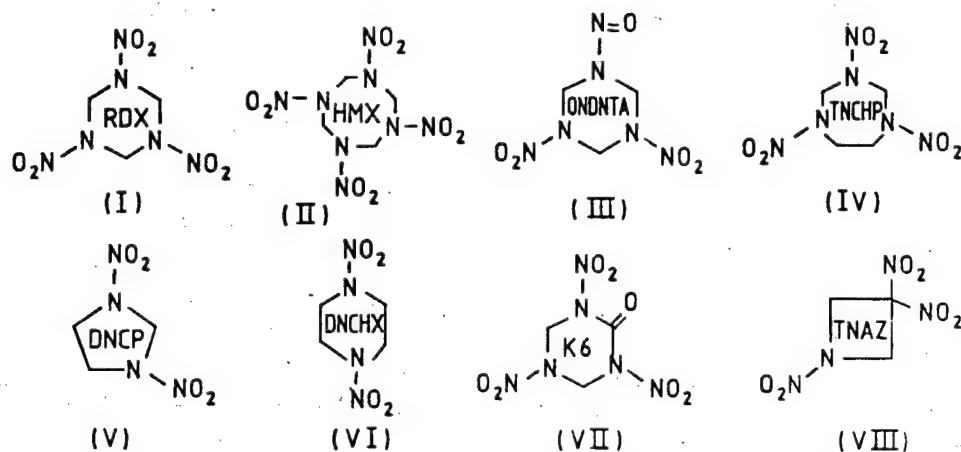


Figure 1. Structures of nitramines currently under investigation.

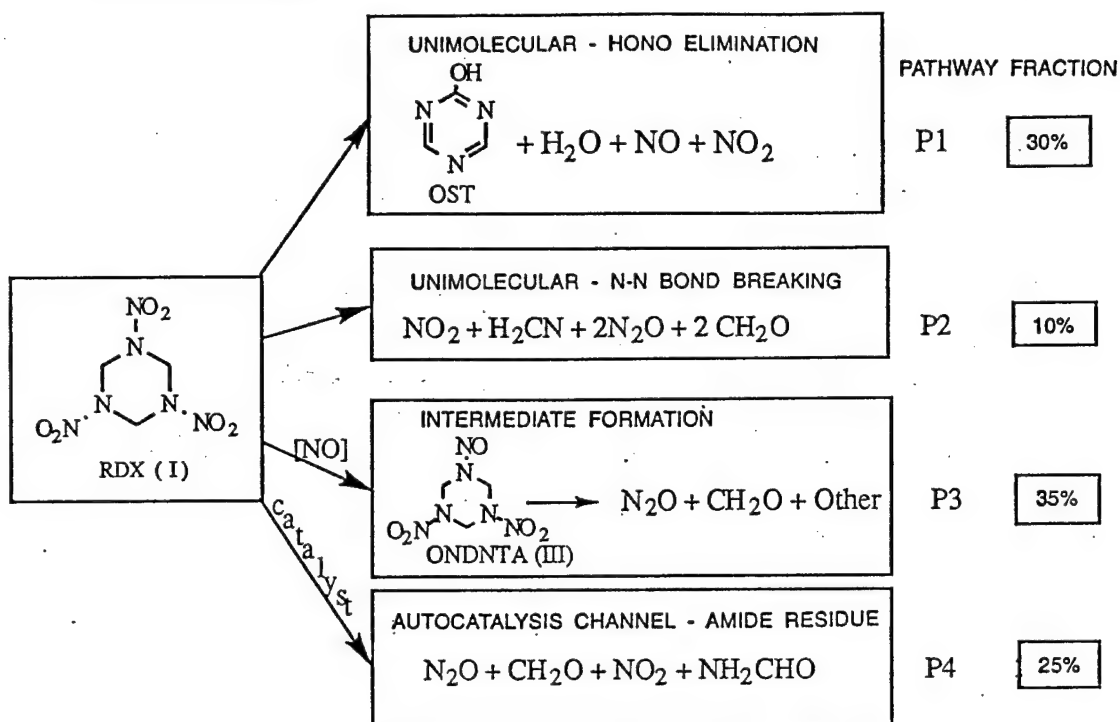


Figure 2. Four major decomposition pathways of RDX in the liquid Phase. (Data from Ref. 19) behavior of the products formed during the thermal decomposition of TNAZ-1-¹⁵NO₂.

molecules or walls of the vacuum chamber. In the region between the reaction cell and the ionization source are located a set of beam defining orifices and a beam modulating wheel. This instrument allows the gas-phase species to be identified and their rates of formation to be measured as a function of time. The decomposition is carried out in the alumina reaction cell from which the gaseous decomposition products may exit only through an orifice whose diameter ranges from 2.5 μm to 1000 μm depending upon the degree of confinement of the decomposition products desired (pressure of the contained gases can be varied between 0 and 2000 torr). The force due to the gas within and exiting the reaction cell (thrust and mass loss) is measured simultaneously with the mass spectra of the evolving gases. The gases are identified from the m/z values of temporally correlated groups of ion signals, from the molecular weight of the neutral molecules evolving from the cell as determined from time-of-flight velocity spectra and by use of isotopically tagged analogues of the molecules being studied. The rates of gas formation are determined in an analysis procedure that utilises the ion signals measured with the mass spectrometer, the force measured by the microbalance and the flow characteristics of the reaction cell orifice. The end result of the experiments and the data analysis procedure is the

rate of gas formation of each species formed during the thermal decomposition as a function of time and of pressure of the contained gases. From this information, insight into the reaction mechanisms that control the decomposition process and the kinetic rate parameters associated with the rate controlling reaction mechanisms is obtained.

2.2 Source of Samples Studied

While RDX and HMX samples were obtained from military sources and purified by repeated crystallisations from acetone, their isotopic analogues and all the other nitramines were made in these laboratories by methods already known. The syntheses of the isotopic analogues of RDX (I) and HMX (II) were described in previous papers^{20,24}. ONDNTA (III) and its deuterium labeled analogue, ONDNTA-d₆, which are intermediates in the decomposition of RDX and RDX-d₆ respectively, were prepared according to previously known methods²⁵ starting with the corresponding hexahydro-1,3,5-trinitroso-s-triazine analogue. The deuterated version of the hexahydro-1,3,5-trinitroso-s-triazine was prepared by the base catalysed deuterium exchange method described in yet another paper²⁶. The nitramines TNCHP²⁷ (IV), DNCP²⁸ (V) and DNCHX²⁹ (VI) were synthesised according to the methods already described

in the early literature on nitramines. The methods of synthesis of K6³⁰ (VII) and TNAZ³¹ (VIII) were also published relatively recently. ¹⁵NO₂-labeled TNAZ was prepared by treating 3,3-dinitroazetidine, an intermediate in the TNAZ synthesis, with *H*¹⁵NO₃.

3. RDX & HMX DECOMPOSITIONS

The decomposition of both RDX and HMX is controlled by multiple pathways whose behaviour depends on the physical state of the sample. In the case of RDX, for example, four major pathways shown in Fig. 2 have been identified¹⁹. The decomposition of both RDX^{19,20} and HMX^{17,18} gives rise to many common products, the nature and relative abundance of each being determined by initial decomposition reactions (i.e., *N*-NO₂ bond breaking and *HONO* elimination) and secondary reactions between the reactant and its decomposition products. Examples of common products are H₂O, N₂O, CH₂O, NO, CO, HCN, NO₂, NH₂CHO and CH₃NHCHO. Products unique to each are OST (oxy-s-triazine, *m/z* 97), ONDNTA (*m/z* 206) from RDX and ONTNTA and (CH₃)₂N-NO from HMX: One important common pathway of decomposition in both RDX and HMX was found¹⁷⁻¹⁹ to be the formation of the mononitroso analogues (1-nitroso-3,5-dinitro-1,3,5-triazine, ONDNTA (III) and 1-nitroso-3,5,7-trinitro-1,3,5,7-tetraazocine, ONTNTA, respectively) of these cyclic nitramines as intermediates in both liquid and solid phases. Isotope scrambling experiments using mixtures of fully ¹⁵N-labeled and unlabeled samples showed that the mononitroso analogues were formed with complete isotope mixing in the liquid phase decompositions and partial mixing in the solid phase decompositions. This implies a re-formation of *N*-NO bond at least in the liquid phase decomposition pathways. Both ONDNTA and ONTNTA undergo further decomposition, contributing to the low molecular weight gaseous products observed in the RDX and HMX decompositions and, therefore, play a significant role in the overall decomposition processes.

3.1 RDX Decomposition in the Liquid Phase

Of the four primary reaction pathways controlling the decomposition of RDX in the liquid phase between 200 and 215 °C (Fig. 2), two pathways are "first order" reactions solely in RDX. One of these produces predominantly OST, NO, and H₂O and accounts for

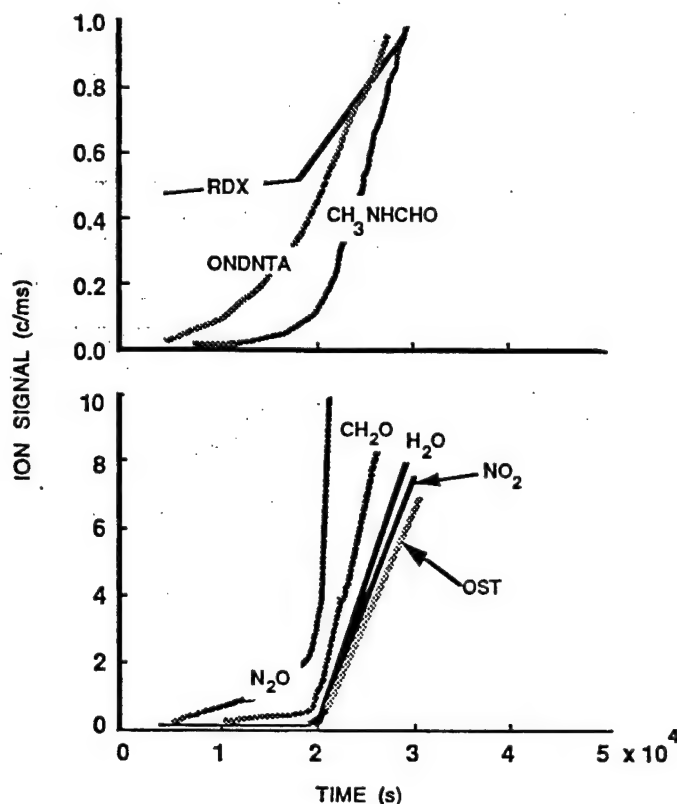


Figure 3. Ion signals associated with the thermal decomposition products formed from pure unlabeled RDX at an isothermal temperature of 190°C. The ONDNTA, N₂O, CH₂O, CH₃NHCHO signals all show a gradual increase prior to the onset of the appearance of the signals associated with the liquid phase decomposition (OST, H₂O and NO₂). Data from Ref. 19.

approximately 30 per cent of the decomposed RDX and the other produces predominantly N₂O and CH₂O with smaller amounts of NO₂, CO, and NH₂CHO and accounts for 10 per cent of the decomposed RDX. The third pathway consists of formation of ONDNTA by reaction between NO and RDX, followed by the decomposition of ONDNTA to predominantly CH₂O and N₂O. The nature of the fourth reaction pathway is less certain. From our original experiments on RDX, we proposed that in the fourth pathway, RDX decomposes by reaction with a catalyst that is formed from the decomposition products of RDX. This conclusion is based on the temporal behaviour of the gas formation rates of the decomposition products. However, from more recent experiments with the independently synthesised mononitroso analogue of RDX, ONDNTA, it appears that this fourth channel may also involve the ONDNTA intermediate. The third and fourth reaction

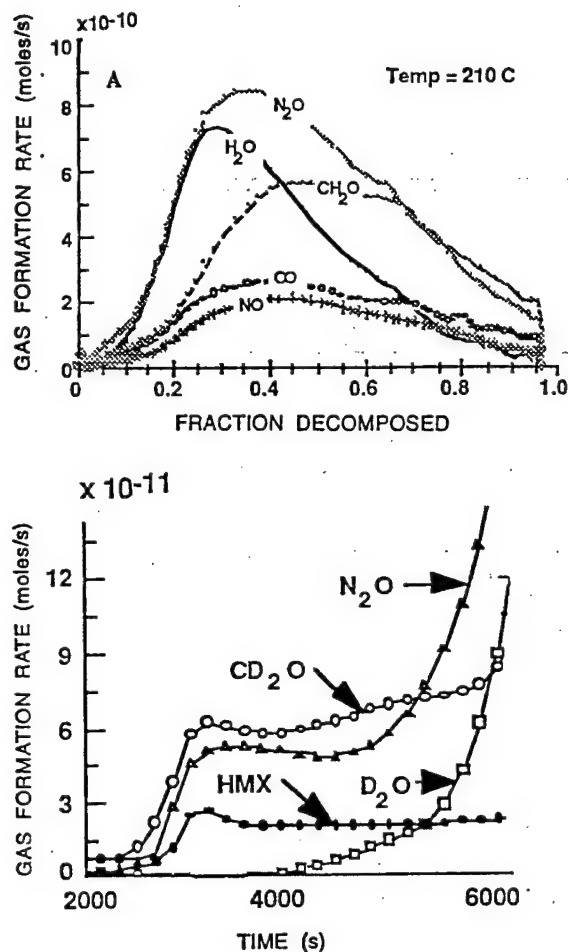


Figure 4. (A) Gas formation rates of the products from the thermal decomposition of HMX at 210 °C. The duration of the decomposition process is about 37000 seconds. (B) Gas formation rates of thermal decomposition products from HMX- d_8 during the induction period and first stage of the acceleration period.

channels each account for approximately 30 per cent of the decomposed RDX.

3.2 RDX Decomposition in the Solid Phase

Experiments with solid phase RDX have shown that its decomposition rate is very much slower than that of liquid phase RDX as can be seen in Fig. 3. ONDNTA is the only product that appears to be formed during the early stages of the decomposition of RDX in the solid phase. As the solid-phase decomposition progresses, N_2O and lesser amounts of CH_2O start to evolve and their rates of evolution increase slowly until products associated with the liquid-phase RDX decomposition

appear and the rates of gas formation of all products rapidly increase. This behaviour strongly suggests that the decomposition of solid RDX occurs through formation of ONDNTA within the lattice. Its subsequent decomposition within the lattice to N_2O and CH_2O , followed by the dispersion of CH_2O in the RDX, leads to the eventual liquefaction of the remaining RDX and the onset of the associated liquid-phase decomposition reactions.

3.3 HMX Decomposition in the Solid Phase

The solid phase decomposition of HMX was studied in detail in the temperature range 210 °C and 235 °C. Since its melting point is about 275 °C, the decomposition in the experiments was predominantly in the solid phase. It was found on the basis of temporal correlations of evolution of products that physical processes played a very important role in controlling the rates of decomposition. The first step in the decomposition appeared to be some gas phase decomposition giving rise to products observed as they exit the reaction cell. Concurrently, decomposition occurs in the solid phase, first forming the mononitroso analogue ONTNTA which then decomposes to low molecular weight products. All these products are presumably trapped within the HMX particles initially, forming bubbles containing N_2O and solutions between HMX and CH_2O which could be localised in the volumes surrounding the bubbles. A polymeric product is also formed in the region of the bubbles and itself undergoes a thermal decomposition process yielding low molecular weight products as well as some polymeric residues. Eventually, the size of the bubbles and the pressure within grow, leading to the cracking of the HMX particles and release of the trapped products.

There was also clear experimental evidence that the HMX decomposition was an autocatalytic process as illustrated in the selected plots of gas formation rates shown in Fig. 4. The extent of this autocatalytic effect was shown to be controlled by the reaction of gaseous products with the unreacted HMX, by comparing the rates of formation of products obtained with 5 and 100 mm exit orifices on the reaction cell, respectively. Autocatalysis was much more pronounced when the gaseous products were more confined in the reaction cell.

The thermal decomposition reactions of HMX in the solid phase may also be divided into four groups of

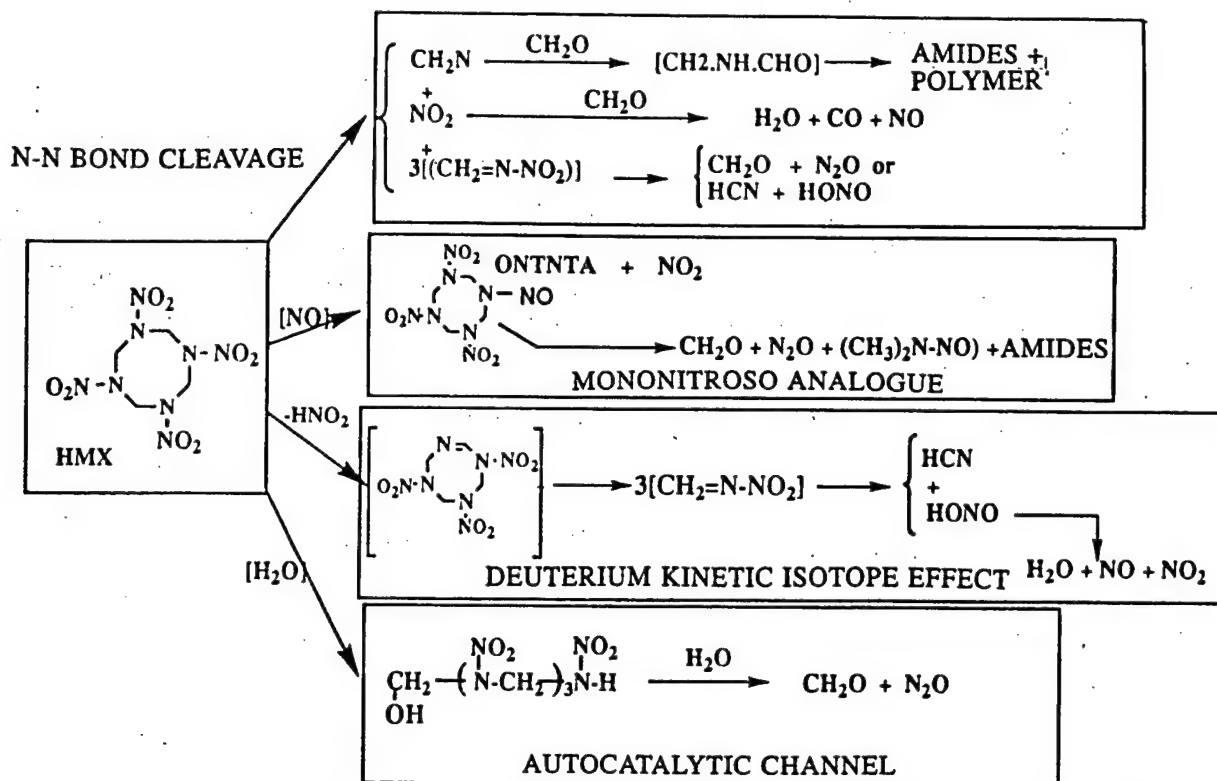


Figure 5. Summary of the proposed reaction pathways controlling the thermal decomposition of HMX in the solid phase. In this scheme, 'methylenenitramine' $[\text{CH}_2=\text{N}-\text{NO}_2]$ is merely assumed intermediate which was actually not detected in the mass spectrometer.

reactions for simplification, constituting four pathways summarised in Fig. 5.

However, some overlap clearly exists between the four branches of the decomposition. One pathway proceeds through *N-N* bond cleavage giving NO_2 , CH_2N , and three methylene nitramine intermediates. In a second pathway, an NO_2 group is replaced by an NO group forming the mononitroso analogue of HMX. In a third pathway, a hydrogen atom transfers to the adjacent NO_2 group giving rise to the observed deuterium kinetic isotope effect and making it a rate-limiting step. A detailed discussion of these reactions and a description of isotope scrambling and deuterium kinetic isotope effect studies is given in Refs. 17 and 18.

3.4 HMX Decomposition in the Liquid Phase

Comparison of the liquid phase decomposition of HMX with that of RDX will show whether decomposition pathways similar to RDX control the decomposition of HMX or whether the higher melting point of HMX and its decomposition in the solid phase prior to melting alter its decomposition mechanism. The liquid phase decomposition products from HMX observed in our experiments include H_2O , HCN , CO , CH_2O , NO , N_2O , NO_2 , formamide, *N*-methylformamide (NMFA), *N,N*-dimethylformamide, and ONTNTA

(Fig. 5). In addition, we observe ion signals at m/z values of 70 and 97. Experiments with ^2H , ^{13}C and ^{15}N isotopically labeled HMX analogues have shown that the ion signals at these two m/z values correspond to ions with formulae of $\text{C}_2\text{N}_2\text{H}_2\text{O}$ (70) and $\text{C}_3\text{N}_3\text{H}_3\text{O}$ (97). For RDX, the ion signals at m/z values of 70 and 97 both arise from the decomposition product, OST. However, for HMX, differences in the relative intensities of these two ions, in addition to differences in their temporal behaviour in the HMX experiments, indicate that they arise from two different decomposition products. These ion signals clearly arise from thermal decomposition products that are similar to the OST formed during the decomposition of RDX. However, without time-of-flight (TOF) velocity-spectra measurements of these ion signals, it is not possible to determine whether the observed ion signals correspond to molecular ions, and thus have the same formula as the thermal decomposition products, or whether they are from daughter ions formed from a decomposition product with a higher molecular weight. In either case, the ion signals at m/z values of 70 and 97 are associated with fragments from the HMX ring formed in a manner similar to reaction pathway P1 for the RDX decomposition (Fig. 2).

The results shown for the decomposition of HMX in Fig. 6 are consistent with the four decomposition

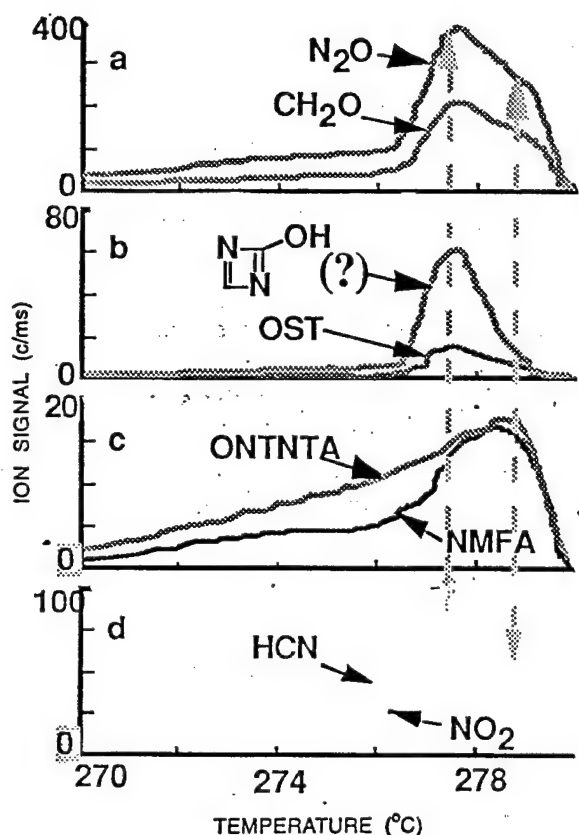


Figure 6. Ion signals associated with various thermal decomposition products formed during the decomposition of HMX as the sample melts. The sample melts at 276 °C. The signals associated with the thermal decomposition fragments of the ring (panel b) only appear in significant quantities as the sample melts. Other products associated with this pathway are indicated by the vertical arrow on the left. After the sample melts, a second set of products that peak later in the decomposition is observed, as indicated by the arrow on the right. These products are associated with the amides, such as the *N*-methylformamide. The heating rate was 2 °C/min.

pathways found for the decomposition of RDX (Fig. 2). A reaction pathway similar to reaction pathway P1 for RDX produces the HMX-ring fragments that are characterised by the ion signals at m/z values of 70 and 97 shown in Panel b of Fig. 6. These two ion signals first appear when the HMX sample liquefies at approximately 276 °C and their signal strengths decrease as the HMX sample is depleted. This behaviour is similar to that observed for OST formed in the decomposition of RDX. The temporal behaviour of the ion signals formed from the mononitroso analogue of HMX, ONTNTA, (shown in Panel c of Fig. 6) is similar to the temporal behaviour

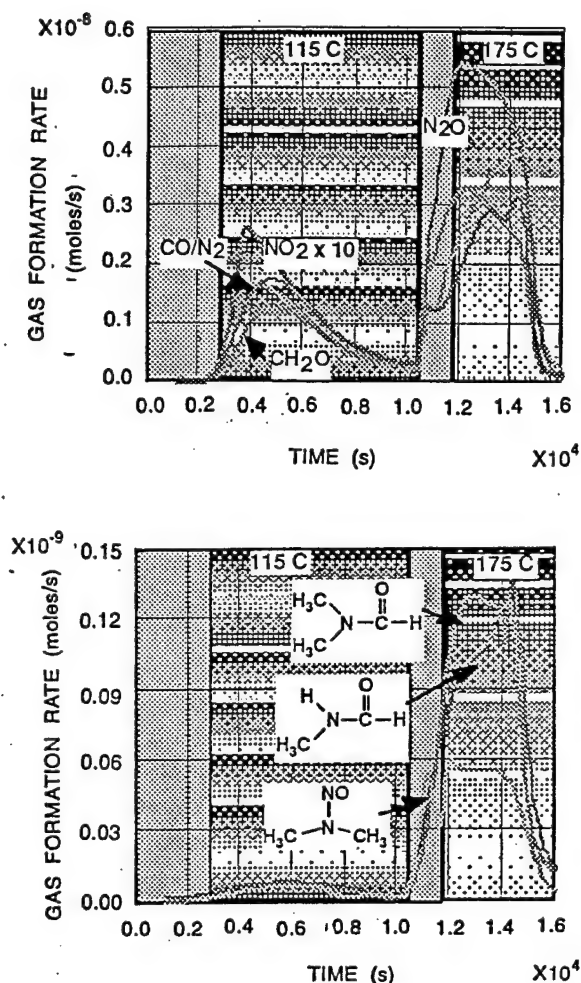


Figure 7. Gas formation rates of decomposition products from the thermal decomposition of ONDNTA in a reaction cell with a 50 μm orifice at isothermal temperatures of 115 °C and 175 °C.

of ONDNTA observed in the liquid-phase RDX decomposition. One significant difference is that a much larger amount of ONTNTA is released from the HMX sample before it liquefies. As can be seen from Fig. 6, the size of the ion signal associated with the ONTNTA product does not show a significant increase as the sample liquefies. This indicates that the decomposition of HMX to its mononitroso analogue is a major decomposition pathway in the solid phase. This is similar to the decomposition of RDX in the solid phase, except that at the higher temperatures associated with the decomposition of HMX, the reaction rate for the formation of ONTNTA is greater and a larger fraction of the HMX sample has decomposed via a reaction pathway similar to pathway P3 prior to the liquefaction of the HMX sample. The temporal behaviour of the ion

signals associated with the CH_2O and N_2O formed during the decomposition of HMX after its liquefaction, have the same broad type of peaks that were observed for these products in the decomposition of RDX. Both the ion signals associated with these products show a rapid increase as the HMX liquefies. The CH_2O and N_2O formed later in the decomposition appear to be correlated with the ONTNTA product and they also display a temporal behavior that is characteristic of an autocatalytic decomposition channel similar to pathway P4 for RDX.

The initial increase in the CH_2O and N_2O signals after the HMX sample liquefies is also similar to that observed in the decomposition of RDX and associated with decomposition via, reaction pathway P2. From the relative sizes of the ion signals associated with the CH_2O and N_2O products and those associated with the HMX ring fragment ion signals at m/z values of 70 and 97 would suggest that the amount of HMX that decomposes by a pathway similar to P2 compared to pathway P1 is greater for HMX than for RDX. In the light of the fact that the decomposition of HMX occurs at a temperature about 70 °C greater than RDX, the behavior of CH_2O and N_2O tends to suggest that reaction pathway P2 may become more dominant than reaction pathway P1 at higher temperatures. However, it is also possible that the increase of the CH_2O and N_2O signals after the HMX sample liquefies is due to an increase in the decomposition rate of ONTNTA, formed in the solid-phase decomposition. Without further quantification of the HMX results, it is not possible at this time to determine exact relative decomposition rates of the various HMX decomposition products

4. THERMAL DECOMPOSITION OF NITRAMINES (III) to (VIII)

4.1 ONDNTA (III) Decomposition

ONDNTA, the intermediate in RDX decomposition, was independently synthesised²⁵ to study its decomposition²¹ separately. This nitramine uniquely decomposes in two separate temperature regions sequentially, one between 95 and 145 °C and the other between 155 and 210 °C. An illustration of this behaviour is shown in Fig. 7 for the decomposition of ONDNTA in a reaction cell with a 50 mm diameter orifice and held at two different isothermal temperatures. The major decomposition products are N_2O , CH_2O , CO/N_2 and NO_2 and the minor ones include several

formamides and dimethylnitrosamine, $(CH_3)_2NNO$. The products obtained from both regions are very similar to those obtained from the decomposition of HMX and RDX in the solid phase with some variation between the two channels of decomposition. It is not understood why the decomposition stops in the intermediate temperature region. However, it is surmised that in this temperature region there is a competition between two processes. One is an autocatalytic process in which gas-phase decomposition products accelerate the decomposition process and the second is some undetectable phase transition that leads to a more stable phase of ONDNTA that is not susceptible to autocatalysis. In support of this conclusion, comparison of the decomposition of ONDNTA in experiments conducted in the reaction cell with 5 mm and 50 mm diameter orifices, respectively, showed that the decomposition occurs 100 times more rapidly with the 5 mm orifice and that the entire sample is consumed in the low temperature channel, presumably due to the autocatalysis by the products.

The behaviour of the decomposition process of ONDNTA under high confinement is illustrated by the data in Fig. 8. The temporal behaviour of the rates of formation of the gaseous products is characterized by two regions. The first region starts at approximately 110 °C and peaks at 125 °C. The second region starts at approximately 140 °C and peaks at 145 °C. A similar temporal behaviour in the two regions was observed during the decomposition of ONDNTA at isothermal temperatures in the 110 to 150 °C range. Thus, it appears that the observed gaseous thermal decomposition products are formed in a series of steps and it is not necessary to increase the temperature as was done in the experiment shown in Fig. 8. The first step in the process leads to the release of CO/N_2 and NO_2 as can be seen from the ion signals in Fig. 8b. These two signals rise and fall sharply. The N_2O and CH_2O signals also rise sharply but decline much more gradually. At 140 °C, after approximately 70 per cent of the sample has decomposed, there is a rapid rise in the rate of formation of a new set of decomposition products as seen in Fig. 8c and 8d. These products include H_2O , N -methylformamide, N,N -dimethylformamide and dimethylnitrosamine. After the sample stops losing gaseous products, between 5 and 10 per cent of the sample remains as a residue.

These results indicate that as ONDNTA decomposes, it gives gaseous products as well as a

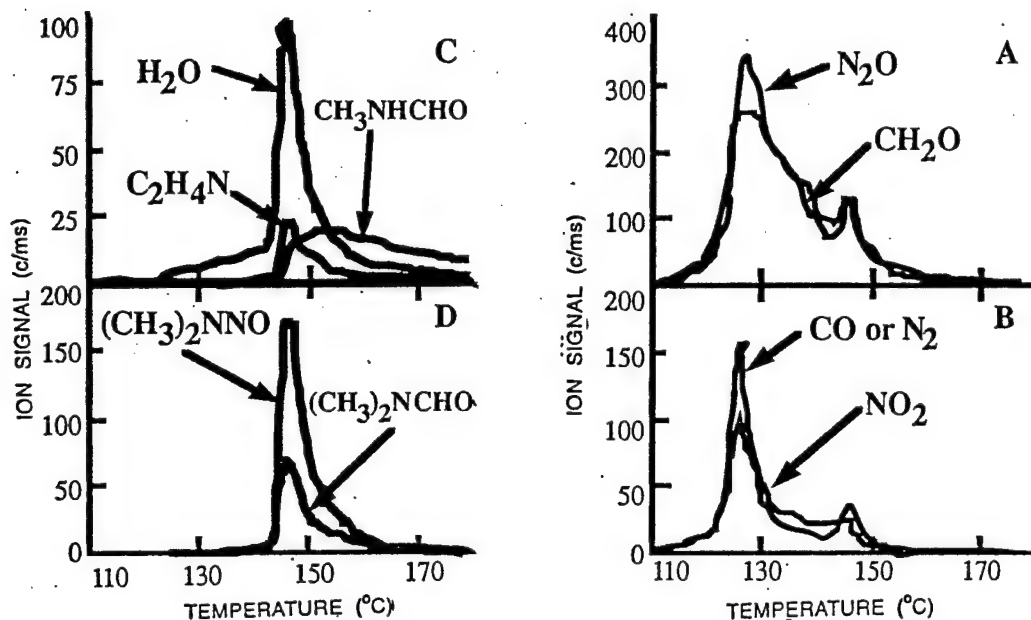


Figure 8. Ion signals in the mass spectrometer from thermal decomposition products of ONDNTA under conditions of high confinement. The heating rate was 2°C/min.

non-volatile compound (possibly polymeric) that is relatively stable. The first step in the process is likely to be scission of the $N\text{-NO}_2$ bond as evidenced by the NO_2 signal, followed immediately by loss of CO/N_2 , N_2O and CH_2O as indicated by the simultaneous rapid rise in these signals. Two different explanations are possible for the sharper decrease in the CO/N_2 and NO_2 signals compared to the N_2O and CH_2 signals. The first one is that the ONDNTA sample is rapidly converted to a nonvolatile product (the rate of conversion is characterized by the NO_2 or CO/N_2 signals) that then undergoes a slower decomposition to form N_2O and CH_2O . The second possible explanation is that the nonvolatile decomposition product interacts with the remaining ONDNTA, thus providing another decomposition pathway that leads to the release of N_2O and CH_2O . The fact that there is an abrupt appearance of a new set of decomposition products later in the process suggests that the first explanation is more likely. This is because the abrupt appearance of the new products occurs in both the thermal ramp and isothermal experiments. It suggests that the nonvolatile product formed in the initial decomposition of ONDNTA itself decomposes, releasing N_2O and CH_2O until it reaches a

point at which the nonvolatile product becomes sufficiently unstable that it starts to decompose more rapidly into water, dimethylnitrosamine and the formamides. This process is quite consistent with the observed data. A discussion of details of this process will be presented in a future paper.

The similarities between the products and their sequence of formation in the thermal decomposition of ONDNTA under high confinement conditions and the products observed in the decomposition of HMX in the solid phase are quite striking. Firstly, the major products formed in the decomposition are the same, namely N_2O , CH_2O and CO/N_2 . Secondly, the products that originate from the decomposition of the nonvolatile product formed in the decomposition of ONDNTA are the same as those observed in the decomposition of HMX in the solid phase [H_2O , $(\text{CH}_3)_2\text{NNO}$, CH_3NHCHO , and $(\text{CH}_3)_2\text{NCHO}$]. Thirdly, a stable residue remains after the decomposition of both the materials.

4.2 Thermal Decomposition of TNCHP

1,3,5-Trinitro-1,3,5-triaza-cycloheptane (TNCHP) is a cyclic nitramine like RDX with an extra carbon atom in the ring. TNCHP is more stable in the liquid phase

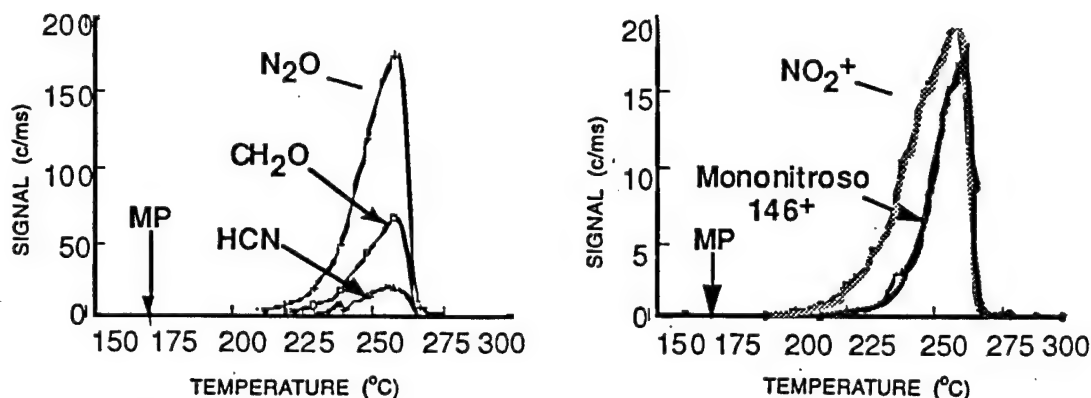


Figure 9. Ion signals associated with the products formed during the thermal decomposition of TNCHP. The heating rate is $2^{\circ}\text{C}/\text{min}$.

than either RDX or HMX. The major products formed in its decomposition are CH_2O and N_2O . Products formed to a lesser extent include: H_2O , HCN , NO and NO_2 . Ion signals, representing other decomposition products, are also observed. Further measurements utilizing deuterium labeled TNCHP and TOF velocity spectra are underway to determine the identity of the thermal decomposition products leading to these other ion signals. The temporal behaviour of the major ion signals is shown in Fig. 9. These results illustrate the increased thermal stability of TNCHP in the liquid phase as compared to RDX. The ion signal at $m/z = 146$ is analogous to the ion signal at $m/z = 132$ that arises from ONDNTPA. Thus, the ion signal at $m/z = 146$ most likely belongs to the mononitroso analogue of TNCHP.

In isothermal experiments with TNCHP, the temporal behaviour of the ion signals associated with the

decomposition products from TNCHP is indicative of several parallel reaction pathways. The temporal behaviour of several of the products is illustrated in Fig. 10. Ion signals associated with processes that are approximately 'first order' in TNCHP are represented by the signals for NO and NO_2 in Fig. 6 and also include signals that represent HCN . Ion signals associated with intermediate products formed during the thermal decomposition are found at m/z values of 55, 84, 130, and 146. The ion signals at m/z values of 55, 84 and 130 have temporal behaviour similar to that of the signal at $m/z = 146$, which probably represents the mononitroso analogue of TNCHP. This suggests that the ion signals at m/z values of 55, 84 and 130 may be ion dissociation products of the TNCHP mononitroso analogue. TOF velocity spectra signals at these m/z values will resolve

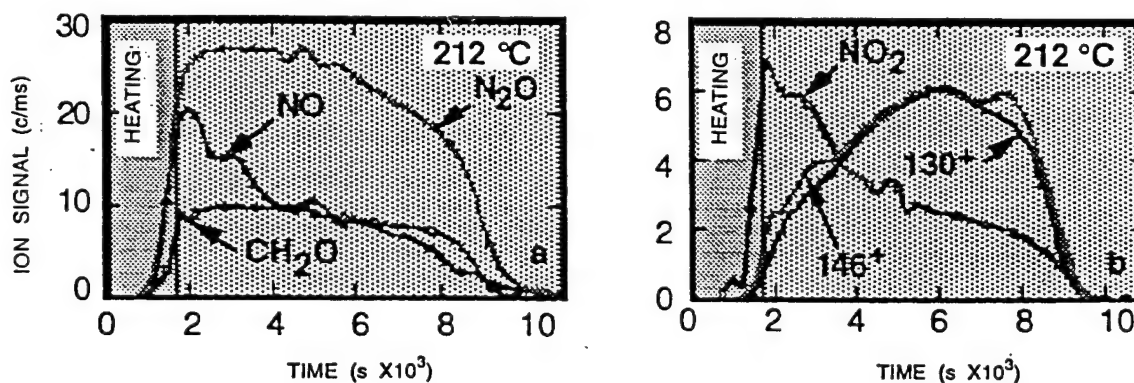


Figure 10. Ion signals associated with the thermal decomposition products from TNCHP. The region in the left shaded panel is the heating portion and the right shaded panel is the isothermal portion of the experiment. The ion signals representing NO and NO_2 appear to be approximately 'first order' in liquid phase TNCHP. The ion signals at m/z values of 130 and 146 are associated with an intermediate formed during the thermal decomposition. The ion signals associated with CH_2O and N_2O probably originate from pathways associated with both the 'first order' process and the decomposition of the intermediate.

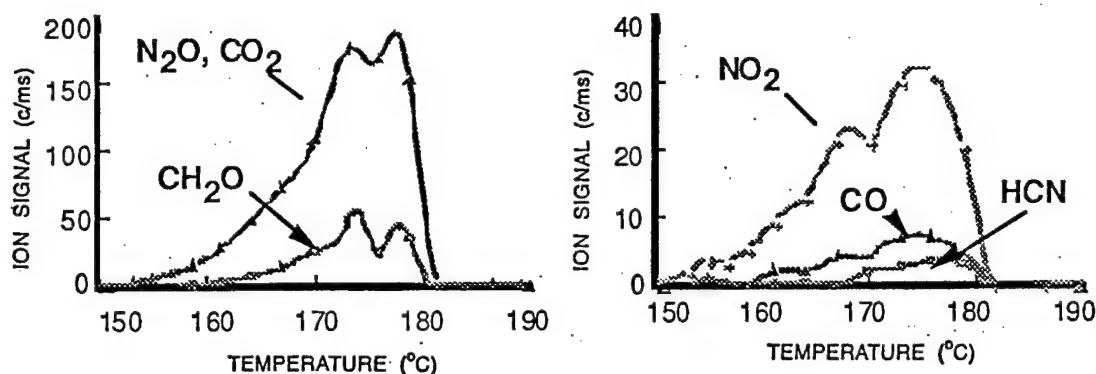


Figure 11. Ion signals formed in the mass spectrometer from products of thermal decomposition of K6.

whether these signals are ion dissociation products formed in the mass spectrometer or whether they arise from additional thermal decomposition products.

A stable product, similar to OST in the decomposition of RDX, was not observed in the thermal decomposition of TNCHP. This inability to form a decomposition product by stabilizing the ring of the cyclic nitramine may be responsible for the increased thermal stability of TNCHP.

4.3 Thermal Decomposition of the Nitramine, K6

The decomposition of K6 is quite different from the other cyclic nitramines used in this study. In addition to its lower thermal stability, K6 also produces fewer and

simpler decomposition products. The decomposition products are mainly CH_2O , N_2O and CO_2 , with minor contributions from HCN , CO , NO and NO_2 .

Unlike the other cyclic nitramines used in this study, K6 does not form any amides, the mononitroso analogue, or a residue. The temporal behaviour of the products formed during the decomposition of K6 is shown in Fig. 11.

The decomposition of K6 (VII) may have been initiated by attack of one of the NO_2 oxygen atoms on the keto group carbon atom, leading to the initial elimination of CO_2 followed by rapid transformation of the remaining fragment into CH_2O and N_2O . The rate of decomposition of K6 through this initial four-centre

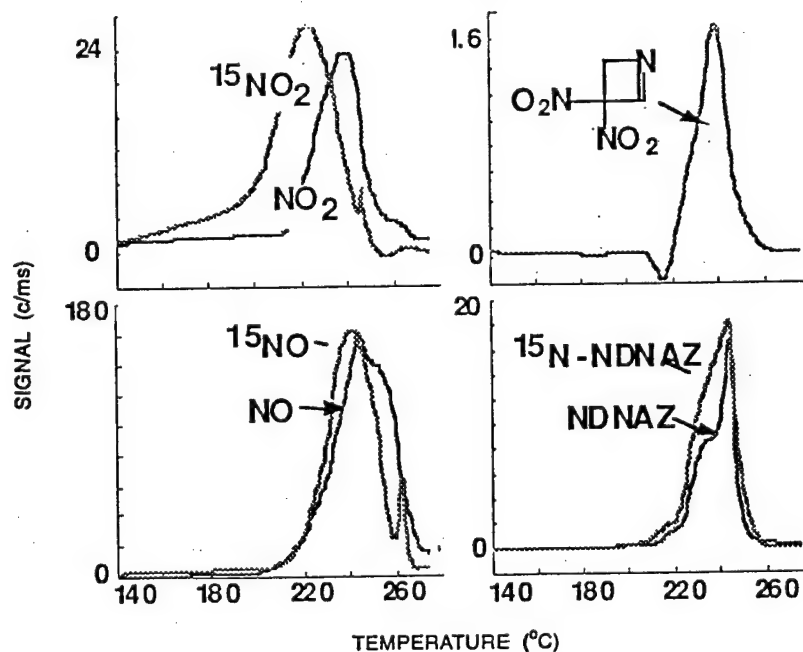


Figure 12. Temporal behaviour of the products formed during the thermal decomposition of $\text{TNAZ-}^{15}\text{NO}_2$.

C-N-N-O complex would appear to be competitive with *N-NO*₂ bond breaking in that no mononitroso analogue or amide products were observed. A more detailed investigation of K6 is currently in progress.

4.4 Thermal Decomposition of the Nitramines, DNCP (V) & DNCHX (VI)

1,3-Dinitro-1,3-diaza-cyclopentane (DNCP) and 1,4-dinitro-1,4-diaza-cyclohexane (DNCHX) are two nitramines with 5- and 6- membered rings, respectively. Only preliminary details of their decompositions are available at present. They exhibit multiple reaction pathways like RDX and HMX, including the formation of the mononitroso analogues²². DNCP is thermally much more stable in the molten state as compared to RDX and HMX while DNCHX (VI) begins to decompose in the solid state similar to the case of HMX. DNCP is exceptional in that it does not give rise to the typical nitramine decomposition products, *CH*₂*O* and *N*₂*O*. Further work on the decomposition mechanism of these nitramines is in progress.

4.5 Thermal Decomposition of TNAZ (VIII)

The last nitramine in Fig. 1 that is being investigated²³, is 1,3,3-trinitro-azetidine (TNAZ) (VIII). This is currently under development as a castable explosive because of its low melting point (100 °C) and unusual thermal stability in its molten state. It is an interesting molecule in that it combines a nitramine and a gem-dinitro [*C*-(*NO*₂)₂] functional groups. In fact, there is a separate paper³² which gives further details of its decomposition than what is given here. Briefly, the major products formed are *NO*₂, *NO*, *H*₂*O*, *HCN*, *CO/N*₂, *CO*₂, and NDNAZ (1-nitroso-3, 3-dinitroazetidine). Hardly any *N*₂*O* and *CH*₂*O* have been detected unlike in the case of the products of RDX and HMX. This study has shown that, in common with RDX and HMX, the nitroso analogue, NDNAZ, plays an important role as an intermediate in the decomposition of TNAZ. The temporal correlations of the decomposition products from TNAZ-1-¹⁵*NO*₂, shown in Fig. 12 suggest a different evolution sequence of product groups and at least four different reaction pathways. As an example, the rate of formation of *NO*₂ increases first followed by a rise in the rate of formation of *NO* and finally, a rise in the rate of formation of NDNAZ. This observation supports the previous conclusion that the nitroso analogue is formed by an initial cleavage of the *N-NO*₂ bond followed by the re-attachment of *NO* to the ring, as

in the case of RDX and HMX. Decomposition of this sample labeled with ¹⁵*NO*₂ in the nitramine group, showed that *NO*₂ originates from both the nitramine and the gem-dinitro groups in the molecule but that the severance of *NO*₂ from the nitramine group precedes that from the *C*-(*NO*₂)₂ group. This can be seen clearly in Fig. 12. As a consequence, the ion signals of ¹⁵*NO* and ¹⁵*N*-NDNAZ are also temporally ahead of those from the unlabeled ones which originate from the *C-NO*₂ groups.

5. CONCLUSION

The comparison of the eight nitramine decompositions studied thus far reveals that the pathway proceeding through the formation of the nitroso analogue is of paramount importance in RDX and HMX and also seems to be significant in the thermal decompositions of four other nitramines (IV, V, VI and VIII). It is not yet known whether the cleavage and reformation of *N-NO* bond seen in RDX and HMX is general to all nitramines since this determination preferably requires synthesis of all the nitramines labeled with nitrogen-15. In at least three nitramines studied (V, VI and VIII) the decomposition products commonly observed from nitramines, namely, *CH*₂*O* and *NO*₂, are not formed or are formed only in very minute amounts among the products. The implications of these differences and similarities among several nitramines are being explored and investigated further. Thus, this initial comparative study has provided, for the first time, a basis for the study of structure and stability/sensitivity correlations within the class of nitramines, which is the goal of these studies in the search for materials superior to RDX or HMX in overall performance. On the basis of available evidence, it appears that TNCHP is considerably less sensitive than RDX with only a slight trade-off in energy output and it is relatively stable in the molten state. It thus exhibits a potential to be a new useful nitramine with valuable applications.

ACKNOWLEDGEMENTS

The authors wish to thank D.M. Puckett for assistance in collecting the mass spectrometry data and Dr Philip Pagoria for a sample of K6. This work was supported by the Memorandum of Understanding (MoU) between the Office of Munitions and the U.S. Department of Energy under contract DE-AC04-94 AL85000 and between the U.S. Army ARDEC and the U.S. Army Research Office, under contract.

REFERENCES

- Robertson, A. J. B., *Trans. Faraday Soc.*, 1949, 45, 85.
- Rauch, F. C. & Fanelli, A. J. *J. Phys. Chem.*, 1969, 73, 1604.
- Cosgrove, J. D. & Owen, A. J. *Combust. Flame*, 1974, 22, 13 & 19.
- (a) Batten, J. J. & Murdie, D. C. *Aust. J. Chem.*, 1970, 23, 737; 749. (b) Batten, J. J. *Aust. J. Chem.*, 1971, 24, 945 & 2025; 1972, 25, 2337.
- Bulusu, S. & Graybush, R. J. Proceedings of the 36th International Congress on Industrial Chemistry, Brussels, Belgium, 1967. *C. R. Ind. Chim. Belge*, 1967, 32, 647.
- Bulusu, S.; Graybush, R. J. & Autera, J. R. *Chem. & Ind. (London)*, 1967, 2177.
- Stals, J. *Trans. Faraday Soc.*, 1971, 67, 1768.
- Goshgarian, B. B. Airforce Rocket Propulsion Laboratory Report, 1976. AFRPL-TR-78-76.
- Farber, M. & Srivastava, R. D. *Chem. Phys. Lett.*, 1979, 64, 307.
- (a) Axworthy, A. E.; Flanagan, J. E. & Woolery, D. O. Proceedings of the 15th JANNAF Combustion Meeting, CPIA Publication 297. Chemical Propulsion Information Agency, Laurel, MD, 1978, Vol II. p. 253. (b) Axworthy, A. E.; Flanagan, J. E.; Woolery, D. O. & Gray, J. C. Proceedings of the 15th JANNAF Combustion Meeting, CPIA Publication 308, Chemical Propulsion Information Agency, Laurel, MD, 1979, Vol III. p. 289.
- Oyumi, Y. & Brill, T. B. *Combust. Flame*, 1985, 62, 213.
- Hoffsommer, J. C.; Glover, D. J. & Elban, W. L. *J. Energ. Materials*, 1985, 3, 149.
- Sharma, J.; Hoffsommer, J. C.; Glover, D. J.; Coffey, C. S.; Forbes, J. W.; Liddiard, T. P.; Elban, W. & Sandiego, F. Proceedings of the Eighth Symposium (International) on Detonation, Albuquerque, NM, 1985. p. 725.
- (a) Boggs, T. L. The thermal decomposition behavior of cyclotrimethylene-trinitramine (RDX) and cyclotetramethylene-tetranitramine (HMX). In *Fundamentals of Solid-Propellant Combustion*, Progress in Astronautics and Aeronautics, Vol. 90., edited by K. K. Kuo, and M. Summerfield. AIAA Inc., New York, NY, 1984. (b) Fifer, R. A., p. 177.
- (a) Schroeder, M. A. Critical Analysis of Nitramine Decomposition Data: Product Distributions from HMX and RDX, BRL-TR-2659, 1985. (b) Critical Analysis of Nitramine Decomposition Data: Activation Energies and Frequency Factors for HMX and RDX Decomposition, BRL-TR-2673, 1985.
- (a) Behrens, R. Jr. *Rev. Sci. Instrum.*, 1986, 58, 451. (b) Behrens, R. Jr. The application of simultaneous thermogravimetric modulated beam mass spectrometry and time-of-flight velocity spectra measurements to the study of the pyrolysis of energetic materials, in "Chemistry and Physics of Energetic Materials", edited by S. N. Bulusu, Proceedings of the NATO Advanced Study Institute, Vol. 309. Kluwer Academic Publishers, Netherlands. 1990. p. 327.
- Behrens, R. Jr. *J. Phys. Chem.*, 1990, 94, 6706.
- Behrens, R. Jr. & Bulusu, S. *J. Phys. Chem.*, 1991, 95, 5838.
- Behrens, R. Jr. & Bulusu, S. *J. Phys. Chem.*, 1992, 96, 8877.
- Behrens, R. Jr. & Bulusu, S. *J. Phys. Chem.*, 1992, 96, 8891.
- Behrens, R. Jr.; Land, T. & Bulusu, S. Proceedings of 30th JANNAF Combustion Meeting, Monterey, CA, November 1993.
- Behrens, R. Jr. & Bulusu, S. Proceedings of 29th JANNAF Combustion Meeting, Hampton, VA, October, 1992.
- Behrens, R. Jr. & Bulusu, S. Proceedings of 32nd JANNAF Combustion Meeting, Huntsville, AL, October, 1995.
- Bulusu, S.; Autera, J. R. & Axenrod, T. J. *Labeled Compds. & Radiopharm.*, 1979, 17(5), 707.
- Brockman, F. J.; Downing, D. C. & Wright, G. F. *Can. J. Res.*, 1949, 27B, 469.
- Boyer, J. H. & Kumar, G. J. *Labeled Compds. & Radiopharm.*, 1985, 22, 1.

27. Meyers, G. S. & Wright, G. F. *Can. J. Res.*, 1949, 27B, 489.
28. Goodman, L. *J. Am. Chem. Soc.*, 1953, 75, 3019.
29. Chute, W.D.; Herring, K.G.; Toombs, L.E. & Wright, G. F. *Can. J. Res.*, 1948, 26B, 80.
30. Mitchell, A. R.; Pagoria, P. F.; Coon, C. L.; Jessop, E. S.; Poco, J. F.; Tarver, C. M.; Breithaupt, R.D. & Moody, G.L. Synthesis, Scale-up, and Characterization of K-6. University of California Report,, February, 1991. UCRL-LR-109404.
31. Archibald, T.G.; Gilardi, R.; Baum, K. & Cohen, M.C. *J. Org. Chem.*, 1990, 55, 2920.
32. Behrens, R. Jr. & Bulusu, S. Proceedings of the International Seminar on High Energy Materials, 19-21 November, 1996, Pune, India.

Thermal Decomposition Studies of a New, *gem*-Dinitroalkyl Nitramine 1,3,3-Trinitroazetidine (TNAZ)

Richard Behrens, Jr.

Combustion Research Facility, Sandia National Laboratories, Livermore, CA 94551

and

Suryanarayana Bulusu

US Army Armament Research, Development & Engineering Center (ARDEC)
Picatinny Arsenal, NJ 07806-5000

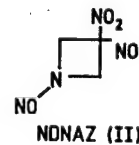
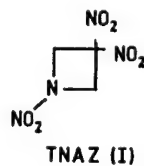
ABSTRACT

The initial results from a study of the thermal decomposition of TNAZ and TNAZ-1-¹⁵N₂O using the simultaneous thermogravimetric modulated beam mass spectrometry (STMBMS) technique are presented. The major products formed in the decomposition of TNAZ are NO₂ and NO with slightly lesser amounts of H₂O, HCN, CO/N₂, CO₂/N₂O and 1-nitroso-3,3-dinitroazetidine (NDNAZ). The last mentioned product (NDNAZ) is shown to be an important intermediate in the decomposition of TNAZ and its decomposition has also been examined by synthesizing it independently. Major products formed in this decomposition of NDNAZ are NO with smaller amounts of H₂O, HCN, CO/N₂ and CO₂/N₂O. The temporal behaviours of the ion signals associated with the various thermal decomposition products from TNAZ, TNAZ-1-¹⁵N₂O and NDNAZ are also presented. They illustrate the evolution sequence of the various products that are associated with the different reaction pathways that control the decomposition of these materials. In particular, the study of the ¹⁵N-labeled sample revealed that NO₂ originates from both the likely sites in the TNAZ molecule and that the cleavage of the nitramine-NO₂ group precedes that of the C-NO₂ cleavage, resulting in similar sequences in the formation of NO and NDNAZ also.

1. INTRODUCTION

TNAZ (1,3,3-trinitroazetidine), (I) is a relatively new energetic material¹ with a strained four membered ring and a *gem*-dinitro group in it. Because of its relatively low m.p. (101 °C) it is melt-castable using steam and is considered to be a useful explosive with valuable applications. Also, TNAZ and mixtures of TNAZ and NDNAZ (1-nitroso-3,3-dinitroazetidine), (II) are new energetic materials with high energy contents which are considered as possible replacements for HMX and TNT. Understanding the thermal decomposition

reactions of these materials is, therefore, important for developing models of their combustion behaviour and their response in abnormal environments. Compared to thermal decomposition studies of the well known cyclic nitramines, RDX and HMX, studies of TNAZ have been new and limited.



Two previous studies of TNAZ have utilized rapid-scan Fourier transform infrared (RSFTIR)² technique in the condensed phase and infrared multiphoton dissociation (IRMPD)³ measurements in the gas phase, to probe the decomposition processes. In the RSFTIR study, based on identification of the lower molecular weight products (i.e., NO_2 , HONO , NO) a mechanism consisting of cleavage of an NO_2 group at either of the C-NO_2 or N-NO_2 sites, elimination of HNO_2 and a nitro-nitrite rearrangement of the C-NO_2 groups was proposed for the decomposition of TNAZ. An uncertainty in this mechanism centers on whether the NO_2 evolves from the nitramine group, the *gem*-dinitro group or both. Another uncertainty was whether the nitro-nitrite rearrangement occurs as postulated, in the condensed phase decomposition.

In the unimolecular decomposition of TNAZ in the molecular beam IRMPD experiments, the results obtained led to the proposal of a mechanism in which the initial step was the loss of NO_2 , followed by opening of the ring, subsequent loss of another NO_2 group and then fragmentation of the ring into N_2O_2 and C_3H_4 . As in the RSFTIR measurements, there is still an uncertainty as to whether the original NO_2 loss was from the nitramine or *gem*-dinitro group. However, a loss of NO_2 as an initial step in the unimolecular decomposition process is clear from these results.³

To develop a reasonable model to characterise the combustion behaviour of TNAZ, it is necessary to characterise the global reaction processes that control its decomposition behaviour. For example, it is not clear whether the first order process as characterised by the results from the IRMPD is also the rate limiting process in a higher pressure environment or whether bimolecular processes should be included to account for other reaction pathways. Furthermore, the appearance of HONO in the RSFTIR measurements, suggests that there is another pathway besides the C-NO_2 or N-NO_2 bond scission. In addition, our previous work on three cyclic nitramines (i.e., RDX^4 , HMX^5 and 1,3,5-trinitro-1,3,5-triazacyclo-heptane, TNCHP^4) suggests that formation of a mono-nitroso analogue of these compounds played an important role in the decomposition. Whether a similar process may be occurring in the decomposition of TNAZ, namely the formation of the nitroso analogue, NDNAZ , is important to determine.

In this paper, we present results of the decomposition of TNAZ and NDNAZ studied by

simultaneous thermogravimetry and molecular beam mass spectrometry (STMBMS) measurements that address the issues of the reaction mechanisms raised above, which indeed, may control the decomposition of TNAZ and NDNAZ . We also present the results of the decomposition study of $\text{TNAZ-1-}^{15}\text{NO}_2$ which shed light on the questions raised. The quantitative gas formation rates of the decomposition products and the associated reaction kinetics are still under investigation.

2. EXPERIMENTAL DETAILS

2.1 Instrument Description

The simultaneous thermogravimetric molecular beam mass spectrometry (STMBMS) apparatus and the basic data analysis procedure have been described previously.^{7,8} This apparatus basically consists of a thermobalance, a specially designed alumina reaction cell in which the decomposition is carried out and a quadrupole mass spectrometer with the ionisation source vertically above the reaction cell. In the region between the reaction cell and the ionisation source are located a set of beam defining orifices and a beam-modulating wheel. In the experimental procedure, a small sample (~10 mg) is placed in an alumina reaction cell that is then mounted on a thermocouple probe which is seated on a microbalance. The reaction cell is enclosed in a high vacuum environment ($< 10^{-6}$ torr) and is radiatively heated by a bifilar-wound tungsten wire on an alumina tube. The molecules from the gaseous mixture in the reaction cell exit through a small diameter orifice (2.5 to 970 μ in these experiments, orifice length is 25 μ) in the cap of the reaction cell, traverse two beam-defining orifices before entering the electron-bombardment ioniser of the mass spectrometer where the ions are formed by collisions of 20 eV electrons with the different molecules in the gas flow.

A relatively low electron energy of 20 eV (compared to 70 eV used on normal mass spectrometry measurements) is used to reduce the extent of fragmentation of the higher molecular weight ions and thus, limit their contribution to ion signals measured at lower m/z values that are associated with the thermal decomposition products. The background pressures in the vacuum chambers are sufficiently low to eliminate significant scattering between molecules from the reaction cell and background molecules in the vacuum chambers. Different m/z value ions are selected with a

quadrupole mass filter and counted with an ion counter. The gas flow is modulated with a chopping wheel and only the modulated ion signal is recorded. This instrument allows the concentration and rate of formation of each gas-phase species in the reaction cell to be measured as a function of time by correlating the ion signals at different m/z values measured with the mass spectrometer with the force measured by a microbalance at any instant. The containment time of gas in the reaction cell is a function of the orifice area, the free volume within the reaction cell, and the characteristics of the flow of gas through the orifice. The reaction cell used in the experiments has been described in detail previously⁸ and the cap in the reaction cell which showed some leakage of products other than from the orifice, is now sealed effectively using vacuum grease and an O-ring between the taper plug and the gold

foil pinhole orifice. The time constant for exhausting gas from the cell is small compared to the duration of the experiments (> 1000 s). Note that the containment time of gas within the reaction cell is short once the gas molecules are in the free volume of the cell, but it may be much longer if the gas is trapped in the condensed phase of the material within the cell. The pressure of the gas products within the reaction cell ranges from less than 1 torr for experiments with the larger diameter orifices ($970\ \mu$) to greater than 1000 torr for experiments with the smallest diameter orifices ($2.5\ \mu$).

2.2 Sample Preparation

The TNAZ was prepared by a previously described method.¹ The $^{15}\text{NO}_2$ -labeled TNAZ was prepared by treating 1-acetyl-3,3-dinitroazetidine with $H^{15}\text{NO}_3$. The NDNAZ was obtained from M. Hiskey (Los Alamos National Laboratory). The samples were characterised by NMR and IR measurements. To check whether any impurity evolved from the sample, the sample was evaporated in the STMBMS apparatus prior to conducting the decomposition experiments. The results for TNAZ indicate that it was greater than 99 per cent pure and the results for NDNAZ indicate that there was about 1 per cent TNAZ impurity.

2.3 Data Analysis

The details of the procedure for identifying the pyrolysis products by correlating the temporal behaviour of the various ion signals measured with the mass spectrometer and the analysis of time-of-flight (TOF) velocity spectra have been described previously.⁹ The latter technique allows one to determine the neutral precursor of each ion observed in the mass spectrometer and thus discriminate between true thermal decomposition products and electron impact-induced products from evaporating parent compound.

In this paper, we present the qualitative results of the decomposition based on the temporal behaviour of the ion signals measured with the mass spectrometer and associated with the various thermal decomposition products. Because these results are qualitative, strict comparison of the ion signal intensities from one experiment to another can be misleading. However, quantitative results derived from these runs will be presented in a later paper.

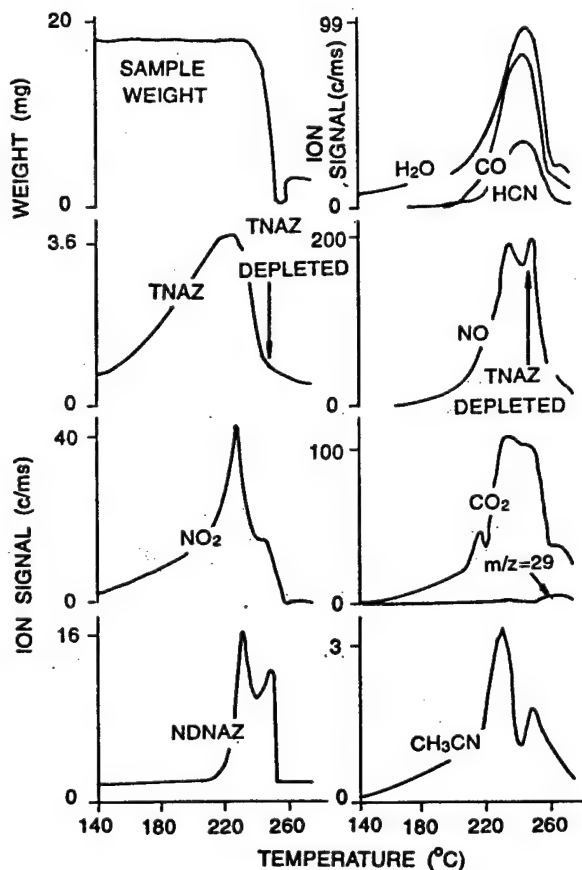


Figure 1. Ion signals representing the major decomposition products from TNAZ. The ion signals have been corrected for the evaporation of TNAZ. The m/z values representing each product are: TNAZ (145), NDNAZ (176), NO_2 (46), $\text{CO}_2/\text{N}_2\text{O}$ (44), NO (30), CO/N_2 (28), HCN (27), CH_3CN (41). Orifice diameter = $2.5\ \mu$, heating rate = $15\ ^\circ\text{C}/\text{min}$.

3. RESULTS & DISCUSSION

3.1 Identity and Temporal Behaviour of the Decomposition Products from TNAZ

The two major products observed in the decomposition of TNAZ are NO (mass spec. ion signal at $m/z=30$) and NO_2 ($m/z=46$). Other major decomposition products observed include: H_2O ($m/z=18$), HCN ($m/z=27$), CO/N_2 ($m/z=28$), CH_3CN ($m/z=41$), and $NDNAZ$ ($m/z=176$). Loss of TNAZ itself is monitored by tracking ($m/z=145$) which is an important fragment in the mass spectrum of TNAZ (Table 1). Smaller ion signals are observed at a number of other m/z values which will be described in a later publication. The temporal behaviour of both the thermogravimetric analysis (TGA) data and the ion signals representing these major products of TNAZ heated at $15\text{ }^\circ\text{C/min}$ in a reaction cell with a $2.5\text{ }\mu$ diameter orifice, are shown in Fig. 1. A close examination of the data illustrates the processes that occur during the decomposition of TNAZ. Firstly, TNAZ starts to evolve in significant quantities from the reaction cell at approximately $150\text{ }^\circ\text{C}$ as can be seen from the sample weight and the ion signal associated with TNAZ. Even though TNAZ has a relatively high vapour pressure for an energetic material, its rate of evolution from the cell is limited due to the small $2.5\text{ }\mu$ orifice diameter used in these experiments. The ion signal associated with TNAZ increases with temperature as its vapour pressure

Table 1. Mass spectra of TNAZ and NDNAZ*

TNAZ		NDNAZ	
Mass	Rel. Intensity (%)	Mass	Rel. Intensity (%)
28	2.1	27	1.5
30	4.2	28	2.9
41	7.0	30	50.2
42	0.6	41	1.4
46	54.5	46	0.7
53	1.0	53	0.6
68	0.7	54	0.8
99	6.5	129	0.6
100	1.4	130	5.5
116	1.1	176	29.3
145	9.9	177	1.5
146	6.8	-	-

* Mass spectra recorded using electron energy of 20 eV.

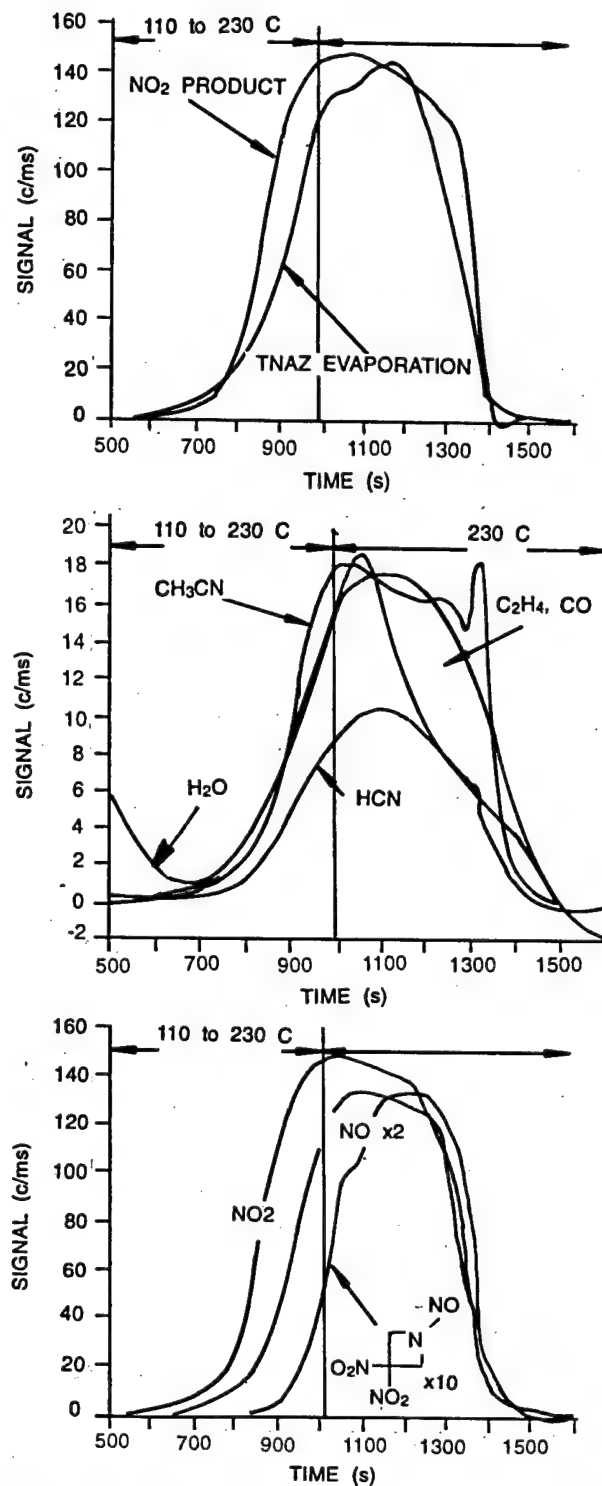


Figure 2. Ion signals representing thermal decomposition products formed from TNAZ heated to $230\text{ }^\circ\text{C}$ at $15\text{ }^\circ\text{C/min}$ and held there in the reaction cell with $2.5\text{ }\mu$ diameter orifice.

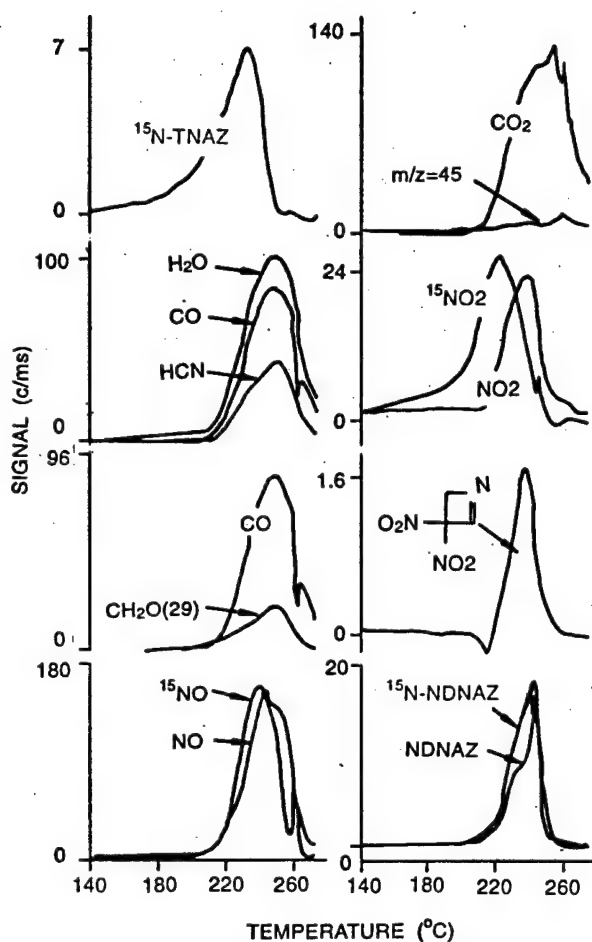


Figure 3. Ion signals representing the thermal decomposition products formed from TNAZ-1- $^{15}\text{NO}_2$ heated at $15^\circ\text{C}/\text{min}$, in a reaction cell with 2.5μ diameter orifice. The products and their m/z values are: H_2O (18), HCN (27), CO (28) CH_2O (29), NO (30), ^{15}NO (31), CO_2 (44), $^{15}\text{NNO}/\text{HCONH}_2$ (45), NO_2 (46), $^{15}\text{NO}_2$ (47), $\text{C}_3\text{H}_3\text{N}_3\text{O}_4$ (145), $\text{C}_3\text{H}_4\text{N}_4\text{O}_5$ (176) and $\text{C}_3\text{H}_4^{15}\text{N}_3\text{O}_5$ (177). The ion signals have been corrected for the contribution of signals from evaporating TNAZ-1- $^{15}\text{NO}_2$.

risers until the TNAZ in the reaction cell is depleted as shown in Fig. 1. Secondly, examination of the ion signal representing NO_2 shows that its evolution commences at approximately 140°C , reaches a peak at 230°C and then decreases. This behaviour is consistent with a reaction that is first order in TNAZ because the rate of decomposition of TNAZ to NO_2 increases with temperature and then decreases as the amount of TNAZ in the reaction cell decreases. This behaviour also indicates that TNAZ is decomposing in both the liquid

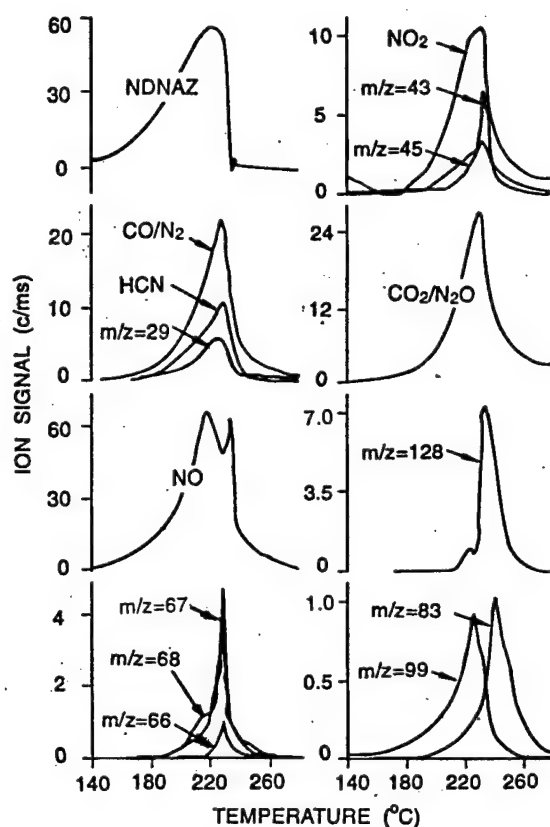


Figure 4. Ion signals representing the major decomposition products from NDNAZ. The ion signals have been corrected for the evaporation of NDNAZ. The m/z values representing each product are: NDNAZ(176), HCN (27), CO/N_2 (28), NO (30), NO_2 (46), and $\text{CO}_2/\text{N}_2\text{O}$ (44). Reaction cell orifice diameter, 2.5μ ; heating rate, $15^\circ\text{C}/\text{min}$.

and gas phases since the rate of NO_2 formation is proportional to the total amount of TNAZ in the cell and not just the amount of TNAZ in the gas phase (which continues to increase until it nears depletion). Thirdly, the evolution of the signals at m/z values 44 (CO_2), 176 (NDNAZ), 30 (NO), 28 (CO or N_2), 27 (HCN) and 41 (CH_3CN) continues beyond the temperatures (and times) corresponding to the evolution of NO_2 and also TNAZ itself. This indicates that another reaction pathway competes with the direct decomposition of TNAZ to NO_2 and other low molecular weight gas phase products, as observed in the RSFTIR and IRMPD experiments.

The formation of the mononitroso analogue of TNAZ, namely NDNAZ, in the decomposition of TNAZ appears to be the other major reaction pathway as will be shown in the following discussions. Formation of the nitrosamine ($N\text{-NO}$) from the nitramine ($N\text{-NO}_2$) group

is shown to play an important role in controlling the decomposition pathway similar to the other cyclic nitramines (i.e., RDX, HMX and TNCHP). Decomposition through the mononitroso intermediate is consistent with several of the features of the data shown in Fig. 1. For example, NDNaz first appears at about 200 °C and increases as the amount of NO increases, suggesting that NO reacts with TNAZ to form NDNaz. The fact that the NDNaz signal decreases as the amount of TNAZ decreases is also consistent with a direct reaction with NO. The increase in the NDNaz signal as the TNAZ in the cell nears depletion is consistent with an increasing mole fraction of NDNaz in the liquid phase and the resulting increase in its partial pressure in the reaction cell. Finally, evolution of CO₂/N₂O, NO, HCN and CO/N₂ after the depletion of TNAZ suggests that they are the thermal decomposition products from NDNaz.

The results from an isothermal decomposition experiment with TNAZ also support a reaction mechanism consisting of parallel reaction pathways. These results at 230 °C are shown in Fig. 2. The *m/z* values representing each decomposition product are: TNAZ (145), NDNaz (176), NO₂ (46), NO (30), CO/N₂/C₂H₄ (28), HCN (27), CH₃CN (41). The ion signals have been corrected for the contribution of signal from evaporating TNAZ. NO₂ is an abundant decomposition product and its rate of formation falls as the amount of TNAZ falls. However, the ion signal associated with NO₂ (*m/z*=46) does not fall as rapidly as the ion signals associated with H₂O and HCN. This suggests that H₂O and HCN originate from reactions associated with a decomposition reaction that is first order in the total TNAZ in the reaction cell (both phases), whereas, NO₂ may originate from more than one source. The formation of NDNaz from TNAZ is also clearly illustrated in Fig. 2. First an increase in the rate of formation of NO₂ is observed, followed by a rise in the rate of formation of NO and finally a rise in the rate of formation of NDNaz. This is reminiscent of the RDX decomposition³ in which NO₂ is replaced by NO to form the nitrosamine, ONDNTA. The behaviour of NO₂, NO and NDNaz from TNAZ is, therefore, consistent with a mechanism analogous to the one that gives ONDNTA from RDX. This suggests that the nitramine NO₂ group is replaced by NO in TNAZ also to form the nitrosamine analogue, as in the case of RDX.

3.2 Thermal Decomposition of TNAZ-1-¹⁵NO₂

Figure 3 presents the ion signals obtained from the decomposition of TNAZ-1-¹⁵NO₂ heated at 15 °C/min. The most interesting differences between these signals and those obtained from unlabelled TNAZ (Fig. 1) are first, the appearance of both ¹⁵NO₂ and NO₂ signals which are of nearly equal intensity and uncorrelated. Likewise, there are separate signals each for ¹⁵NO/NO and ¹⁵N-NDNaz/NDNaz, also uncorrelated and of equal intensity. This clearly suggests that NO₂ is formed from both the possible sites in the TNAZ molecule, namely, the nitramine group and the *gem*-dinitro group, but the former precedes the other significantly earlier. However, the time lags between the ¹⁵N-labelled and unlabelled species of NO and NDNaz are much smaller than for NO₂. The thermal decomposition product, *m/z* = 145 (193-48) presumably derives from elimination of H¹⁵NO₂ exclusively from the nitramine function and an adjacent H but not from the C-NO₂ function analogous to the previous nitramines studied. The earlier conclusion that the nitroso-NDNaz is derived by a reattachment of ¹⁵NO or NO to the initial radical produced by the loss of nitramine-NO₂ is borne out by the correlations of ¹⁵NO/NO and ¹⁵N-NDNaz/NDNaz.

It is apparent from an examination of the ¹⁵N and unlabelled species shown in the plots of Fig. 3 that NO₂ originates from both the possible sites in the TNAZ molecule and that the cleavage of the nitramine-NO₂ precedes that of the C-NO₂ cleavage. This also results in similar sequences of ¹⁵NO/NO and ¹⁵N-NDNaz/NDNaz. This observation is consistent with the fact that N-NO₂ bond is weaker than C-NO₂ bond. Once an N-NO₂ bond cleaves, other C-NO₂ bonds can cleave more readily as predicted by the calculations of Melius¹⁰. It is also worth mentioning that the lack of ¹⁵N-isotopic shifts show that *m/z* = 44 and *m/z* = 28 are predominantly CO₂ and CO, respectively and not N₂O and N₂.

3.3 Thermal Decomposition of Independently Synthesized NDNaz

The thermal decomposition of NDNaz is controlled by a complex process that forms both gas-phase and liquid-phase products. Ion signals associated with thermal decomposition products formed from NDNaz are shown in Fig. 4 for a 12 mg sample of NDNaz heated at 15 °C/min in a reaction cell with a 2.5 μ diameter orifice. The vapour pressure of NDNaz is relatively high as can be seen from the large ion signal

associated with the evaporation of NDNaz in Fig. 4. The NDNaz in this experiment is depleted when the sample reaches a temperature of $\sim 235^\circ\text{C}$. Examination of the ion signals associated with the thermal decomposition products show continued evolution from the reaction cell after the NDNaz is depleted. This suggests that products with low volatility are formed in liquid-phase during the decomposition and their evolution and decomposition continues as the sample is heated further

Table 2. Probable composition of the unidentified m/z species in Fig. 4

m/z	$\text{C}_3\text{H}_4\text{N}_4\text{O}_5(\text{NDNAZ})$	Composition
66	176 - 110 ($2\text{HNO}_2 + \text{O}$)	$\text{C}_3\text{H}_2\text{N}_2$
67	176 - 109 ($\text{HNO}_2 + \text{NO}_2 + \text{O}$)	$\text{C}_3\text{H}_3\text{N}_2$
68	176 - 108 ($2\text{NO}_2 + \text{O}$)	$\text{C}_3\text{H}_4\text{N}_2$
83	176 - 93 ($\text{HNO}_2 + \text{NO}_2$)	$\text{C}_3\text{H}_3\text{N}_2\text{O}$
99	176 - 77 ($\text{HNO}_2 + \text{NO}$)	$\text{C}_3\text{H}_3\text{N}_2\text{O}_2$
128	176 - 48 ($\text{NO} + \text{H}_2\text{O}$)	$\text{C}_3\text{H}_2\text{N}_3\text{O}_3$

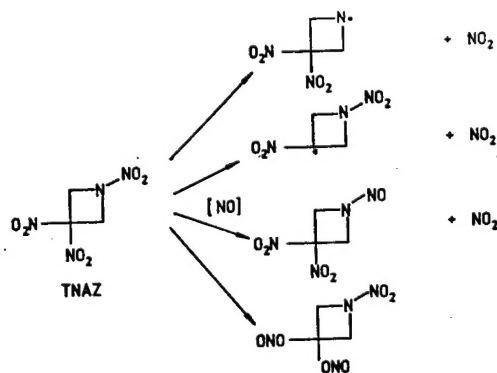
NDNAZ decomposes at significant rates in these experiments starting at approximately 160°C as indicated by the first appearance of the ion signals associated with the thermal decomposition products. The rates of formation of several of the lower molecular weight gaseous products, such as CO/N_2 and HCN , fall to zero as the NDNaz sample is depleted indicating that they are formed directly from the decomposition of NDNaz. In contrast, some products start evolving at a higher temperature and also fall-off as the NDNaz is depleted. For example, a product associated with ion signals at m/z values of 66, 67 and 68 starts appearing at approximately 180°C and its rate of formation increases rapidly at $\sim 210^\circ\text{C}$. Further, other products start evolving at a higher temperature and continue to evolve after the NDNaz is depleted. Examples of this behaviour are seen with the $\text{CO}_2/\text{N}_2\text{O}$ signal and ion signals representing a number of different products at m/z values of 43, 83, 99 and 128. In the case of the product represented by the $m/z = 128$ signal, the rate increases significantly after the NDNaz is gone.

The identities of the thermal decomposition products from NDNaz are similar to those formed in the decomposition of TNAZ. However, the relative amounts of the major products differ significantly. The other most

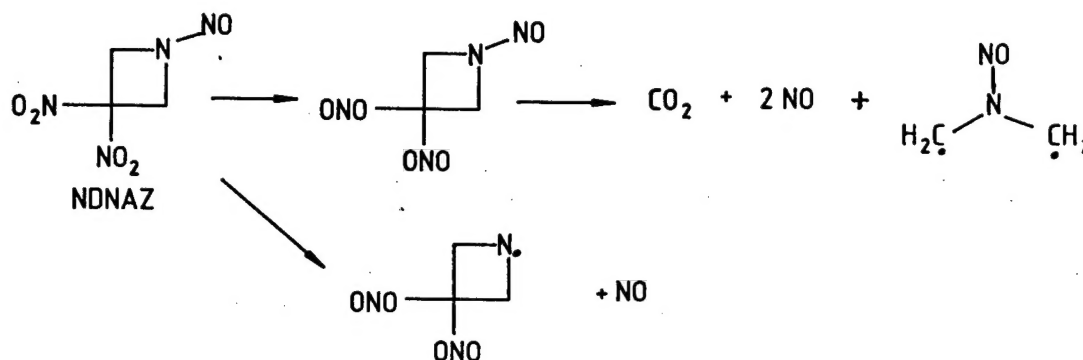
abundant thermal decomposition products from NDNaz are H_2O , HCN , CO/N_2 , CO_2 , NO_2 and some of the less volatile products that remain in the liquid phase, parallel to the behaviour of TNAZ. The identities of the thermal decomposition products associated with the ion signals of various m/z values shown in Fig. 4 require conducting TOF velocity spectra measurements which will be carried out in the future.

3.4 Basic Reaction Pathways for TNAZ

From the STMBMS measurements on TNAZ we have observed that the products are consistent with the direct decomposition mechanisms proposed based on previous RSFTIR measurements² and unimolecular IRMPD measurements³. In addition, we observed the new reaction product, NDNaz, which shows that the reaction pathways other than the unimolecular decomposition alone must be considered in developing a mechanism for the thermal decomposition of TNAZ. The first step in the decomposition of TNAZ appears to be $\text{N}-\text{NO}_2$ and $\text{C}-\text{NO}_2$ bond homolysis, replacement of the nitramine NO_2 group with an NO group and the possible nitro- nitrite rearrangement of NO_2 at the gem-dinitro group. These steps are summarized as follows:



The NO required for the conversion of TNAZ to NDNaz may form through either the nitro-nitrite rearrangement reaction, and the reaction of NO with CH_2O or via the loss of N_2O_2 after the NO_2 loss and the ring opening steps in the IRMPD mechanism. Once the nitroso analogue of TNAZ is formed, it alters the subsequent decomposition pathway by significantly reducing the direct decomposition to NO_2 and enhancing



the rate of formation of NO . Two possible pathways for producing NO from NDNaz are as follows:

The fact that the rate of formation of NO compared to NO_2 is significantly higher in the thermal decomposition of NDNaz indicates that a nitro-nitrite rearrangement reaction is more likely for the nitrosamine than the nitramine. The formation of NO by scission of N-NO bond probably occurs but it cannot account for the significant increase of NO formed in the decomposition.

The ion signals observed in the decomposition of NDNaz (Fig. 4) also include several unassigned mass species in the m/z range 66-128. Given the fact that there are only four possible atomic species (C , H , N , and O), one can speculate on the possible atomic compositions of these species as summarised in Table 2. The identities of the species in the last column will be established with the help of isotopic shifts using ^{15}N -labelled material and time of flight velocity data both of which are currently being obtained.

The mass spectrometry data on the thermal decomposition of TNAZ and NDNaz clearly show many ion signals at different m/z values associated with products of secondary reactions. Several of the products come directly from the ring HCN ($m/z = 27$) and CH_3CN ($m/z = 41$). Others such as H_2O and CO/N_2 come from secondary reactions of thermal decomposition products, while many other ion signals have not yet been associated with specific thermal decomposition products since further information is required to make these assignments.

It is clear from the STMBMS results that the construction of a realistic mechanism to characterise the thermal decomposition process of TNAZ requires the use of several parallel reaction pathways. Construction of a useful model of the decomposition process requires

measuring the temperature-dependent rate constants for each of these pathways.

3.5 Further Work

The work on the thermal decomposition of TNAZ and NDNaz presented in this paper is the first step of examining the decomposition of these materials with the STMBMS technique. Further work on TNAZ will include making TOF velocity spectra measurements of the various ion signals to determine the identities of the secondary products. Quantitative analysis of the data will be made to determine the gas formation rates of the different products as a function of time. Finally, the time and temperature dependence of the gas formation rates of the different products will be analysed to determine the temperature dependence of the rate constants for the different reaction pathways.

4. SUMMARY

The results presented in this paper on the decomposition of TNAZ show that its thermal decomposition is controlled by a number of different competitive and coupled reactions. The formation of NO_2 is consistent with either C-NO_2 and/or N-NO_2 bond homolysis and is in agreement with the pathways determined in the IRMPD experiments. This study shows that in the presence of decomposition products TNAZ reacts with NO to form the nitroso analogue of TNAZ, NDNaz. The temporal behaviours of the decomposition products show that as the amount of NDNaz increases in the TNAZ sample, new products associated with the decomposition of NDNaz appear and contribute to an increase in the overall decomposition of TNAZ. Thus, to adequately characterise even the first step of the decomposition process, bimolecular reactions must be

included. The first decomposition products from TNAZ were observed at $\sim 160^\circ\text{C}$ in the STMBMS experiments and the formation of NDNAZ was first observed starting at $\sim 200^\circ\text{C}$. Decomposition products associated with NDNAZ were observed after all of the TNAZ was thereby consumed suggesting that NDNAZ is thermally more stable than TNAZ.

The decomposition of NDNAZ shows that changing the *N-NO₂* group to *N-NO* group alters the decomposition process. For NDNAZ a much larger proportion of *NO* as compared to *NO₂* is formed in the decomposition process. This may be due to an enhanced propensity to undergo nitro-nitrite rearrangement that leads to the formation of *NO* and the elimination of *CO₂* from the azetidine ring. This is consistent with the results. The decomposition of NDNAZ produces both volatile gaseous products and some products that remain in the liquid phase.

The temporal behaviour of the product species from the thermal decomposition of both TNAZ and NDNAZ indicates that the reactions occur in both the gas and liquid phases.

Further STMBMS experiments and analyses will be conducted to identify other reaction products, obtain more details on the reaction pathways and determine the temperature-dependent rate constants for the different pathways. These experiments are also expected to shed light on the effect of the *gem*-dinitro group on the thermal stability of TNAZ relative to other cyclic nitramines.

ACKNOWLEDGEMENT

We would like to acknowledge the help of David Puckett for collecting the experimental data and to Dr. Michael Hiskey for providing the NDNAZ.

REFERENCES

1. Archibald, T. G.; Gilardi, R.; Baum, K. & Cohen, M. C. *J. Org. Chem.*, 1990, **55**, 2920.
- 2(a). Oyumi, Y. & Brill, T. B. *Combust. Flame*, 1985, **62**, 225.
- 2(b). Oyumi, Y. & Brill, T. B. *Combust. Flame*, 1987, **68**, 209.
3. Anex, D. S.; Allman, J. C. and Lee, Y. T., In *Chemistry of energetic materials*, edited by G. Olah. Academic Press, New York, 1991. p. 27.
4. Behrens, Jr. R. & Bulusu, S. *J. Phys. Chem.*, 1992, **96**, 8877 & 8891.
- 5(a). Behrens, Jr. R. *J. Phys. Chem.*, 1990, **94**, 6706.
- 5(b). Behrens, Jr. R. & Bulusu, S. *J. Phys. Chem.*, 1991, **95**, 5838.
6. Behrens, Jr. R. & Bulusu, S. *Mater. Res. Soc. Symp. Proc.*, 1993, **296**, 13.
- 7(a). Behrens, Jr. R. *Rev. Sci. Instrum.*, 1986, **58**, 451.
- 7(b). Behrens, Jr. R. The application of simultaneous thermogravimetric modulated beam mass spectrometry and time-of-flight velocity spectra measurements to the study of the pyrolysis of energetic materials. In *Chemistry and physics of energetic materials*, edited by S. N. Bulusu, Proceedings of the NATO Advanced Study Institute, Kluwer Academic Publishers, Netherlands, 1990, 309, p. 327.
8. Behrens, Jr. R. *Int. J. Chem. Kinetics*, 1990, **22**, 135.
9. Behrens, Jr. R., *Int. J. Chem. Kinetics*, 1990, **22**, 159.
10. Melius, C. F. and Binkley, J. S. In *Proceedings of the 21st Symposium (International) on Combustion*, 1987, The Combustion Institute, Pittsburgh, PA, 1988.